united nations
educational, scientific
and cultural
organization

international atomic
energy agency

the
abdus salam
international centre for theoretical physics

H4. SMR/1247
Lecture Note: 21

WORKSHOP ON PHYSICS OF MESOSPHERE-STRATOSPHERE-TROPOSPHERE INTERACTIONS WITH SPECIAL EMPHASIS ON MST RADAR TECHNIQUES

(13 - 24 November 2000)

TURBULENCE
ITS NATURE, AND HOW TO HANDLE IT MATHEMATICALLY

Prof. W. K. Hocking

Dept. of Physics
University of Western Ontario
London, Ontario

TURBULENCE

— Its nature, and how to handle it mathematically.

Let us now look at turbulence in the atmosphere in greater detail.

70 Turbulence and radar

University of Canterbury Oct 14 1999. (1)

W. Hocking

In the previous lecture we discussed the different types of scatterers which exist in the atmosphere. We particularly concentrated on specular reflectors.

But probably the main form of scatter is turbulent scatter, and it is therefore appropriate that we spend this lecture discussing the nature of turbulence, and how it relates to radar methods.

[Extracts from Indian Summer School, 1994]

6.1.2 An introduction to turbulence

Turbulence is essentially a quasi-random hybrid of fluid motions which cannot be described in terms of wave motions. It affects its environment in at least two main ways; it may heat the fluid in which it exists, and it causes diffusion of momentum, heat, particles and atmospheric constituents. Turbulence occurs on a wide range of scales, but in this work most discussion will be concentrated on small scale turbulence; that is, scales less than about 5 km in size, where turbulence is at least quasi-isotropic, and can truly be called three- dimensional turbulence. Our later discussions will also incorporate some commentary about the internal nature of turbulence.

A variety of parameters are important in describing turbulence. The rate at which turbulence causes heating of its environment, ε, and the rates at which momentum (K_m) and heat (K_t) diffuse are some of the most important. In theory the rate of diffusion of momentum and heat differ, but in practice they are often taken to be similar. Many measurements made in the mesosphere assume that turbulence obeys Kolmogoroff inertial range theory (Kolmogoroff, 1941; Tatarski, 1961), and this applies between a minimum scale called the "inner scale", ℓ_0, and an outer scale, called the buoyancy scale, L_B. Various levels of sophistication exist for theories connected with turbulence, but given the accuracy with which measurements have been possible, it is often only worth using approximate relations between the various parameters. Such relations will be discussed in due course. In this text, ε and K will be discussed in greatest detail. Typical inner and buoyancy scales as a function of altitude have been presented by Hocking, (1985), and will also be shown here-in.

Turbulence, by it nature, is very variable in intensity, but there are some general features about its altitudinal distribution which we can comment upon. Clearly it can be quite intense in the Earth's boundary layer and troposphere, especially during storm conditions. Within the boundary layer, the nature of turbulence differs from that at greater altitudes, in that the proximity to the ground affects the nature of the scatterers and the rates of diffusion. Turbulence strengths above the tropopause generally diminish compared to the tropospheric values, and then increase again above about 60 km altitude. In the boundary layer, turbulence is often caused by orographic effects, but above the tropopause the main sources of turbulence are almost certainly gravity waves and (to a lesser extent) tides. These generate turbulence by processes such as non-linear breaking, shear instabilities, convective overturning and critical-level interactions (Lindzen, 1981; Teitelbaum and Sidi, 1976; Sidi and Teitelbaum, 1978; Hodges, 1967; Jones and Houghton, 1971). Measurements of turbulence by

rocket techniques (e.g. Blamont and Barat, 1964) have shown that turbulence often appears in horizontal laminae of thicknesses of a few kilometres, interspersed with non-turbulent regions, and it appears that turbulence is both spatially and temporally intermittent. Turbulence appears to occur in patches; Anandarao et al., (1978), Teitelbaum, (1966) and Zimmerman and Murphy, (1977) have presented data to suggest that turbulence occurs between 30% and 80% of the time, with the lower percentage occurring at lower heights. Radar studies, and particularly high resolution VHF studies, have also confirmed the intermittent nature of turbulence at these higher altitudes (e.g. Czechowsky et al., 1979; Roettger et al., 1979; Woodman et al., 1980; Woodman, 1980; Sato et al., 1985; Sato and Woodman, 1982).

Generally, turbulence is important to an upper altitude of somewhere between 90 and 110 km (the exact limit varies with time within this range), whereupon the atmospheric viscosity becomes so large that it quickly damps any tendency for turbulence to form. This transition region is called the "turbopause".

GENERAL THEORY

In the following section, we will discuss just how turbulence arises from the fluid dynamical equations, and then consider the various quantities which can be measured in connection with these motions. Discussion of typical scales will be left to a later section.

6.2.1 The fluid dynamical equations of motion.

The equations considered are the standard fluid-dynamical equations

$$\frac{D\underline{u}}{Dt} + 2\underline{\Omega} \times \underline{u} + \underline{g} + \frac{1}{\rho}\underline{\nabla} p - \nu \nabla^2 \underline{u} = 0 \tag{1}$$

$$\frac{D\rho}{Dt} = \frac{1}{c_s^2}\frac{Dp}{Dt} \tag{2}$$

$$\frac{D\rho}{Dt} + \rho \underline{\nabla} \cdot \underline{u} = 0 \tag{3}$$

$$\frac{D\Theta}{Dt} = \frac{\kappa}{\rho}\nabla^2 \Theta \tag{4}$$

where D/Dt represents differentiation following the motion. The total velocity is $\underline{u}$, the density ρ, $\underline{\Omega}$ is the Earth's angular rotation rate, $\times$ means cross product, $\underline{g}$ is the acceleration due to gravity = (0,0,-g), p is the pressure, c_s^2 is the speed of sound squared, $\underline{\nabla}$ represents the gradient differential operator and "." means the dot product. Θ represents potential temperature, κ the heat diffusion coefficient, and ν is the kinematic viscosity coefficient.

In the following sections, it will be briefly shown how these equations are modified for dealing with turbulence, and the important parameters required in any useful study will be defined.

In the case of turbulence studies, different modifications are made to the equations of motion. To begin, Coriolis effects are unimportant, and often the gravity term is also unimportant for turbulence. In this case, (1) becomes

$$\frac{D\underline{u}}{Dt} = -\frac{1}{\rho}\underline{\nabla} p + \nu\nabla^2\underline{u} \tag{17}$$

Furthermore, in the case of turbulence the fluid is usually assumed incompressible, in which case c_s^2 is taken to be infinity in (2). Compressibility due to vertical displacement (the so-called Boussinesq approximation) is usually allowed, but it is assumed that at any one height the air is incompressible.

In the case of turbulence, motions are generally very complex. Therefore there is no value in trying to produce exact descriptions (e.g. sinusoidal solutions) of the fluid motions, and the normal approach is to change the equations and express them in terms of energies. The fluid motions are written as the sum of a "mean" and a "fluctuating" component, such as $u = \overline{u} + u'$, and this is then re-inserted in the equations. In this case we do *not* ignore second-order terms, but because we are interested only in a statistical description, we take a time-average. Thus second order terms like $v'\frac{\partial \overline{u}}{\partial y}$ cancel out, since the average of v' is zero by definition. However, terms involving cross-terms of two fluctuating quantities do *not* necessary cancel out. Carrying out this expansion, performing the time-average, and ignoring the viscous terms ($\nu\nabla^2\underline{u}$) produces a new set of equations, called the "mean momentum equations", as described in Bradshaw, (1975). Let $\underline{u} = (\overline{u}, \overline{v}, \overline{w})$, and $\underline{u}' = (u', v', w')$. Then the x component of equation (17) now becomes

$$\frac{\partial \overline{u}}{\partial t} + (\overline{u}, \overline{v}, \overline{w}) \cdot \underline{\nabla}\overline{u} = \frac{-1}{\rho_0}\frac{\partial \overline{p}}{\partial x} - \left[\overline{\frac{\partial}{\partial x}(u')^2} + \overline{\frac{\partial}{\partial y}(u'v')} + \overline{\frac{\partial}{\partial z}(u'w')}\right] \tag{18}$$

Similar equations exist for the y and z components. It will be noted that this looks very much like (17), except that the total velocity vector $\underline{u}$ has been replaced by the mean velocity vector $\overline{\underline{u}}$, and the term $\nu\nabla^2 u$ is now replaced by terms like $-d/dz(\overline{\rho u'w'})$.

The term $\rho\overline{u'w'}$ represents the vertical flux of horizontal momentum. Terms like this are also called "Reynold's stress" terms. Note that there would have been nothing to stop us from doing this in the case of gravity wave motions, and indeed we will see later that the Reynolds' stress terms are also quantities which are often sought after for gravity wave motions. However, at the present time we will continue to pursue their meaning with respect to turbulence.

Now we noted above that our equation looks very much like equation (17), but that the term $\nu\nabla^2\underline{u}$ has been replaced by the Reynolds' stress terms. Therefore in turbulence theory we often replace these terms with an expression that looks a lot like $\nu\nabla^2\underline{u}$; in fact we use a term like $K_{zz}\nabla^2\overline{\underline{u}}$ to replace the term $-\overline{\frac{\partial}{\partial z}(u'w')}$. In molecular flow, the kinematic viscosity is defined by the relation $f_d = -\rho\nu d/dz(\overline{u})$ where f_d is the drag force per unit area. In the case of flow with fluctuating motions, the Reynold's stress acts like the viscous drag, and either by noting the similarity between the Reynold's stress and the viscous drag, or by comparing (17) and (18), with ν in (17) replaced by the turbulent diffusivity K_{zz}, we see that the momentum diffusivity K_{zz} is defined through the relation

$$\rho\overline{u'w'} = -\rho K_{zz}\frac{d\overline{u}}{dz} \tag{19}$$

K_{zz} (also denoted K_m, where the "m" stands for "momentum") is also called the (vertical) turbulent viscosity, since it has a strong analogy with molecular viscosity, ν. There are other "diffusion coefficients" K_{xx}, K_{xy}, which relate to the rates of horizontal diffusion, and in general there is an asymmetry in the rate of diffusion as a function of the direction being considered. In most of this article, the effects of turbulence at scales less than about 5 km (small scale) will be examined. At such scales, the rate of diffusion is approximately independent of direction; the rates of diffusion in the vertical and horizontal are at least similar to within a factor of 2 or 3. The eddy diffusion coefficients obtained at these scales are also appropriate for calculation of vertical diffusion rates at larger scales, since buoyancy effects limit the vertical extent of eddies, and most of the energy of turbulence occurs in the eddies with vertical scales less than about 5 km. Horizontal diffusion rates, however, can become quite large at larger scales. Some very preliminary estimates of horizontal diffusion coefficients have been made by Ebel, (1980). In this work it is primarily the vertical and small scale diffusion coefficients which are of interest, so we will concentrate mostly on K_{zz}.

Just as K_m, the momentum diffusion coefficient, is the turbulent analog of the molecular diffusion coefficient ν, the analog of the thermal diffusion coefficient κ_T is the turbulent heat diffusion coefficient, K_T. The rate of diffusion of atmospheric constituents is also controlled by K_T.

The ratio of the molecular viscosity to the thermal diffusivity, ν/κ_T, is called the Prandtl number, and for air it is about 0.7. Similarly a "turbulent Prandtl number", $P_r = K_m/K_T$ is defined for turbulent processes, and often it is assumed that the value for this turbulent Prandtl number is also about 0.7, although this assumption is rarely justified. For example, Justus, (1967a) has made measurements with rockets which suggest that P_r may have a numerical value of about 2 or 3. Recently, physical reasons have been advanced to explain why P_r might be quite large when considered over long time scales and large spatial scales (Fritts and Dunkerton, 1985). Recent model calculations have also suggested that the diffusivities of momentum (Garcia and Solomon, 1985) and heat (Strobel et al., 1987; Strobel, 1989) seem to be quite different, but further substantiation is needed.

Often K_T and K_m are treated as a similar parameter, usually denoted by "K", despite the fact that $P_r \neq 1$, and given the accuracy with which these parameters have been measured in the past, this was not entirely unreasonable. Recently demands for greater accuracy in the measurements of K_T and K_m have arisen, and the need to consider these parameters as distinct may be more important in the future.

Finally, an important warning should be sounded. We have made some mileage in our discussions about turbulence by intercomparing molecular and turbulent diffusion. Sometimes this is even taken further; it is sometimes noted that the molecular diffusion coefficient is proportional to the mean free path between collisions for a molecule, multiplied by the molecular speed. Sometimes a "diffusion coefficient" is likewise inferred in the turbulence case by multiplying a typical turbulent speed by a typical "scale". This works in a broad sense, but one must be very careful. Bradshaw (1975) sounds warnings against such crass comparisons. Indeed, one can recognize that there is not a simple correspondence between the molecular and turbulent diffusion cases in the following manner. If a cloud of gas is released in air and expands by molecular diffusion, then the mean square radius of this cloud expands according to a law of the type $r^2 = 2\nu t$, where t represents time since the moment of release. However, this is not true for turbulent diffusion, for in that case the cloud expands according to a law of the type $r^2 \propto t^3$, at least out to values of r comparable with the size of the largest eddy. This occurs because as the cloud expands, larger scale eddies become more important in the diffusion process (Batchelor, 1977).

Thus, whilst many developments of "turbulent parameters" have their basis in comparisons with molecular diffusion processes, one must be very wary about this procedure.

Finally, it should be noted that we have thus far ignored the *real* term $\nu\nabla^2\underline{u}$ in all our discussions (see equation (17)). It is normally acceptable to ignore it for scales greater than the so-called "inner scale" (typically a few *mm* in the troposphere, and up to a few tens of metres at higher altitudes), but at smaller scales it *does* become important. It is in fact the term responsible for dissipation of dynamical motion into heating. We will consider this term in more detail shortly.

"Solutions" for turbulence approximations; similitude analysis and structure functions.

In this section, we will concentrate on the so-called Kolmogoroff solutions for description of turbulence. In contrast to the case of gravity wave studies, these are not rigorous solutions per se'. Rather, because of the statistical nature of turbulence, we cannot describe the motions of individual particles, but we describe the statistics of the motions of a collection of particles. This necessitates a different approach to finding "solutions". Before showing how this is done, however, we should first make some comments about the relevance of this theory in modern-day atmospheric science.

A large number of turbulence studies are made and interpreted under the assumption that the turbulence being observed obeys the classical Kolmogoroff theory of inertial- range turbulence (Kolmogoroff, 1941; Tatarski, 1961). Many authors who use this theory comment on its possible inappropriateness, but due to lack of alternative theories are forced to use it. More recently, better models have been developed (e.g. Hill and Clifford, 1978; Driscoll and Kennedy, 1985) but the Kolmogoroff theory is still used a great deal in experimental situations because of its simplicity.

Indeed it would be surprising if the Kolmogoroff theory did rigorously apply throughout the atmosphere, especially in the upper part. For example, parts of the region (stratosphere and lower thermosphere) generally have a very stable temperature profile, so buoyancy forces could well be important in producing anisotropic turbulence in such regions. However, high resolution measurements in the stratosphere (Barat, 1982c) have shown that in any turbulent layer, there is some part of the spatial spectrum which obeys the spectrum predicted by Kolmogoroff, and the measured values of the smallest and largest scales of the inertial range also agree nicely with theory.

A more serious difficulty for the thermospheric and upper mesospheric cases is the separation of the smallest and largest scales, or, equivalently, the value of the Reynold's number. For Kolmogoroff's theory to apply, it is necessary that the Reynold's number be very large (Batchelor, 1953). The Reynold's number for the atmosphere is defined as

$$R_e = \frac{L_B v_L}{\nu} \tag{33}$$

in analogy with flow in pipes, where L_B is a typical "outer scale", and v_L is the velocity associated with scale L_B . In the troposphere, $\nu \sim 10^{-5} m^2 s^{-1}$, $L_B \sim 100m - 1km$, and $v_L \sim 1 - 10ms^{-1}$. Hence $R_e \sim 10^7 - 10^9$, which is satisfactorily large. However, in the lower thermosphere $\nu \sim 1ms^{-1}$, whilst L_B and v_L are similar to the tropospheric values. Hence R_e can be less than 100, and this may not be large enough to maintain an inertial subrange.

Nevertheless, the little experimental data available suggests that the turbulence at least tries to tend to a Kolmogoroff spectral shape (Zimmerman et al., 1971; Booker and Cohen, 1956, Blix et al., 1990; Luebken et al., 1987), at least in conditions of weak to moderate wind shear. For stronger wind shears, other theories (e.g. Tchen, 1954) have occasionally been invoked. Theoretical studies such as those by Hill and Clifford, (1978) and Driscoll and Kennedy, (1985) also show that there is something like an inertial range of turbulence with the classical Kolmogoroff shape, although interesting departures occur near the scales at which viscous energy dissipation occurs.

The upper atmosphere is an especially difficult region to study. It is, for example, too low for in-situ satellite measurements, yet too high for aircraft. Measurements of ε and K must be made by somewhat indirect means, and are therefore difficult. Given the tendency for the atmosphere to at least try and approach an "inertial" spectrum, and given that an experimental bias which will be followed in these lectures, it will be assumed in this article that the Kolmogoroff theory may be approximately applied.

We now embark on a description of some of the important quantities used in turbulence studies.

EDDIES AND SPECTRA.

Turbulence is by definition a rotational motion. We envisage turbulence being generated in regions of large wind shear, or unstable temperature gradient, by the creation of large vertical rolls.

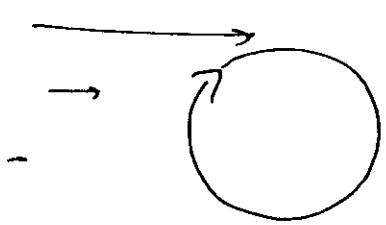

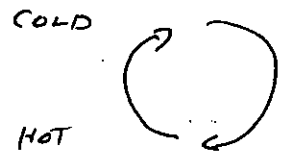

These rotational motions then produce shears in the local air-speed vectors, and thus generate other, smaller "eddies". These in turn produce even smaller ones, and so forth. The circular motion is also distorted as time progresses, and turbulent structure become highly convoluted and distorted, often being very "string-like".

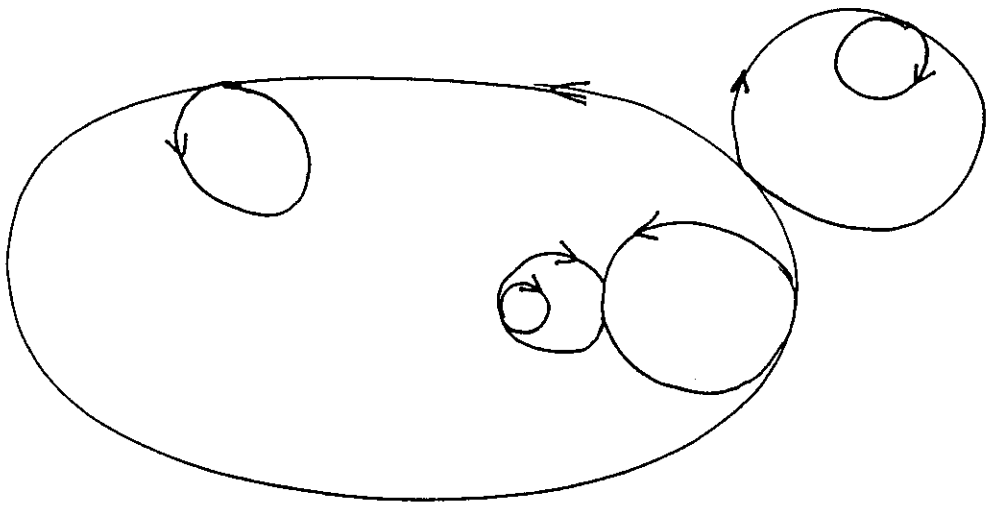

~~FIG~~ Illustration of eddy energy cascade.

The above diagram shows a schematic of this so-called "energy cascade.

However, "eddies" are not a good way to describe turbulence mathematically. For mathematical progress, we turn to a FOURIER REPRESENTATION of the velocity and density distributions.

We consider the fluctuations in a volume of space to be a summation of sinusoidal like oscillations with different "wavelengths" and orientations.

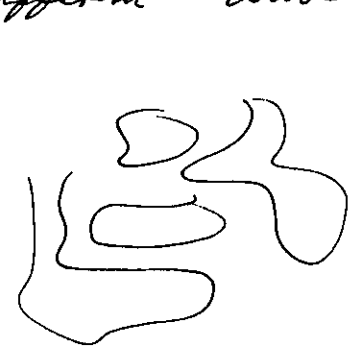

Turbulent field.

≡

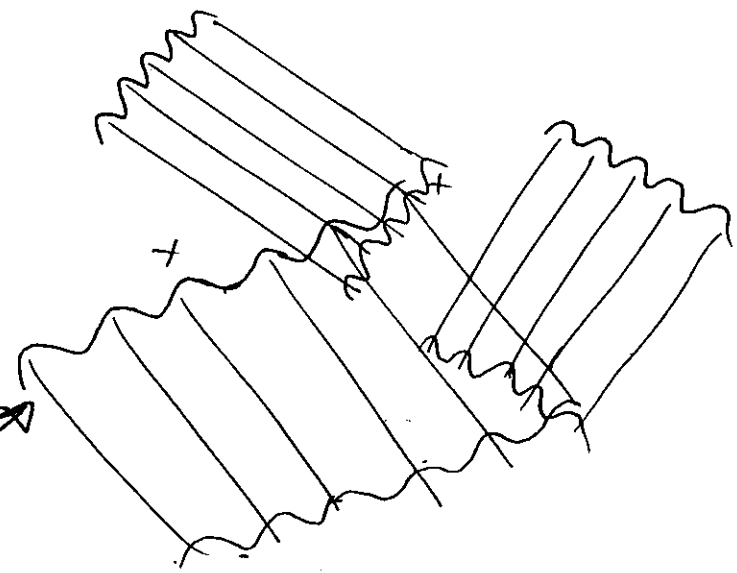

add these oscillations to produce original amplitude distribution.

The distribution of these sinusoidal oscillations is represented as a SPECTRUM. There are various types of spectra, which we will consider in due course.

One simple spectral representation is to add up all the sinusoidal powers at a particular wave-number k, irrespective of the orientation $\underline{k}$, and determine this summation as a value $E(k)$ which represents the energy per unit wave-number. This then produces a graph like that below. There is more energy at larger scales (small k), and less at small scales (large k).

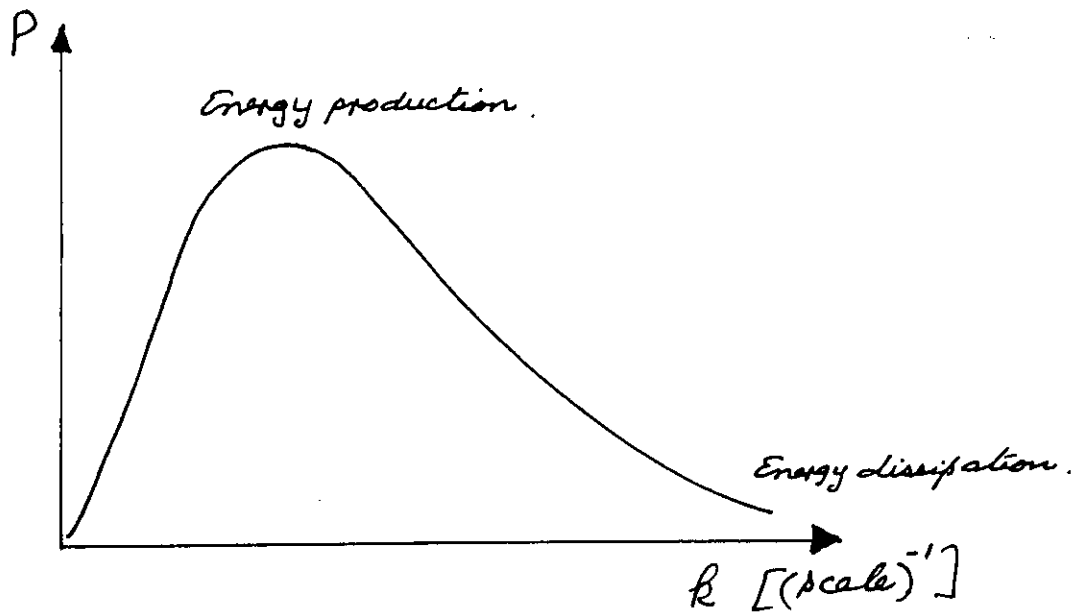

FIG. 3. Crude illustration of energy distribution vs. scale.

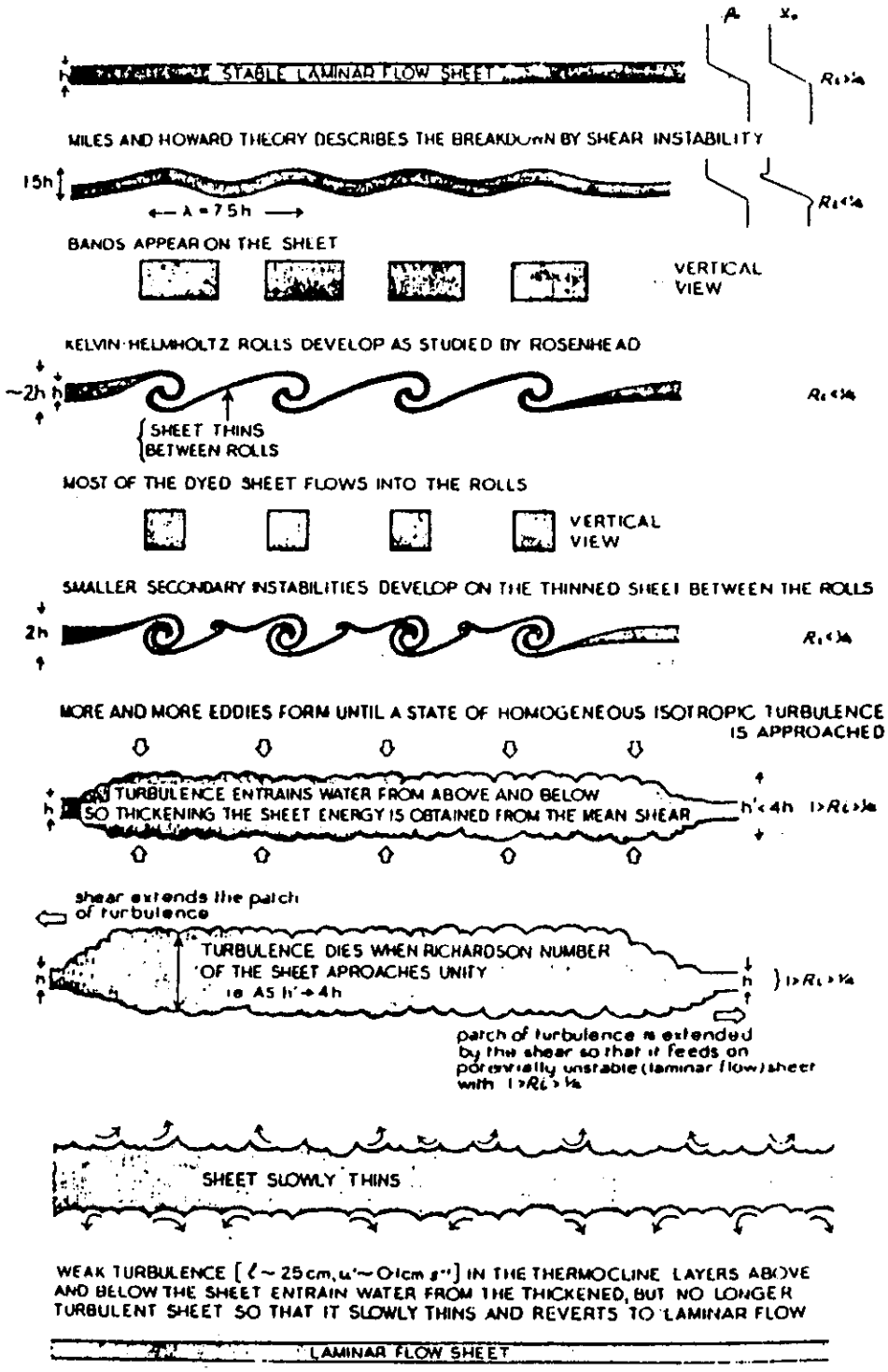

Fig. 4 Illustration of the development of turbulence in stratified flow, via the Kelvin-Helmholtz process. From Woods, 1969.

Derivation of the shape of the turbulence spectrum, and some important scales.

We have established that the energy spectrum contains most energy at smaller wavenumbers (larger scales), and cascades down through the smaller scales.

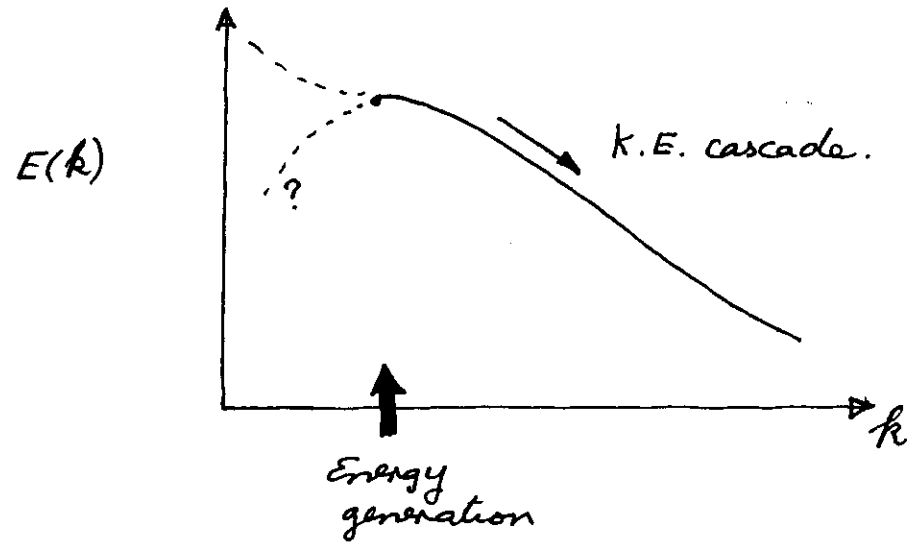

We can determine a spectral shape for $E(k)$ in several ways.

The first is by dimensional analysis on $E(k)$.

We recognize that $E(k)$ has units of

kinetic energy per unit mass per unit wavenumber

i.e.

$$\underbrace{[M]([L][T]^{-1})^2}_{KE \propto mv^2} \div \underbrace{[M]}_{\text{mass}} \div \underbrace{([L]^{-1})}_{\text{wavenumber has units of } (\text{length})^{-1}}.$$

where $[M]$ represents mass, $[L]$ represent dimensions of length, and $[T]$ represent dimensions of time.

$\therefore$ the units of $E(k)$ are $[L]^2 [T]^{-2} \cdot [L]$

or $\boxed{[L]^3 [T^{-2}]}$ (1)

We now assume that in the inertial range, $E(k)$ depends only on the energy dissipation rate, ε, and the wave-number k. (We assume no dependence on direction spatially, no dependence on the strength of the source (except through ε), and no dependence on ν (the kinematic viscosity). We assume a power-law dependence on ε & k

Then $\boxed{E(k) \propto \varepsilon^a k^b}$ (2)

We now attempt to derive values for "a" and "b".

ε represents kinetic energy dissipation per unit mass. It therefore has units

$[M]([L][T^{-1}])^2 \quad [T]^{-1} \quad [M]^{-1}$

$KE \propto mv^2$; ε = KE dissipation PER UNIT TIME ; "per unit mass"

$\therefore \boxed{\varepsilon \text{ has units of } [L]^2 [T]^{-3}}$ (3)

The wavenumber "k", of course, has units of $[L]^{-1}$ (4).

Therefore, (2) tells us that, dimensionally,

$[L]^3 [T]^{-2} \equiv ([L]^2 [T]^{-3})^a \cdot ([L]^{-1})^b$

units of $E(k)$ from (1) ; $[\varepsilon^a]$ from (3) ; k^b from (4)

$$\therefore \quad [L]^3 [T]^{-2} = [L]^{2a-b} [T]^{-3a}$$

Equating powers gives

$$3 = 2a - b$$
$$-2 = -3a.$$

$$\therefore \quad a = \tfrac{2}{3} \quad b = -\tfrac{5}{3}, \text{ giving}$$

$$\boxed{E(k) = C_\varepsilon \, \varepsilon^{\frac{2}{3}} k^{-\frac{5}{3}}} \qquad (5)$$

C_ε ← dimensionless constant

This therefore gives the spectral shape of $E(k)$ in the inertial range.

Alternative derivation, - STRUCTURE FUNCTIONS

One problem with the previous derivation is that we really have not been too careful about defining what we mean by $E(k)$. There are different types of energy spectra, and we have only referred to $E(k)$ as an "energy spectrum". This is therefore somewhat incomplete. We will see more about energy spectra later.

STRUCTURE FUNCTION APPROACH

A much better approach is to follow that of Kolmogoroff, and as espoused by Tatarskii, (1961). The basic ideas of isotropy and homogeneity are still maintained, but the roots of the equations of turbulence are much more clearly defined.

Kolmogoroff theory starts by defining the *structure function* of a turbulent medium. This a function of the form

$$D = \overline{| u(x+r) - u(x) |^2}. \tag{36}$$

Now notice that I have deliberately been a little unclear here, by not clearly indicating whether u is a vector or a wind component. This is because there are in fact many different *types* of structure function, which I will now describe in more detail.

We begin by imagining a large number of turbulence probes distributed through the fluid, which can measure all components of the fluid motion at any time. Then the *longitudinal structure function* is defined as

$$D_{\|} = \overline{| u_{\|}(\underline{x}+\underline{r}) - u_{\|}(\underline{x}) |^2}. \tag{37}$$

where $u_{\|}$ is the *component* of the fluid flow vector at each point in the direction parallel to $\underline{r}$ i.e. in the direction parallel to the line joining $\underline{x}$ and $\underline{x}+\underline{r}$.

We may also define a *tangential structure function* as

$$D_{\perp} = \overline{| u_{\perp}(\underline{x}+\underline{r}) - u_{\perp}(\underline{x}) |^2}. \tag{38}$$

where $u_{\perp}$ is the *component* of the fluid flow vector at each point in the direction perpendicular to $\underline{r}$ i.e. in the direction parallel to the line joining $\underline{x}$ and $\underline{x}+\underline{r}$.

There is also a *total* structure function

$$D_{tot} = \overline{| \underline{u}(\underline{x}+\underline{r}) - \underline{u}(\underline{x}) |^2}. \tag{39}$$

Note that this involves a *vector difference.*

All of these structure functions are important.

Kolmogoroff theory then applies our arguments about isotropy and homogeneity to recognize that each of these functions D are independent of direction, and dependent only on separation r and the energy dissipation rate ε. Thus if we take the longitudinal structure function as an example, we expect

$$D_{\parallel} = C\varepsilon^s r^t \tag{40}$$

where C is a dimensionless constant. Dimensional analysis then gives that $s = 2/3$, t = +2/3. Note that this expression only applies in the *inertial range* of the spectrum.

Careful experiments in the boundary layer give a value for C of about 2.0. This expression is also written as

$$D_{\parallel} = C_v^2 r^{2/3} \tag{41}$$

where $C_v^2 = C\varepsilon^{2/3}$.

Similar expressions exist for the other structure functions. For example, the tangential structure function is given by

$$D_{\perp} = \frac{4}{3} C_v^2 r^{2/3}. \tag{42}$$

Note especially the factor $\frac{4}{3}$. The reasons for this are subtle, but arise form the fact that when one forms a longitudinal structure function, part of the turbulent motions are "lost" to the mean, so subtract out to zero.

The "total" structure function in the inertial range is

$$D_{tot} = \frac{11}{3} C_v^2 r^{2/3}. \tag{43}$$

Kolmogoroff (and Tatarskii, 1961) then go on to show how these structure functions may be related to relevant spectra, of which there are several types. We will see these in due course. *It is an important requirement of any student of turbulence theory to recognize that there are several different forms of spectra used in turbulence theory, and to be able to properly employ them.*

4. Relation between structure functions and spectra

The structure function relates very simply to the autocorrelation function, viz

$$D = |\underline{u}(\underline{r}) - \underline{u}(\underline{r}+\underline{\xi})|^2$$

$$= \overline{|\underline{u}(\underline{r})|^2} + \overline{|\underline{u}(\underline{r}+\underline{\xi})|^2} - 2\,\overline{\underline{u}(\underline{r})\,\underline{u}(\underline{r}+\underline{\xi})}$$

Assuming that $\overline{|\underline{u}(\underline{r})|^2} = \overline{|\underline{u}(\underline{r}+\underline{\xi})|^2}$,

which is true provided the medium is statistically homogeneous, we have

$$\underline{D}(\underline{\xi}) = 2\rho(\underline{0}) - 2\rho(\underline{r})$$

where $\rho(\underline{\xi}) = \overline{\underline{u}(\underline{r})\,\underline{u}(\underline{r}+\underline{\xi})}$ is the autocorrelation function.

$$\therefore \quad D(\underline{\xi}) = \tfrac{1}{2}\left(\rho(\underline{0}) - \rho(\underline{\xi})\right), \qquad (9)$$

showing that the autocorrelation function relates very simply to the structure function.

The spectrum can then be easily derived as a FOURIER TRANSFORM of the autocorrelation function. I will leave you to verify that this returns you to equation (5)

(or see Tatarskii if you have troubles).

Thus we have derived the shape of the turbulence spectrum, and structure functions, in the inertial range.

Scales

We now ask the question: "what defines the "beginning" and "end" of the inertial range of the spectr

Let us begin with the "end"? At some stage, the turbulent region must deposit its energy as heat (or it would never die out!). This happens at the smallest scales, where the windshear are in fact largest.

Let us look for a typical scale ℓ (which we will call "η") at which the energy transfer TO that scale from larger scales approximately matches the energy it loses as heat. This scale will give us some idea about the "end" of the inertial range.

In order to do this, we need to first develop a term which describes heat loss.

Recall that the Navier Stokes equation gives an expression something like

$$\frac{D\underline{u}}{Dt} = \underbrace{-\frac{1}{\rho}\nabla p + \ldots}_{\text{Forcing terms: pressure, Coriolis, Joule heating, etc.}} + \underbrace{\nu \nabla^2 \underline{u}}_{\text{viscous drag.}} \quad (10)$$

This really just says

$$\underline{a} = \frac{\underline{F}}{m}$$

where $\underline{a}$ = acceleration, $\underline{F}$ = force, m = mass (Newton's 2nd law

The term $\nu \nabla^2 u$ is a "retarding" force per unit mass.
Now we want a heat loss.

Recall that

Work = Force × distance

So that work (or energy) gained or lost per unit time is

$$W/t \sim F \times \text{speed}.$$

Thus if $\nu \nabla^2 u$ represents a retarding force per unit mass,

then $\boxed{(\nu \nabla^2 \underline{u}) \times \underline{u}}$ represents energy loss per unit mass and per unit time – ie heating.

We may therefore write the following:

Energy gained at our scale η is $\sim \mathcal{E} \sim \frac{v_\eta^2}{t_\eta}$ (per unit mass per unit time)

But $v_\eta \sim \frac{\eta}{t_\eta} \Rightarrow t_\eta \sim \eta / v_\eta$

$$\mathcal{E} \sim v_\eta^2 \cdot (v_\eta/\eta) \sim v_\eta^3/\eta$$

$$\therefore \boxed{\dot{N}_\eta \sim (\mathcal{E}\eta)^{1/3}} \qquad (12)$$

Now the energy lost per unit mass per unit time in the so-called "viscous range" (ie the "end" of the inertial range) is

$$\mathcal{E}_H \sim \nu (\nabla^2 u)\, u \qquad (13)$$

But $\nabla^2 u \sim \left(\frac{u_1'}{\ell} - \frac{u_2'}{\ell}\right)/\ell \sim u''/\ell^2.$

We ascribe u'' to v_η, so that

We also scale u to v_η. Thus

$$\boxed{\mathcal{E}_H \sim \nu \cdot \frac{v_\eta^2}{\eta^2} \cdot v_\eta} \qquad (14)$$

(Note that this is really only a dimensional-type analysis, so we don't worry about distinguishing u and u' or u'' too much).

We now recognize that we are searching for a scale η at which $\mathcal{E} = \mathcal{E}_H$ (heat gained = heat lost)
So we can replace $\mathcal{E}_H$ in (14) by $\mathcal{E}$. We also use v_η from (12).

Hence (14) becomes:-

$$\mathcal{E} \sim \frac{\nu}{\eta^2} \cdot \left((\mathcal{E}\eta)^{\frac{1}{3}}\right)^2$$

or $\mathcal{E} \sim \nu \cdot \mathcal{E}^{\frac{2}{3}} \eta^{-\frac{4}{3}}$

Hence $\mathcal{E}^{\frac{1}{3}} \sim \nu \eta^{-\frac{4}{3}}$

or $\boxed{\eta \sim \left(\frac{\nu^3}{\mathcal{E}}\right)^{\frac{1}{4}}} \qquad (15)$.

This is called the KOLMOGOROFF MICROSCALE.

It isn't really the "end" of the inertial range - it is a scale deep into the VISCOUS range. But it gives us a "feel" for where the inertial range ends, and is a useful scaling term.

The actual "end" of the inertial range is at a scale called the "inner scale", l_0.

The value of l_0 is proportional to η.

$$\boxed{l_0 \sim \gamma\eta} \qquad (14)$$

where γ is a value of $\sim 7-15$, depending on various factors relating to the type of spectrum under investigation.

For more detail about how l_0 is defined, see Tatarskii. (1961, 1971)

Hill & Clifford (1978) gives $\gamma = 7.2$ for density fluctuat^{ns}
For velocity fluctuations, $l_0 \sim 12-13$.

What about the "large-scale" end of the inertial range?

This can be derived fairly easily if you assume that the inertial range motions are limited to time scales less than, or of the order of, the Brunt-Vaisala frequency.

Then, (as in equation (12) & thereabouts) we write

$$\varepsilon \sim v_L^2 / t_L \;?$$

But $v_L \sim L/t \sim L_B \omega_B$

where L_B is the largest scale in the inertial range and ω_B is the associated inverse time scale (Brunt Vaisala angular frequency).

$$\therefore \quad \varepsilon \sim (L_B \cdot \omega_B)^2 \cdot \left(\frac{1}{\omega_B}\right)$$

$$\text{or} \quad \boxed{L_B \sim \varepsilon^{\frac{1}{2}} \omega_B^{-\frac{3}{2}}} \qquad (15)$$

More careful analysis gives

$$\boxed{L_B \sim .10\, \varepsilon^{\frac{1}{2}} \omega_R^{-\frac{3}{2}}} \quad (16)$$

($\frac{2\pi}{0.62}$ is the constant according to Weinstock)

Thus we have learnt a lot about our spectra

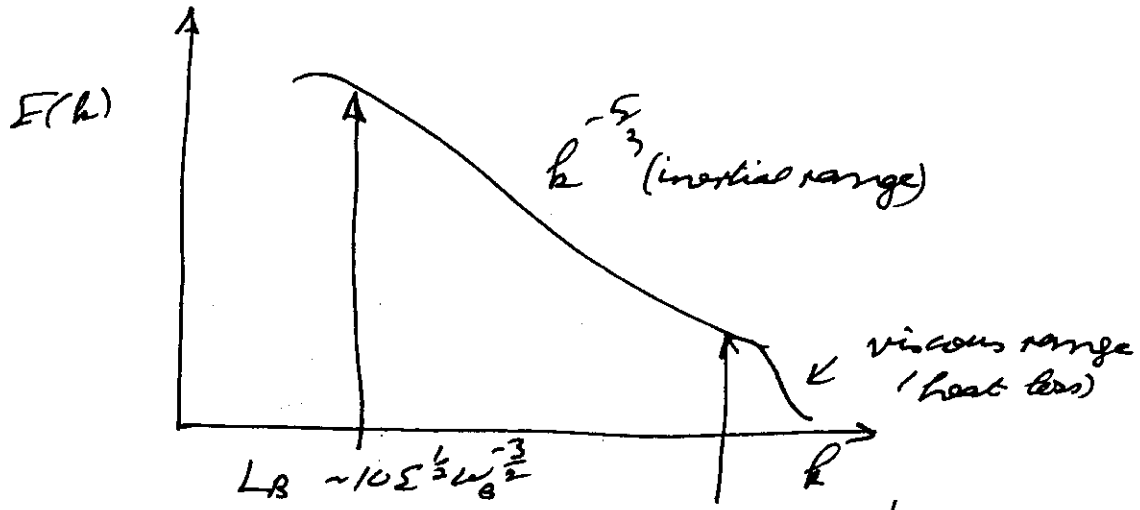

$$l_0 \sim 10\left(\frac{\nu^3}{\varepsilon}\right)^{\frac{1}{4}}$$

$\eta = \left(\frac{\nu^3}{\varepsilon}\right)^{\frac{1}{4}}$ = Kolmogoroff microscale

TYPICAL SCALES IN THE ATMOSPHERE.

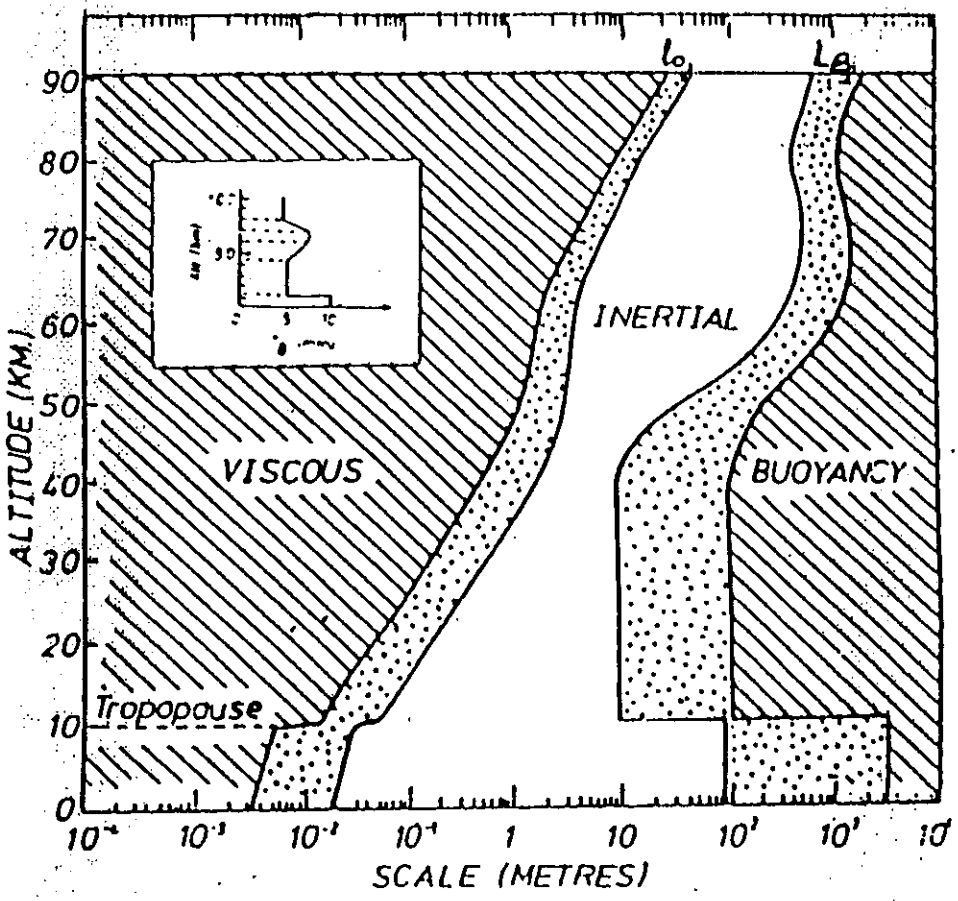

It must be emphasized again that this is the total energy spectrum. There are other types of energy spectra, and there are other types of spectra too! You need to be continually aware of this.

Indeed, there is one spectral type which is especially important to radar studies - and this is the (potential) refractive index spectrum. This is what defines radar backscatter.

Some Observational notes.

Before we progress further, it is worthwhile to look at some different instruments used to measure turbulence, because this will help us understand the reasons for the different spectra which we will introduce.

It should also be recognized that turbulence tends to occur ~~spasm~~ in layers, and short "bursts" in the upper atmosphere. This is important to recognize - some examples occur below.

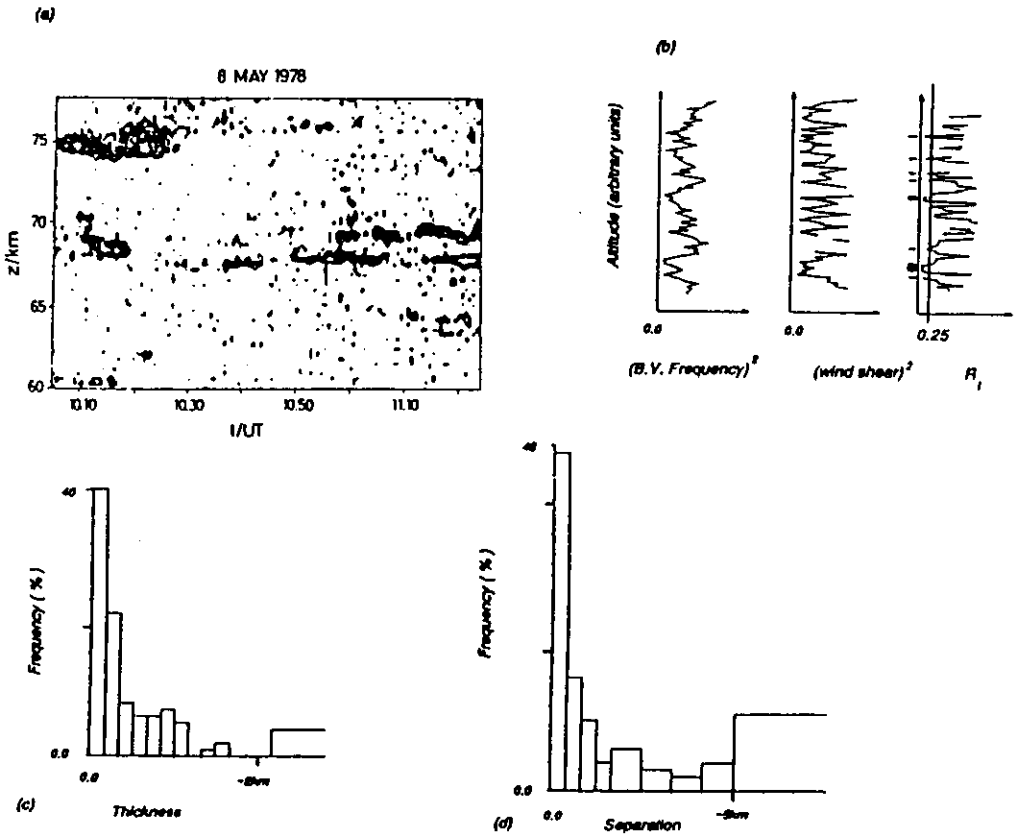

Fig. 8 (a) Typical plot of turbulent layering observed with a VHF radar. Note the intermittency both in time and space (from CZECHOWSKY *et al.*, 1979). (b) Profiles of Brunt-Vaisala frequency squared, wind shear squared and Richardson number for an ensemble of gravity waves in the atmosphere (adapted from simulations using oceanic internal gravity waves performed by DESAUBIES and SMITH, 1982). Absolute scales are different for the atmosphere and the oceans, so scales are not shown for the first two graphs). (c) Histogram of typical layer thickness distributions, again adapted from DESAUBIES and SMITH (1982). Scales are not shown precisely because they are different for the oceanic and atmospheric cases, but approximate scales are shown based on experimental experience. (d) Distribution of layer separations, again from DESAUBIES and SMITH (1982). Similar comments apply with respect to scales as for (c).

The following pages show some of the different instruments used for studies of turbulence

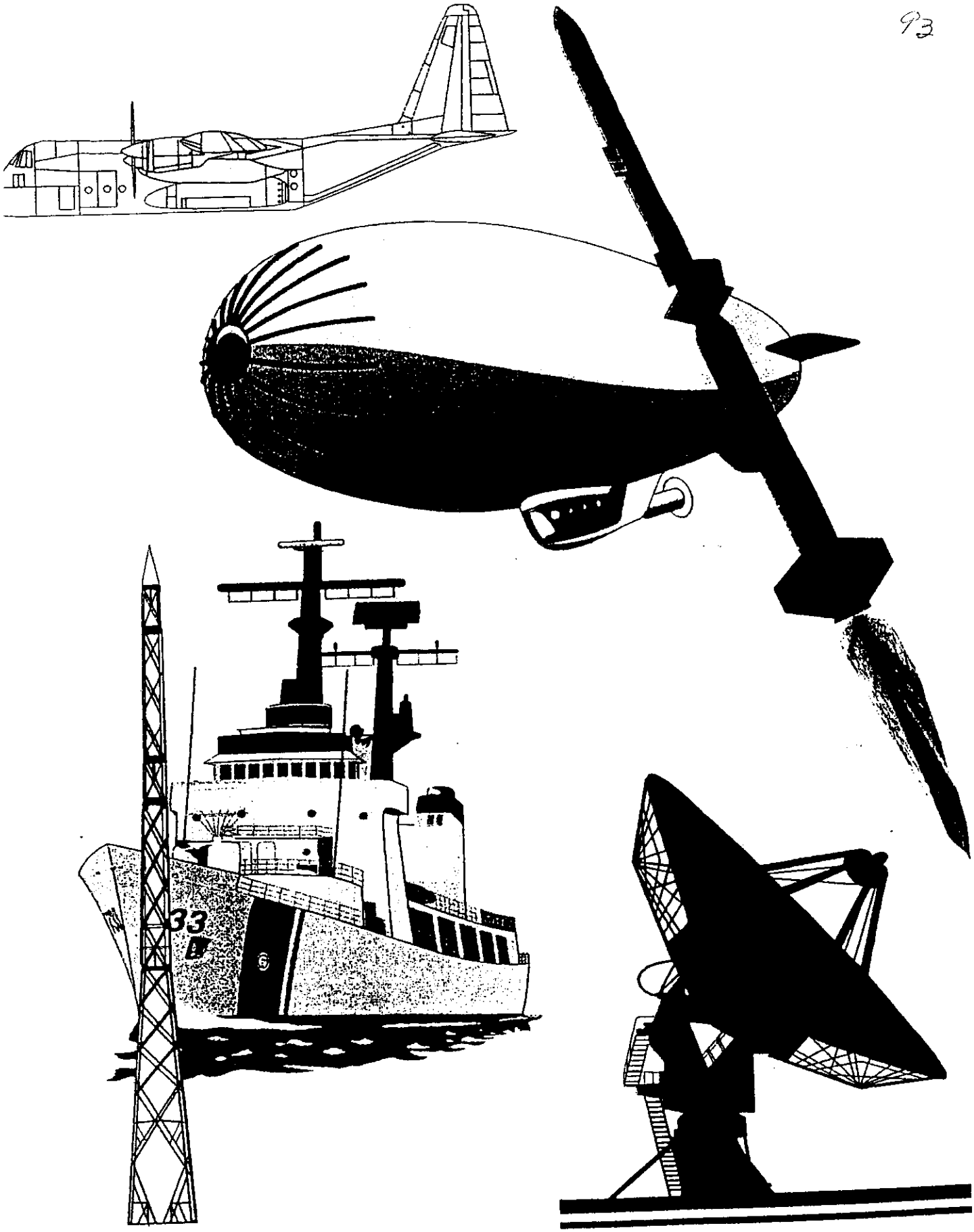
33

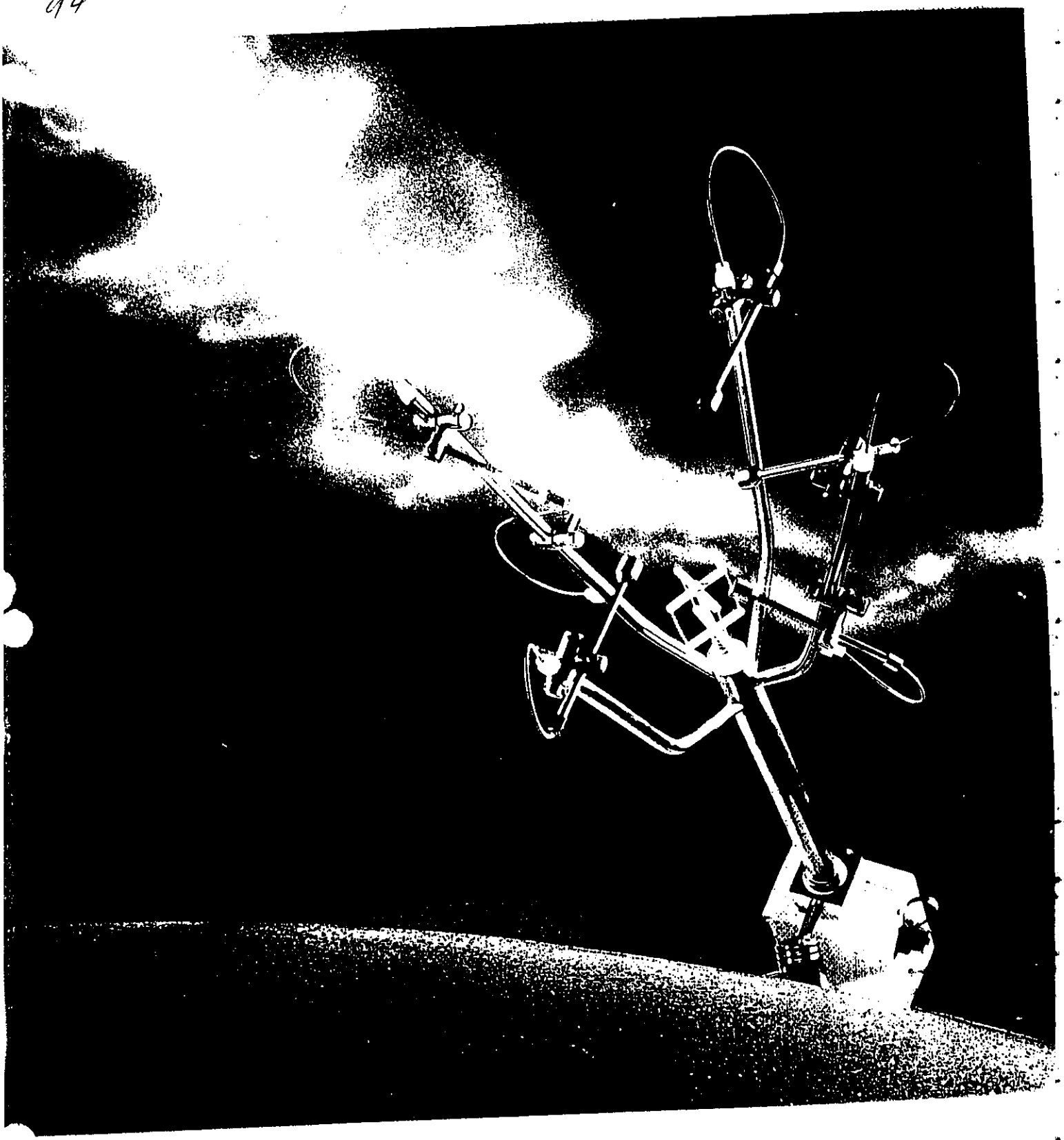

IONIC ANEMOMETER

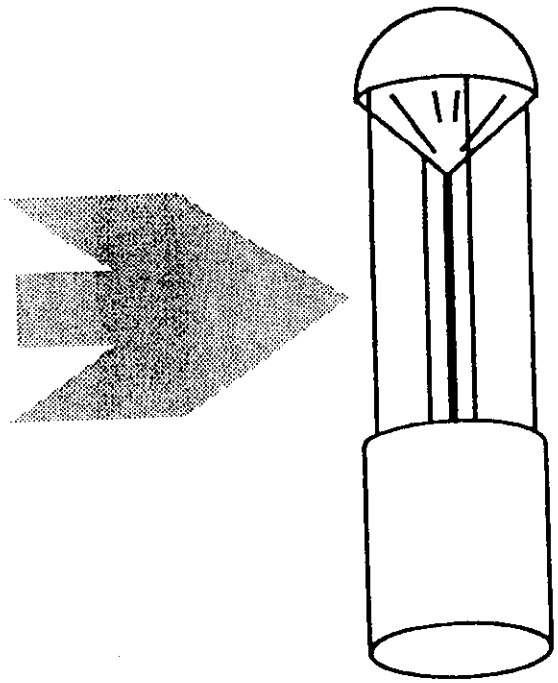

Side View

Top View

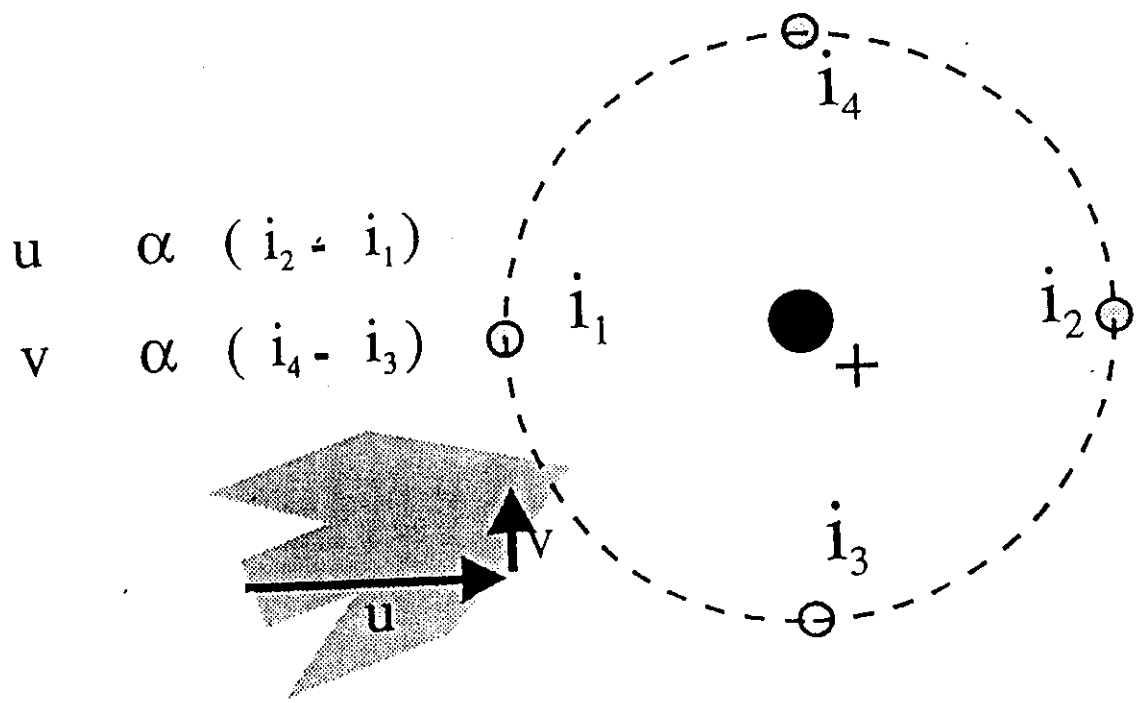

$u \quad \alpha \quad (i_2 - i_1)$

$v \quad \alpha \quad (i_4 - i_3)$

96

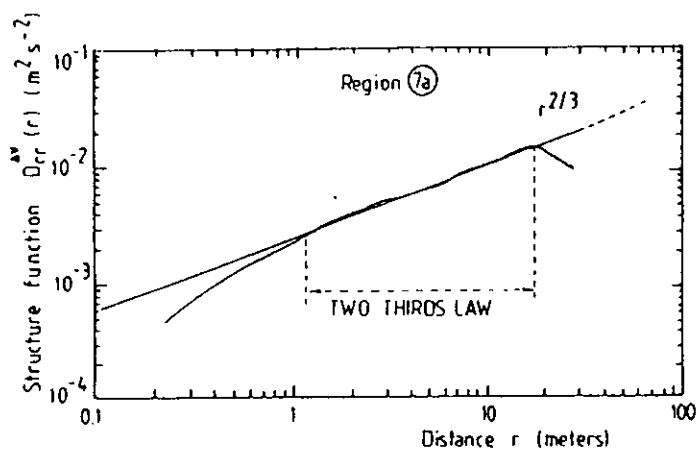
Region (7a)
$r^{2/3}$
TWO THIRDS LAW
Structure function $D^{LL}_{rr}(r)$ $(m^2 s^{-2})$
10^{-1}
10^{-2}
10^{-3}
10^{-4}
0.1
1
10
100
Distance r (meters)

(a)

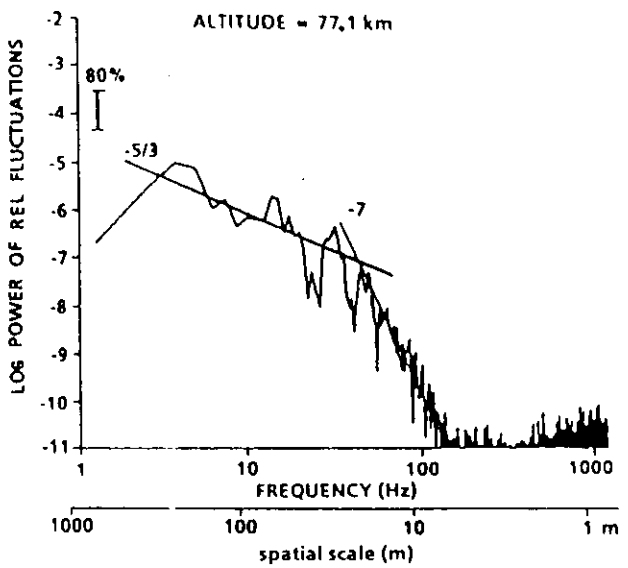
ALTITUDE = 77,1 km
80%
-5/3
-7
LOG POWER OF REL FLUCTUATIONS
-2
-3
-4
-5
-6
-7
-8
-9
-10
-11
1
10
100
1000
FREQUENCY (Hz)
1000
100
10
1 m
spatial scale (m)

(b)

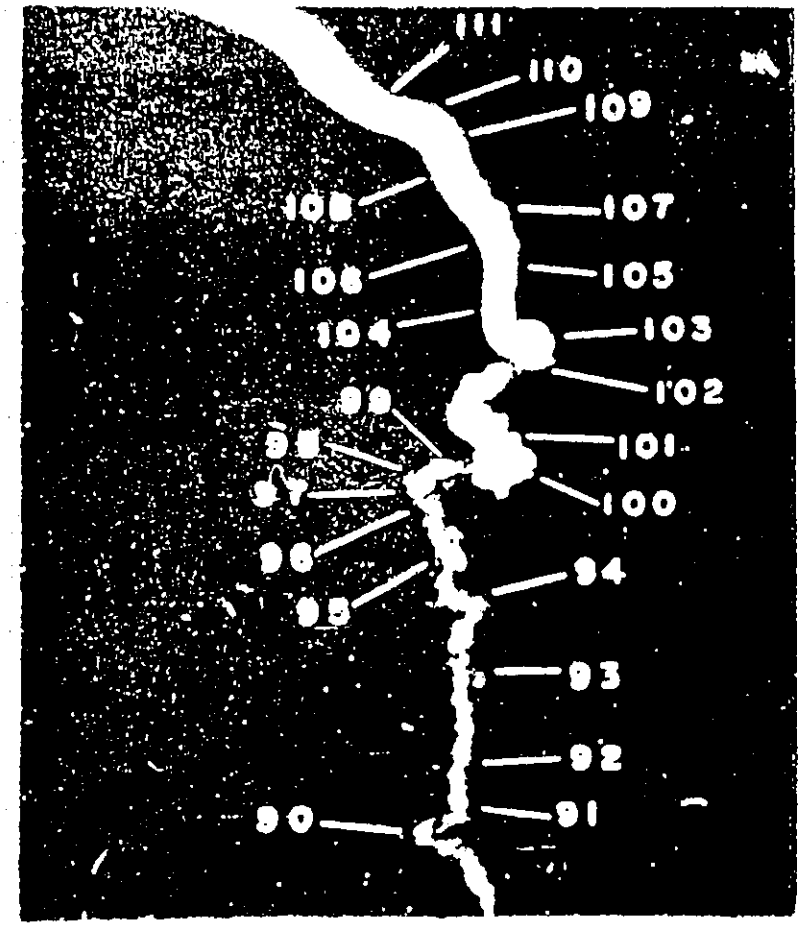
111
110
109
107
105
103
102
101
100
94
93
92
91
90

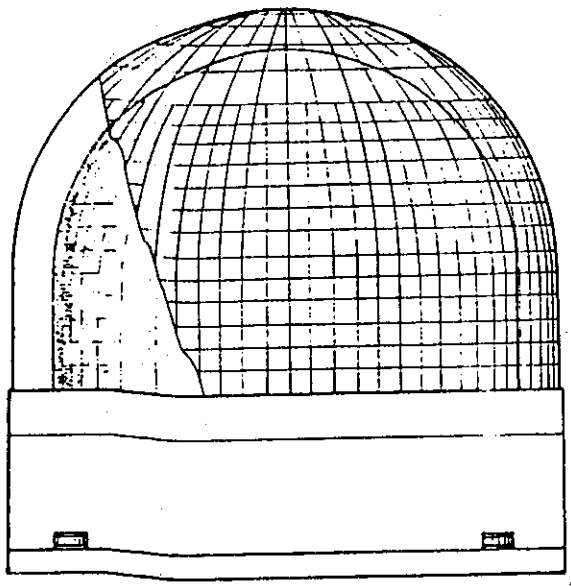

Fig. 2. Schematic view of the ion probe flown during the MAP WINE campaign 1983/1984.

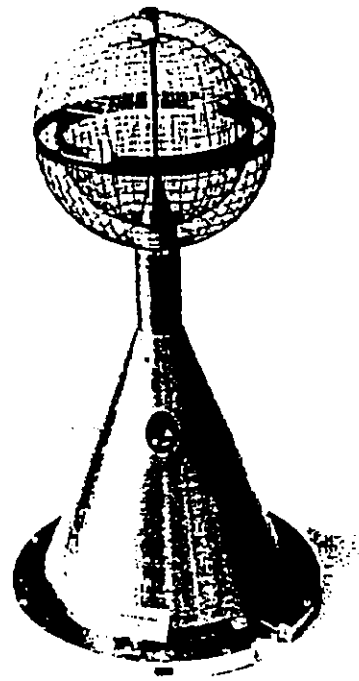

Fig. 3. The double-gridded ion probe flown during the MAC Epsilon campaign 1987

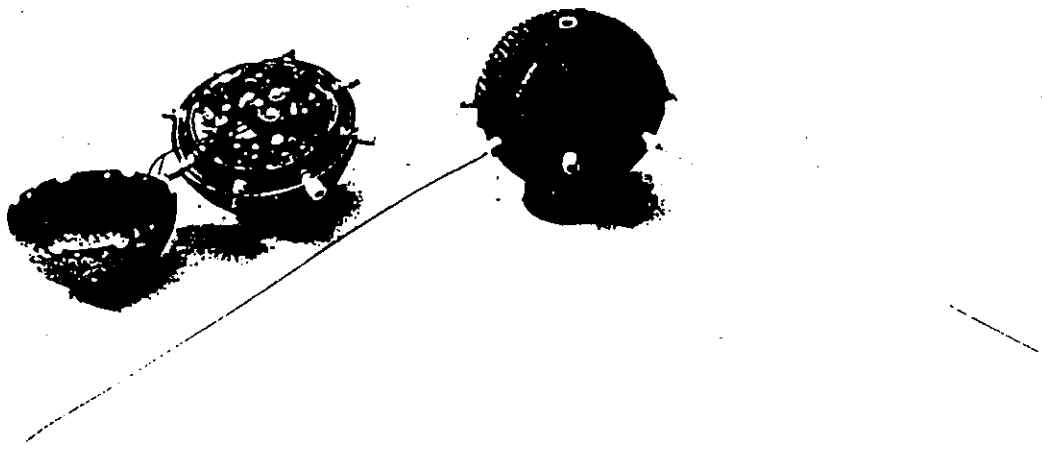

Fig. 1. The free-flying ion probe (dropsonde), disassembled and fully assembled, flown during the EBC 1980.

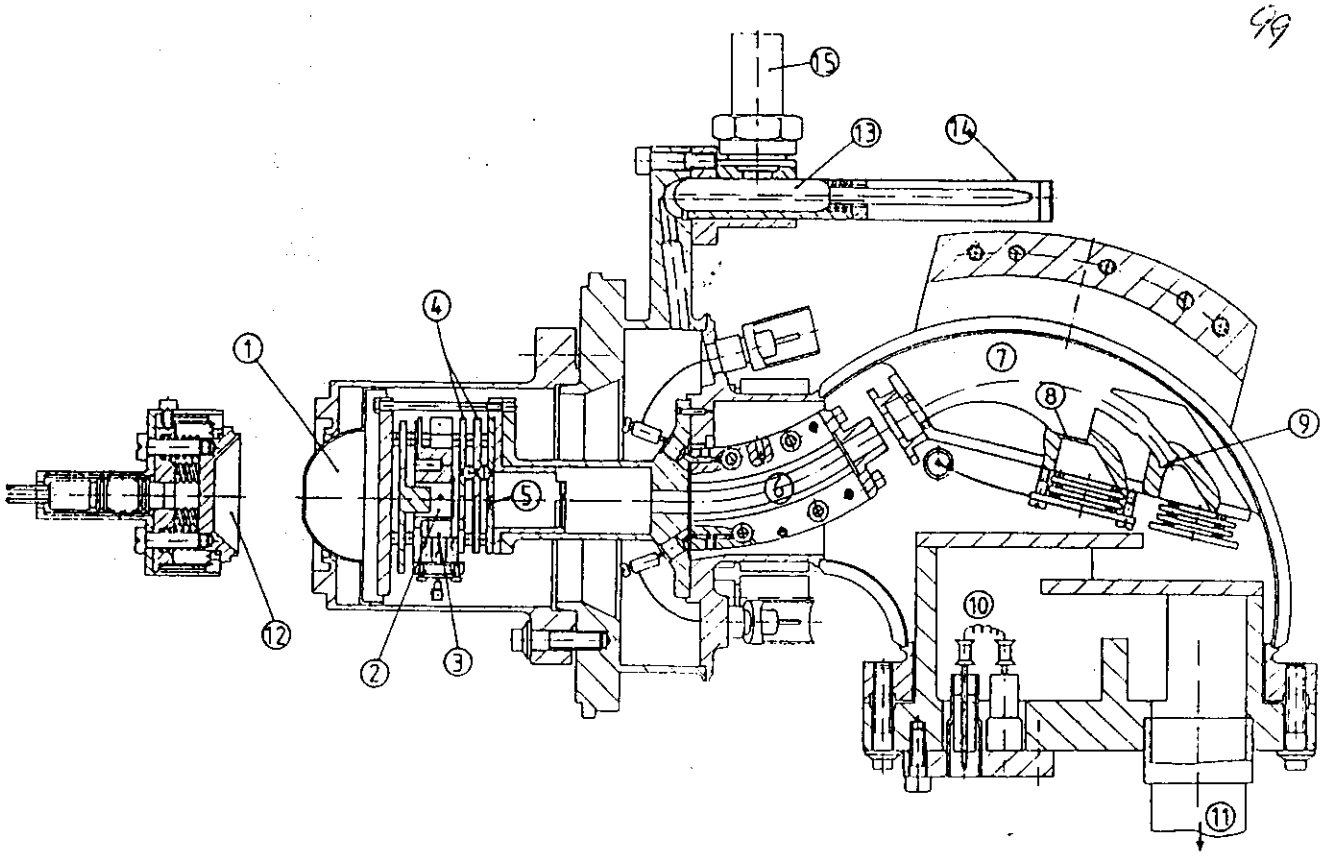

Fig. 3. Cross section of the BUGATTI mass spectrometer. For a detailed description and the number references, see section 5.1.

We now can look at turbulent spectra in more detail.

6.5.2 Turbulence spectra

Proper treatment of any turbulence study in the atmosphere requires a detailed understanding of the many types of spectra which are used in turbulence studies. This means we need to relate structure functions, (as introduced earlier) to these spectra. We will begin by looking at velocity spectra.

6.5.2.1 Velocity Spectra

As an intermediate step, then, we first recognize that the structure function is closely related to the autocovariance function. Consider for example the parallel structure function. Then we may write

$$D_{\|} = \overline{\mid u_{\|}(\underline{x}+\underline{r}) - u_{\|}(\underline{x}) \mid^2}. \tag{59}$$

Let us suppose that for simplicity we consider $\underline{x}$ and $\underline{x}+\underline{r}$ to be both on the x axis. Then $\underline{u}_{\|}$ is just the x component of $\underline{u}$, or simply u. If we now expand this out, we obtain

$$D_{\|} = \overline{u^2(x+r)} + \overline{u^2(x)} - 2\overline{u(x)u(x+r)}. \tag{60}$$

If the turbulence is homogeneous, the averages shown in the first two terms are identical, and can be written as $\overline{u^2}$. Then we may write

$$D_{\|} = 2\overline{u^2}\left[1 - \frac{\overline{u(x)u(x+r)}}{\overline{u^2}}\right] \tag{61}$$

The last term in the brackets is simply the autocorrelation function $\rho_{\|}(r)$, so we may write

$$D_{\|} = 2\overline{u^2}\left[1 - \rho_{\|}(r)\right]. \tag{62}$$

Alternatively we may write

$$D_{\|} = 2\left[R_{\|}(0) - R_{\|}(r)\right] \tag{63}$$

where $R_{\|}(r)$ is the spatial autocovariance function.

Thus the structure function relates simply to the autocovariance function. But of course, as anyone who has done a course on Fourier Methods will know, the autocovariance function is simply related to a spectrum $\phi(k)$. In this case k is the wavenumber corresponding to spatial scales along the x axis. R and ϕ are related as follows:

$$R(r) = \int_{-\infty}^{\infty} e^{ikr}\phi(k)dk \tag{64}$$

and

$$\phi(k) = \frac{1}{2\pi}\int_{-\infty}^{\infty} e^{-ikr} R(r) dr \tag{65}$$

There are in fact a plethora of autocovariance functions and related spectra. I will simply list some of them below: a full derivation of all of them is beyond the scope of this course. The interested reader is referred to *Batchelor, 1953* for a more thorough discourse on these spectra.

First, consider a line along the x axis. Suppose we cross-correlate the velocity component u_k with the component u_j; for example, if $k = 1$, and $j = 2$, we are cross-correlating the x-component of the velocity with the v-component. Then the autocovariance function is called $R_{kj}(r_1, 0, 0)$, and the relevant spectrum is

$$\Theta_{kj}(k_1) = \frac{1}{2\pi}\int_{-\infty}^{\infty} e^{-ikr_1} R_{kj}(r_1) dr_1 \tag{66}$$

(Note: do not confuse this Θ with our use of Θ for potential temperature earlier in these notes). Thus we see we already have 9 different spectra (though of course some are identical). Note that R_{11} corresponds to the parallel structure function, whilst R_{22} and R_{33} both correspond to the transverse structure function.

As a point of (important) interest, if $D_{\|}$ is proportional to $\varepsilon^{2/3} r^{2/3}$, then Θ_{11} is proportional to $\varepsilon^{2/3} k^{-5/3}$.

We may go further. If we define

$$D_{33}(\underline{r}) = \overline{|\, \mathrm{w}(\underline{x} + \underline{r}) - \mathrm{w}(\underline{x}) \,|^2} \tag{67}$$

then we recognize that this is a *three-dimensional* structure function averaged over *all* directions, using only the velocity component along the z axis. This has an associated autocovariance function $R_{33}(\underline{r})$ and an associated spectrum $\Phi_{33}(\underline{k})$. In general,

$$\Phi_{kj}(\underline{k}) = \frac{1}{8\pi^3}\int_{-\infty}^{\infty}\int_{-\infty}^{\infty}\int_{-\infty}^{\infty} e^{-i\underline{k}\cdot\underline{r}} R_{kj}(\underline{r}) d\underline{r}. \tag{68}$$

There are obviously a large number of these types of spectra too!

Now this function forms a spectral density function of (k_1, k_2, k_3) i.e. all of k-space. If turbulence is isotropic, then this function will be spherically symmetric, and in this case it is sometimes of interest to know not Φ, but rather the integrated spectral density over a shell of radius k and thickness dk. (Note k is a scalar, $\underline{k}$ is a vector, and $k = |\, \underline{k} \,|$.) This is illustrated in the following diagram.

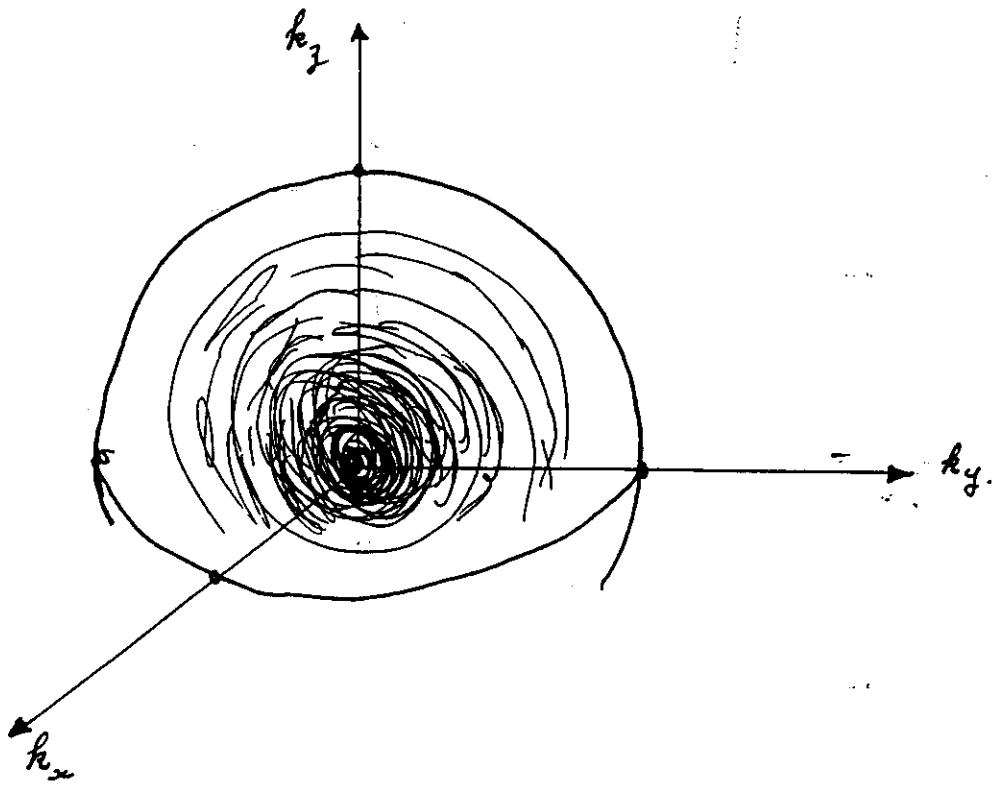

FIG. 10a

3D spectral function. High density towards centre, falling off towards edges.

Then this new function is

$$\Psi_{kj}(k) = \oint \Phi_{kj}(\underline{k})k^2 d\Omega_k \tag{69}$$

($d\Omega_k$ = solid angle in k-space)

Now of course this corresponds to the spectrum related to the correlation between velocity components u_k and u_j. Sometimes we want the *total* energy associated with the turbulence at scale k, and to get this we need to sum Ψ_{11} and Ψ_{22} and Ψ_{33}. In fact, in order to have a proper measure of the *kinetic energy* per unit mass, we sum and divide by 2 (c.f. $KE = \frac{1}{2}mv^2$.)

Thus we define a new function

$$E(k) = \frac{1}{2}(\Psi_{11} + \Psi_{22} + \Psi_{133}) \tag{70}$$

This is the *total energy* spectrum. It is the function which people implicitly assume when they derive equations like (34), but unfortunately they often really do not *what* function they are doing the dimensional analysis for - they just know it is a "spectrum".

Note that if we integrate over all scales, we see that

$$\int E(k)dk = \frac{1}{2}\overline{u_{tot}^2} \tag{71}$$

i.e. the total kinetic energy per unit mass.

[Special note: The function I have called $E(k)$ is *not* the same as that used by Tatarskii; my definition follows that of Batchelor. Tatarskii's $E(k)$ is related to ours as $E_{tatarskii} = E/(4\pi k^2)$.]

The function $E(k)$ is somewhat unique in its definition, in that the factor $\frac{1}{2}$ is introduced. If, for example, we integrate over Φ_{11}, we do not obtain $\frac{1}{2}\overline{u_1^2}$, but rather $\overline{u_1^2}$. We will need to recognize this later.

i.e.

$$\int \Phi_{11}(k)dk = \overline{u_1^2} \quad \text{(no factor of } \tfrac{1}{2}\text{)} \tag{72}$$

6.5.2.2 Inter-relations between turbulence spectra

In the previous section we introduced several different types of spectra. Clearly once we have our assumed Kolmogoroff structure function, $D_{ll} \propto \varepsilon^{2/3} r^{2/3}$, it is a trivial matter to convert to an appropriate spectrum. Once we know the inter-relationship between the different types of spectra, we can then obtain forms for *all* spectra. Such derivations have been carried out by *Tataskii, 1961, 1971)* and *Batchelor, (1953)*. In this short lecture series, we will not repeat these derivations: we will simply repeat the main results.

One of the first things to notice is the difference between the Θ and the Φ spectra. For example, suppose we compare $\Theta_{11}(k_1)$ and $\Phi_{11}(k_1,0,0)$. Are these in fact the same thing? Afterall, they both involve correlating longitudinal components along the x axis, and both involve a k_1 vector. But in fact they are *not* the same. The first involves fluctuations due to *all* scales which are measured as one moves along the x axis, whilst the second involves fluctuations due *only* to scales which are orientated with wave vectors parallel to the x axis.

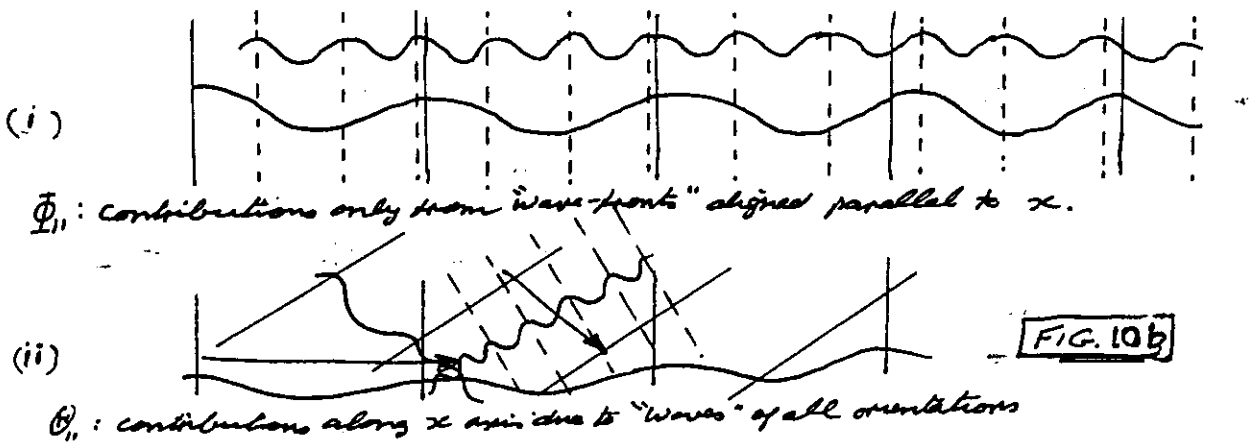

FIG. 10b

In fact the two functions are related by

$$\Theta_{kj}(k_1) = \int_{-\infty}^{\infty}\int_{-\infty}^{\infty} \Phi_{kj}(k_1, k_2, k_3)dk_1dk_2 \tag{73}$$

It is very important to recognize differences of this type.

The rest of the major relations between spectra will be listed below without proof.

$$\Phi_{kj}(\underline{k}) = \frac{E(k)}{4\pi k^4}\cdot(k^2\delta_{kj} - k_k k_j) \tag{74}$$

For isotropic turbulence, this implies

$$\Phi_{ii}(\underline{k}) = \frac{2E(k)}{4\pi k^2} \tag{75}$$

where we have used the summation convention the $\Phi_{ii} = \Phi_{11} + \Phi_{22} + \Phi_{33}$.

We can also show that

$$E(k) = k^3\frac{d}{dk}\left[\frac{1}{k}\frac{d}{dk}\Theta_{11}(K)\right] \tag{76}$$

In the special case that Θ_{11} is proportional to $k^{-5/3}$, then $E(k)$ is also proportional to $k^{-5/3}$ (Kolmogoroff turbulence). Therefore people often confuse these two spectra - you should be sure to recognize that they are in fact different!

For inertial range, homogeneous, **Kolmogoroff**-style turbulence, we have the following relations.

$$D_{\parallel} = C_v^2 r^{2/3} \tag{77}$$

where $C_v^2 = C\varepsilon^{2/3}$, and C is close to 2.0.

$$D_{\perp} = \frac{4}{3} C_v^2 r^{2/3} \tag{78}$$

Then in the spectral domain we have

$$E(k) = \alpha \varepsilon^{2/3} k^{-5/3} \tag{79}$$

where $\alpha = \frac{11\Gamma(\frac{8}{3})\sin(\frac{\pi}{3})C}{6\pi^2} = 0.76655C$.

Furthermore

$$\frac{E(k)}{4\pi k^2} = A\varepsilon^{2/3} k^{-11/3} \tag{80}$$

where $A = \alpha/\ 4\pi = \frac{11\Gamma(\frac{8}{3})\sin(\frac{\pi}{3})C}{24\pi^2}$, or $A = 0.061C$.

We should also recall the relation (74) viz.

$$\Phi_{kj}(\underline{k}) = \frac{E(k)}{4\pi k^4} \cdot (k^2 \delta_{kj} - k_k k_j) \tag{81}$$

Then we can show that

$$\Theta_{11} = \alpha'_{11} \varepsilon^{2/3} k^{-5/3} \tag{82}$$

where $\alpha'_{11} = \frac{9}{55}\alpha = 0.1244C$.

Likewise

$$\Theta_{22} = \alpha'_{22} \varepsilon^{2/3} k^{-5/3} \tag{83}$$

where $\alpha'_{22} = \frac{4}{3}\alpha'_{11}$.

If we use $C = 2.0$, then we have

$$E(k) = 1.53\varepsilon^{2/3} k^{-5/3} \tag{84}$$

Different authors use different values for the constant 1.53 - anything between 1.35 and 1.5 are common. Note, however, that if one adjusts this constant then the constant C also needs adjustment. I prefer to use $C = 2.0$ because it has at least been measured with good accuracy in the atmosphere (e.g. CAUGHEY et al., 1978, Kaimal etc.).

Additionally, for this choice of C, we have

$$\Theta_{11} = 0.25\varepsilon^{2/3}k^{-5/3} \tag{85}$$

and

$$\Theta_{22} = 0.67\varepsilon^{2/3}k^{-5/3} \tag{86}$$

However, one final warning is warranted here. The last two spectral forms assume that k may be both positive and negative. Because of the obvious symmetry, many experimentalists often "fold" their negative spectral densities over onto their positive ones. If this procedure is used, the amplitudes above double, and so we have

$$\Theta'_{11} = 0.50\varepsilon^{2/3}k^{-5/3} \tag{87}$$

and

$$\Theta'_{22} = 1.34\varepsilon^{2/3}k^{-5/3} \tag{88}$$

This therefore completes the main spectra you will need when dealing with velocity fluctuations. Unfortunately, it is not yet the end of the story! We still need to consider the spectra associated with *scalar* fluctuations!

6.5.2.3 Spectra for scalar quantities

Just as we may form structure functions and spectra for velocities, we may also form them for scalar parameters. These should ideally be parameters which are unaffected by movement within the turbulence - so-called conservative quantities. An example is potential temperature; others might include artificially added tracers, or inert constituents. We will denote the concentration of this scalar as θ. Then the following are the most important spectra.

The structure function is taken to obey a law of the type

$$D_\theta(r) = C_\theta^2 r^{2/3}. \tag{89}$$

The first important spectral form is $\Phi_\theta(\underline{k})$, which is the full three-dimensional spectral density function. For Kolmogoroff Turbulence, it is given by

$$\Phi_\theta(\underline{k}) = 0.033C_\theta \mid \underline{k} \mid^{-11/3} \tag{90}$$

in the inertial range.

This function has been chosen to be normalized so that

$$\int_{-\infty}^{\infty}\int_{-\infty}^{\infty}\int_{-\infty}^{\infty}\Phi_\theta(\underline{k})d\underline{k} = \overline{(\theta')^2}. \tag{91}$$

As for the velocity spectra, we are also on occasion interested in the integrated spectral density on a spherical shell of radius k. For isotropic turbulence this then gives

$$E_\theta(k) = 4\pi k^2\Phi_\theta(k) = 0.132C_\theta^2 k^{-5/3} = 0.415C_\theta^2 k^{-5/3} \tag{92}$$

where $k = |\,\underline{k}\,|$.

Finally, we present the spectrum seen if we record along a straight line. This is the spectrum which a probe moving through a patch of turbulence would measure, and is very similar to Θ_{11} from the section on velocity spectra. This is given by

$$S_\theta(k_1) = \int_{-\infty}^{\infty}\int_{-\infty}^{\infty}\Phi_\theta(\underline{k})dk_2dk_3 \tag{93}$$

which, for the case of Kolmogoroff turbulence, becomes

$$S_\theta(k) = 0.125C_\theta^2 k^{-5/3} \tag{94}$$

If we fold negative wavenumbers onto positive, we obtain

$$S'_\theta(k) = 0.25C_\theta^2 k^{-5/3} \tag{95}$$

RADAR BACKSCATTER

We are now in a position to (finally!) be able to employ our knowledge to determine how strongly turbulence backscatters radio waves.

To determine the strength of backscatter of radio waves, we need to consider a "parcel" of air in a turbulent patch.

If a parcel is displaced vertically, it will expand adiabatically. If the background mean gradient is NOT adiabatic, the parcel will have a density different to that of its surroundings

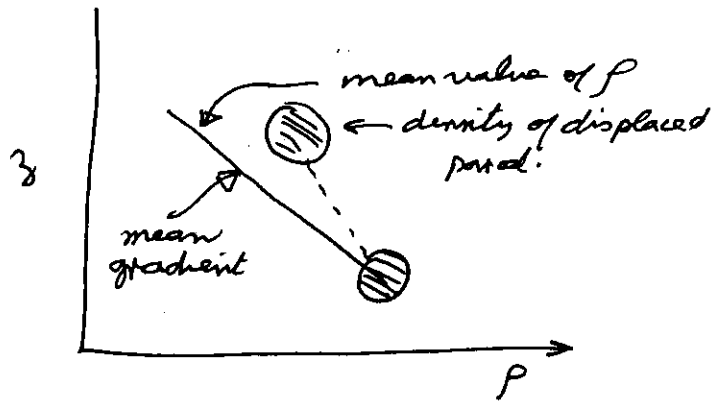

We therefore have a discrete "blob" with a density (& refractive index) different from its surroundings. (This has a lot in common with our Gaussian blobs we discussed last lecture).

We expect the backscattered power to depend in some way on this refractive index difference between the parcel and its surroundings. We also expect the degree of fluctuation in the turbulent patch to depend on this difference.

If we look at the previous equation (90), & let θ be the refractive index, then

$$\Phi_n(k) = 0.033\, C_n^2\, k^{-\frac{11}{3}}$$

Where we have replaced C_θ by C_n^2 for historical reasons

But the returned power is also proportional to the strength of the Fourier component at a scale

$$k_r = \frac{4\pi}{\lambda}$$

where λ is the radar wavelength. (see Dr. Lawrence's notes on Bragg scatter).

Thus the backscattered power is proportional to

(i) k^4

(ii) $\Phi_n(k)$.

$$\therefore \quad P \propto k^4 \cdot \underbrace{(0.033\, C_n^2 k^{-\frac{11}{3}})}_{\Phi_n}$$

$$\text{or} \quad \boxed{P \propto C_n^2 k^{\frac{1}{3}} \quad \propto C_n^2 \lambda^{-\frac{1}{3}}}$$

More precisely,

$$P \approx (0.015)\left[C_n^2\, P_T \cdot A_R \cdot e^2 \Delta z\right] \cdot \frac{\lambda^{-\frac{1}{3}}}{r^2}$$

(see Hocking, Radio Science, 20, 1403-1422, 1985 for more explicit derivations).

Where P_T = transmitted power, A_R = effective collecting area of the radar, e = efficiency, Δz = radar pulse-length, and r is the range to the scatterer from the radar.

Thus C_n^2 gives a measure of the "degree of fluctuation" of the refractive index n inside the turbulent patch.

We expect this "degree of fluctuation" to depend on the difference in gradient of the mean value $\bar{n}$, & the gradient associated with displacement of a parcel of air.

We will denote this "differential gradient" by M_n.

We also expect the degree of fluctuation to be more if a parcel of air is allowed to be displaced vertically by a larger amount.

Hence we expect C_n^2 to be monotonic in M_n, and monotonic in L_B (the outer scale).

Tatarskii, 1961, p51, shows that

$$\boxed{C_n^2 \propto L_B^{\frac{4}{3}} M_n^2}$$

But recall that

$$L_B \propto \varepsilon^{\frac{1}{2}} \omega_B^{-\frac{3}{2}}$$

Hence

$$\boxed{C_n^2 \propto \varepsilon^{\frac{2}{3}} \omega_B^{-2} M_n^2} \qquad (*)$$

Note that C_n^2 depends on ε to the $\frac{2}{3}$ power.

Now what about the radar backscatter? We return to equation (49) of Dr. Lawrence's notes.

Then we see that the returned power is proportional to k^4.

Thus we may derive an estimate for ε in the following way

(1) Determined the backscattered power received by the radar

(2) Use the previous equation, & knowledge of your radar parameters (collecting area, transmitted power etc.) to deduce $\underline{\underline{C_n^2}}$

(3) Then from $C_n^2 \propto \varepsilon^{\frac{2}{3}} \omega_B^{-2} M_n^2$ -

we can deduce ε if we know M_n and ω_B.

The exact relation for this ~~form~~ equation is

$$C_n^2 = \frac{1}{\gamma} \varepsilon^{2/3} \omega_B^{-2} M_n^2$$

where γ actually depends on the Richardson number, but is often taken to be 0.25.

An extensive discussion about γ can be found in Hocking and Mu, J. Atmospheric & Solar-Terrestrial Phys., 59, 1979, 199 and Hocking, Advances in Space Research, 12(10), 207-213, 1992.

~~Those~~ The relevant sections from these papers now follow, (after some brief additional note.)

First, We state without proof that:

(see Tatarskii, 1961, + Hocking, 1985 for proofs)

The "potential refractive index gradient" is given in the troposphere and stratosphere by

$$M = -77.6 \times 10^{-6} \frac{P}{T} \left(\frac{\partial ln\Theta}{\partial z} \right) \left[1 + \frac{15500q}{T} \left(1 - \frac{1}{2} \frac{\partial lnq/\partial z}{\partial ln\Theta/\partial z} \right) \right] \tag{97}$$

where z is height, Θ is the potential temperature, q is the specific humidity, T is the absolute temperature and P is the atmospheric pressure in millibars. The term in square brackets was denoted as χ by VanZandt et al., 1978; indeed this particular form of the equation was first introduced by these authors. Note that χ tends to 1 as the humidity terms tend to zero.

In the ionosphere, where humidity is no longer important but electron density is, we have

$$M = \frac{\partial n}{\partial N} \left[\frac{N}{\Theta} - \frac{dN}{dz} + \frac{N}{\rho} \cdot \frac{d\rho}{dz} \right] \tag{98}$$

where again we have used the symbol Θ for potential temperature and N is the electron density. The term ρ is the neutral density. The function $\frac{\partial n}{\partial N}$ needs to be determined from electro-ionic theory (e.g. Hartree; Sen and Wyller, etc.) +

These functions and relations now give us the tools to make useful radar measurements of the strength of turbulence.

+ Footnote: for a VHF radar, with radiation scattered from the ionosphere

$$\frac{\partial n}{\partial N} = \frac{1}{2} \pi^{-1} r_e \lambda^2$$

where r_e is the classical electron radius.

Extra factors.

An extra complication arises if the turbulence does not fill the radar volume, and indeed this often appears to be the case. It appears that in the stratosphere and mesosphere, turbulence occurs in relatively thin layers with thicknesses ranging from a few tens of metres to perhaps a kilometre or so, but generally of the order of 10-100m. At any one instant, only a small fraction of the radar volume contains turbulence, and this should be taken into account when calculating ϵ. In other words, the calculated value of C_n^2 is actually too small by a factor F_t, where F_t is the fraction of the radar volume which is filled with turbulence at any one time. Thus one normally calculates

$$C_n^2(turb) = C_n^2(radar)/F_t, \tag{14}$$

where $C_n^2(radar)$ is the value determined from the radar measurements. VANZANDT et al.(1978, 1981) have developed models for the variation of F as a function of atmospheric conditions, enabling estimates of ϵ to be made.

Hence we must modify our earlier $C_n^2 \leftrightarrow \varepsilon$ relation to the following.

The energy dissipation rate is related to the potential refractive index structure constant by

$$\bar{\varepsilon} = \left(\gamma \overline{C_n^2} \frac{\omega_B^2}{F^{1/3}} M^{-2}\right)^{3/2} \tag{96}$$

where ω_B is the Vaisala-Brunt frequency. The parameter F represents the fraction of the radar volume which is filled by turbulence, while γ is a constant which will be discussed in much more detail shortly.

Furthermore, one is often interested in the mean value of ϵ averaged over the radar volume, so VANZANDT et al. suggested calculating the quantity

$$\bar{\epsilon} = F_t \epsilon_{turb} \tag{15}$$

For tropospheric and stratospheric studies at VHF, GAGE et al. (1980) used a simplified model based on VanZandt's model, in which they showed that the parameter $F_t^{\frac{1}{3}}\omega_B^2$ could be determined to moderate accuracy from climatological data, so that the simplified expression

$$\bar{\epsilon} = \gamma[C_n^2(radar)]^{\frac{3}{2}}[\frac{T}{P}^3] \tag{16}$$

could be used, where $\gamma = 1.08 \times 10^{22}$ for a dry troposphere and $\gamma = 3.25 \times 10^{21}$ for the stratosphere. Here, P is in millibars, T in Kelvin, C_n^2 is in units of $m^{-\frac{2}{3}}$ and ϵ is in units of Wkg^{-1}. Variations on these principles have also been presented by CRANE (1980) and WEINSTOCK (1981). Similar simplifications are not yet available for the ionosphere - but layer thicknesses are generally of the order of $100m$ and more in the ionosphere, so that F_t can at least be taken to be in the range 0.1 to 1 - layers with depths of only a few tens of metres are much less common than in the stratosphere (e.g. see fig. 1, Hocking, Radio Sci., 20, 1403, (1985)).

Detailed studies, and more in-depth discussions of these points above matters are available in the literature

Please note - we have not even discussed another important method for determining ε by radar - the so called "Spectral width" method.

6.6.3.3 C_n^2 methods for determining ε

One simple but effective method for deducing information about the scatterers is to record the backscattered power. In many experiments powers are compared in a relative way; for example, power variations as a function of time and height are usually studied in most experiments. Even this simple process can give useful results, but it is even more effective if the radar can be calibrated in an absolute sense. This requires some careful work by the user, but if this is done it is then possible to convert the measured powers to effective reflection coefficients, backscatter cross-sections, and perhaps estimates of the turbulence intensity.

The basis of this method is described in the following articles.

1/6

Adv. Space Res. Vol.12, No.10, pp.(10)207–(10)213, 1992
Printed in Great Britain.

0273-1177/92 $15.00

ON THE RELATIONSHIP BETWEEN THE STRENGTH OF ATMOSPHERIC RADAR BACKSCATTER AND THE INTENSITY OF ATMOSPHERIC TURBULENCE

W. K. Hocking

Department of Physics and Mathematical Physics, University of Adelaide, Adelaide, S.A. 5001, Australia

ABSTRACT

A commonly accepted expression relating the strength of radar backscatter and the strength of atmospheric turbulence is re-investigated. It is found that the previously accepted relation between the two quantities should have an extra dependence on the Richardson number included, and the implications for radar and in-situ studies of the atmosphere are discussed.

INTRODUCTION

An expression which is used frequently to relate turbulent structure function "constants" and the turbulent energy dissipation rate is the following:

$$\epsilon = [\ \gamma\ C_\xi^2\ \ \omega_B^2\ \ M_\xi^{-2}\ ]^{3/2} \qquad (1)$$

where ϵ is the turbulent energy dissipation rate, C_ξ^2 is the structure constant for fluctuations in any passive and conservative tracer ξ, ω_B is the Vaisala-Brunt frequency in radians per second, and M_ξ is the mean gradient of the quantity ξ across the turbulent patch. In the case of radar backscatter from the mesosphere, for example, in which electron density fluctuations are the main cause of the radar backscatter, ξ is the potential refractive index, and M_ξ is given approximately by $M_n = (\partial n/\partial N)M_N$, where N is the electron density. In this case,

$$M_N = N\left[-\frac{1}{N}\frac{dN}{dz} + \frac{1}{\gamma p}\frac{dp}{dz} \right]$$
$$= \left[\frac{N}{\theta}\frac{d\theta}{dz} - \frac{dN}{dz} + \frac{N}{\rho}\frac{d\rho}{dz} \right] \qquad (2)$$

Corresponding expressions exist for scatter from other parts of the atmosphere ; for example in the troposphere the backscattered signal strength is a function of pressure, temperature and humidity (e.g. /1/).

However, various expressions for the "constant" γ have appeared in the literature. For example, /1,2/ give

$$\gamma = \frac{b^{2/3}}{a^2\,\alpha'\,R_{i(c)}} \qquad (3)$$

where $R_{i(c)}$ is the critical Richardson's number (usually taken as 0.25), α' is the inverse of the turbulent Prandtl number, a^2 is a constant which /1,2/ took to be 2.8, and b is a constant which /2/ took to be 1.0. In fact it seems likely that b is significantly different from 1.0, as will be seen shortly, but this does not bear too strongly on this particular paper Formally, b is defined through the relation

$$\epsilon = b\ S^{3/2}\ L_0^2\ , \qquad (4)$$

where L_0 is Tatarskii's "outer scale" /3/ and S is the square of the vertical shear in the mean horizontal wind.

Alternatively, /4/ and /5/ give

$$\gamma = 1/(\ a^2\,\alpha'\ B\ c_3) \qquad (5)$$

where B is a constant which should normally be 1 and certainly never more than 3, and c_2 is a constant normally taken to be 0.8. Formally, c_2 is defined through the relation

$$K_m = c_2 \epsilon / \omega_B^2 \tag{6}$$

where K_m is the diffusion coefficient for momentum.

If we assume that (3) and (5) are equivalent, then b = 0.175 and the two approaches are consistent. In all cases, however, it has been assumed that γ is indeed a constant. In this article, it is shown that this is not so, and γ is in fact a function of the Richardson number. For γ to be a true constant would require that the ratio between the kinetic and potential energy spectra is a universal constant, an assumption which is shown to be unreasonable.

POTENTIAL AND KINETIC ENERGY SPECTRA

For simplicity, all the following derivations will be done for the case of electron density fluctuations in the mesosphere, but analagous expresssions can be derived at any other level in the atmosphere and for any other appropriate scalar. We begin by deriving expressions for the spectral potential and kinetic energy densities per unit wave-number in terms of the electron density fluctuations and velocity fluctuations.

For the potential energy (PE), consider first a small parcel displaced from its equilibrium position, and calculate its potential energy. The PE per unit mass at displacement Δz is

$$\int_{\xi=0}^{\xi=\Delta z} g \frac{\Delta\rho'}{\rho} \, d\xi \tag{7}$$

where $\Delta\rho' = -M_\rho . \xi$ at displacement ξ, and where M_ρ is the background potential density gradient. Note that M_ρ is not the gradient of the background density, but gives the rate of change of the difference of the density of the parcel and the background as a function of height. Hence

$$\text{PE per unit mass at displacement } \Delta z = -g/\rho \, M_\rho \, (\Delta z)^2/2 . \tag{8}$$

Now use the relation $\Delta N'/\Delta z = \partial N'/\partial z = M_N$, where $\Delta N'$ is the difference of the parcel's ion density and that of the environment, so that $\Delta z = \Delta N'/M_N$, and substituting for Δz above gives

$$\text{PE per unit mass} = -\frac{g}{\rho} M_\rho \frac{1}{2} \frac{(\Delta N')^2}{M_N^2} . \tag{9}$$

We may now use the fact that $\omega_B^2 = -(g/\rho) M_\rho$ to write that the potential energy per unit mass is

$$\text{PE per unit mass} = \frac{1}{2} \frac{\omega_B^2}{M_N^2} \langle (\Delta N')^2 \rangle \tag{10}$$

The total kinetic energy (KE) per unit mass is of course 1/2 $\overline{u^2}$, $\overline{u^2}$ being the total mean square velocity fluctuation.

We can measure the total velocity and electron density fluctuations as a function of position in space and Fourier transform the resultant series to form spectra. For example, according to Kolmogoroff theory (e.g. /3/), the total kinetic energy for wave numbers with magnitudes between |k| and |k+dk| is

$$E_K(k) \, dk = aC \epsilon^{2/3} k^{-5/3} \, dk \tag{11}$$

where a = 0.061 (4π), and C is a constant which has been experimentally determined to be very close to 2.0 /6,7/.

Likewise the spectral density of the electron density fluctuations in the same wave-number range is /3/

$$E_N(k) = (6/11) \, a \, C_N^2 \, k^{-5/3} . \tag{12}$$

We discussed $(\Delta N')^2$ above as the total mean square electron density fluctuation, but we can equally consider it as the density fluctuation in the wavenumber range between |k| and |k+dk|. Then, by (10), the potential energy per unit wave number in this range is

$$E_p(k) = \frac{1}{2} \frac{\omega_B^2}{M_N^2} \frac{6}{11} a C_N^2 k^{-5/3} \quad (13)$$

It has been suggested /8/ that the kinetic and potential energy should be equally partitioned in a turbulent patch, in which case we can equate (11) and (13) to give

$$\epsilon = \left[\frac{3 C_N^2 \omega_B^2}{22 M_N^2} \right]^{3/2} \quad (14)$$

However, let us now consider the equipartition assumption itself in more detail. Assume that the KE spectrum and the PE spectrum are not equipartitioned, but are related through

$$E_p/E_K = d' \quad (15)$$

/9,10/ have used a similar expression, but used 2d/3 in place of d'. In that case, d was equal to the ratio of the rates of flow of potential and kinetic energy down through the scales of the turbulence spectrum. Then the "equipartition of KE and PE" is modified so that

$$\frac{\omega_B^2}{M_N^2} \frac{3}{11} a C_N^2 / [a C \epsilon^{2/3}] = d'$$

$$\text{or} \quad \epsilon = \left[\frac{3 C_N^2 \omega_B^2}{22 d' M_N^2} \right]^{3/2} \quad \text{for} \quad C = 2.0 \quad (16)$$

Values of d' are not very well known. However, if atmospheric turbulence occurs in regions where the temperature lapse rate is adiabatic, for example, there will be *no* temperature fluctuations induced by the turbulence. Thus E_p tends to zero, even though E_K is finite, so that d' approaches zero. Hence it is clearly NOT valid to assume that the two forms of energy are always equipartitioned.

We therefore need to look in more detail at this constant d', and this is done in the following section.

RELATION OF THE QUANTITY d' TO THE RICHARDSON NUMBER

Consider a turbulent layer of thickness D. The available KE for generation of turbulence is (appendix A)

$$AKE = \frac{1}{24} D^2 \left(\frac{du}{dz} \right)^2 \quad (17)$$

The available PE for generation of turbulence is (also see appendix A)

$$APE = -\frac{1}{24} D^2 \omega_B^2. \quad (18)$$

(This is negative because when ω_B^2 is positive (a stable stratification), the potential energy acts to stabilize the region, rather than supply energy for turbulence.)

The total available energy for conversion to turbulent KE is therefore

$$AE = \frac{1}{24} D^2 \left[\left(\frac{du}{dz} \right)^2 - \omega_B^2 \right]. \quad (19)$$

The spectral density of the kinetic energy density spectrum will be proportional to the total available energy, since all the available energy is converted into energy of motion. We expect that the potential energy spectrum is proportional to the available potential energy APE for any given ϵ. Then we can say that the potential energy spectral density relative to the kinetic energy density will be equal to

$$\frac{APE}{AE} = d' = \frac{\left| \omega_B^2 \right|}{\left(\frac{du}{dz} \right)^2 - \omega_B^2}. \quad (20)$$

Note that the PE spectrum is independent of the sign of ω_B^2, since fluctuations tend to zero near $\omega_B^2 = 0$, but become non-zero at $\omega_B^2 \neq 0$ for both positive and negative ω_B^2. (spectra are by definition of course positive definite). A positive displacement results in a positive value for $\Delta\rho'$ when $\omega_B^2 > 0$, and a negative value for $\Delta\rho'$ when $\omega_B^2 < 0$, but of course the square of $\Delta\rho'$ is always positive. The available KE is very critically dependent on the sign of ω_B^2, however. If ω_B^2 is negative, the buoyancy can supply energy to the turbulence,

rather than extract from the available kinetic energy. Dividing (20) through by $(du/dz)^2$, and noting that $(du/dz)^2$ is always positive (in contrast to ω_B^2, which may be either positive or negative), we see that

$$\frac{E_P}{E_K} = d' = \frac{|R_i|}{1 - R_i} = \left| \frac{R_i}{1 - R_i} \right| = \left| \frac{1}{\frac{1}{R_i} - 1} \right| \qquad (21)$$

This is true for both $\omega_B^2 > 0$ and $\omega_B^2 < 0$, provided $R_i < 1$. If $R_i > 1$, it means no turbulence is to be expected because APE > AKE, and the available kinetic energy cannot overcome the stabilization due to the potential energy. A graph of d' vs R_i is shown in fig 1.

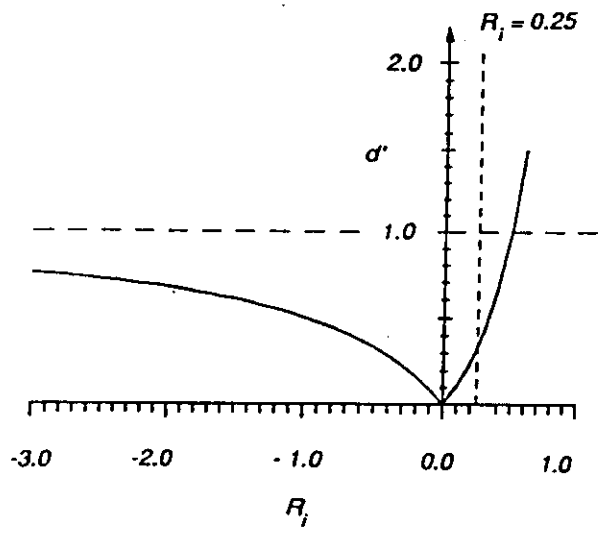

Fig. 1. The ratio of the potential and kinetic energy spectral densities, d', plotted as a function of the Richardson number, R_i. Note that the ratio tends to infinity as R_i tends to 1, and tends to 1 as R_i approaches minus infinity.

This expression represents the main point of this article. We now see that d' is a function of R_i, and so therefore so is γ. In fact (16) can now be rewritten as

$$\epsilon = \left[\frac{3\, C_N^2\, \omega_B^2}{22\, \frac{|R_i|}{|1 - R_i|}\, M_N^2} \right]^{3/2} \quad \text{for } C = 2.0 . \qquad (22)$$

Comparing this to (1), we see that

$$\gamma = \frac{3}{22} \frac{|1 - R_i|}{|R_i|} \quad (R_i < 1) \qquad (23)$$

Similar expressions apply for other scalar parameters. For example, if one measures the temperature structure function "constant" C_T^2, then M_N^2 is replaced by $M_\theta^2 = (d\theta/dz)^2 = (g/\theta\, \omega_B^2)^2$, and we have

$$\epsilon = \left[\frac{3\, C_T^2\, g^2}{22\, \frac{|R_i|}{|1 - R_i|}\, \theta^2 \omega_B^2} \right]^{3/2} \quad \text{for } C = 2.0 \qquad (24)$$

TURBULENT ENERGY DISSIPATION RATE AS A FUNCTION OF LAYER DEPTH

We can in fact take this further. It is an interesting exercise to get a crude estimate of the energy dissipation rate in a layer of some specified thickness, and specified wind shear and temperature profile.

We have already seen an expression for the available energy (AE) in such a layer (ie(19)).

Let us say that this energy will be lost in a time τ equal to the time for one convective cycle of the largest eddy. Then

$$\epsilon = AE/\tau \quad . \tag{25}$$

What is τ? We can write

$$\tau \approx D/u_0 \tag{26}$$

where u_0 is the velocity associated with the largest eddy, and I have assumed that the largest eddy has scale ~ D.

As a simple estimate of u_0, we can say that it is of the order of the total RMS velocity of all eddies, u_{RMS}, since this integral will be dominated by the largest scales. Evaluating u_{RMS} by integrating over the spectrum in (11), we have

$$\frac{1}{2} u_{RMS}^2 = \int_{k_B}^{\infty} \alpha \; C \; \epsilon^{2/3} k^{-5/3} dk$$

$$= 1.15 \; C \; \epsilon^{2/3} \; k_B^{-2/3}$$

$$\text{so} \quad \epsilon = \frac{u_{RMS}^3}{L_B} \cdot \frac{2\pi}{(2.3\,C)^{3/2}} = 0.6 \frac{u_{RMS}^3}{L_B} \qquad \text{for } C = 2.0 \tag{27}$$

Of course u_0 is less than u_{RMS}, so let us write

$$\epsilon \approx \psi \, u_0^3 / L_B \tag{28}$$

where ψ is a constant, greater than about 0.6. We shall assume that it lies in the range between 1 and 5, which is a wide range and is therefore likely to include the correct value.

Thus from (19), (25) and (28), we have

$$\epsilon \approx \frac{AE}{\tau} \approx \frac{1}{24} D^2 \left[\left(\frac{du}{dz}\right)^2 - \omega_B^2 \right] \left(\frac{\epsilon L_B}{\psi} \right)^{1/3} / D \tag{29a}$$

According to /11/, the actual layer thickness of typical stratospheric layers is 5 to 10 times the buoyancy scale L_B, so the most energetic eddies could be a few times larger than L_B. In order to allow for this possibility, write L_B as a fraction of D, $= \chi D$, where χ lies somewhere between 0.2 and 1, so that

$$\epsilon^{2/3} \approx \frac{1}{24} D^{4/3} \left(\frac{\chi}{\psi}\right)^{1/3} \omega_B^2 \left(\frac{1}{R_i} - 1 \right) \tag{29b}$$

If R_i approaches zero, this expression does not "blow up", but can be written

$$\epsilon^{2/3} = \frac{1}{24} D^{4/3} (\chi/\psi)^{1/3} \left(\frac{du}{dz} \right)^2 \tag{30}$$

Note that (χ/ψ) only appears as a weak power (1/3), and $(\chi/\psi)^{1/3}$ varies between about $(.2/5)^{1/3}$ and $(1/1)^{1/3}$ ie between 0.34 and 1.

For example, if $R_i = 1/4$, $D = 10^3$m, and $\omega_B = .01$, then ϵ lies between 0.008 and 0.04 W kg^{-1}.

Thus this seemingly rather approximate method for estimates of ϵ has a possible error of around plus or minus a factor of 2. Thus it is still a reasonable procedure to use for approximate estimates of turbulent energy dissipation rates if there are no other more direct means available.

Finally, it is possible to gain an estimate of the lifetime of such a layer of turbulence. For simplicity, assume that there is no source of energy maintaining the current temperature and wind gradients, so that once all the available energy is exhausted, there is no other source of energy to maintain the turbulence. Thus the lifetime of the layer can crudely be determined by dividing the available energy by the turbulent energy dissipation rate. Of course this is not exact, because as the available energy depletes, so the wind and temperature gradients change and so the turbulent energy dissipation rate also reduces.

For the example discussed above, the total available energy is about 12.5 J kg^{-1}, and ϵ ~0.01 W kg^{-1}. Thus the lifetime of such a layer would be about 20 mins.

CONCLUSIONS

An improved expression relating the turbulent energy dissipation rate to the potential electron density structure constant has been presented, and a new dependence on the Richardson number has been highlighted. The relation has been given in equation (22). Similar relations exist for other structure constants (e.g. (24)). A relation between the potential and kinetic energy spectra has also been given in terms of the Richardson number. Finally, a simple treatment has been presented to allow approximate estimates of the turbulent energy dissipation rate from measurements of the layer depth, the Richardson number and the Brunt-Vaisala frequency. Experimental tests of these expressions are still needed.

APPENDIX A

In this appendix we derive expressions for the total available kinetic and potential energy in a turbulent layer.

As seen in equation (8), assuming that displacement occurs in a region in which ω_B^2 is constant as a function of height, then the potential energy per unit mass stored by displacing a parcel a vertical distance z is given by

$$PE(z) = \omega_B^2 z^2/2 \qquad (A1)$$

But if we need the total energy stored in a layer, we need to carry this one step further. Imagine taking thin sub-layers of thickness δz at a reference height z=0 and successively shifting each sub-layer to a new altitude at height $z_b + (i-1)\delta z$, i being the sub-layer number. Taking the layers to have cross-sectional area ΔA and letting δz tend to dz, then the work done to do this is

$$W_{tot} = \int_{z_b}^{z_T} \omega_B^2 \frac{z^2}{2} \rho \Delta A \, dz \qquad (A2)$$

(Note we multiply by $\rho \Delta A \, dz$, the mass of the layer, to convert the potential energy per unit mass in (A1) to a total energy).

Then the total energy per unit mass stored in the layer is given by the integral in (A2) divided by the total mass of the layer ($= \rho \Delta A (z_T - z_b)$), or

$$\text{PE per unit mass of whole layer} = (1/6)\, \omega_B^2 (z_T^3 - z_b^3)/(z_T - z_b) \qquad (A3)$$

For a fixed layer depth ($z_T - z_b$ = constant), this has a local minimum when $z_T = -z_b$, as can readily be found by setting $z_T = z_b + D$, where D is the layer depth, differentiating with respect to z_b, and setting the derivative to zero.

Thus if the sub-layers are distributed between -D/2 and +D/2, the minimum amount of energy is expended in forming the layer. Conversely, if we wish to drive the layer to adiabatic, it can be done in the least expensive way by making the new potential temperature of the whole layer equal to the previous potential temperature of the midpoint of the layer. We can consider this minimum amount of energy as the "available potential energy" of the layer. This is the energy required to produce this layer from an adiabatic state, so we can think of the layer possessing "potential energy" equal to the negative of this. Using $z_b = -D/2$ and $z_T = D/2$, we see that the available potential energy per unit mass is

$$APE = -(1/24)\, \omega_B^2 D^2. \qquad (A4)$$

A similar approach may be used to examine the "available kinetic energy" in the turbulent layer. We imagine a layer with a wind shear du/dz and consider the total kinetic energy in the layer. Let the wind at the midpoint of the layer be u_0. Let each sub-layer have thickness dz and area A. Then the total kinetic energy contained in the layer is given by

$$KE_{tot} = \int_{-D/2}^{D/2} \frac{1}{2} \left[u_0 + \left(\frac{du}{dz}\right) z\right]^2 \rho A \, dz \qquad (A5)$$

or

$$KE_{tot} = \rho A D \left[(1/2) u_0^2 + (1/24) (du/dz)^2 D^2 \right] \qquad (A6)$$

The total kinetic energy per unit mass can be found simply by dividing by ρAD.

Turbulence will extract energy from this shear, and transfer it to heat, but it alone cannot change the total momentum of the layer. To extract all available kinetic energy from the flow and at the same time conserve momentum, the layer must be driven to a final state in which the velocity throughout the layer is a constant, equal to u_0. The kinetic energy per unit mass in this case will clearly be $(1/2) u_0^2$, so that from (A6) the available kinetic energy is just

$$AKE = (1/24) (du/dz)^2 D^2. \qquad (A7)$$

(A4) and (A7) represent two expressions used frequently in the body of the text. The first gives the potential energy stored by the layer, and the second the available kinetic energy within the layer for producing turbulence.

Acknowledgements

Special thanks to Jim Brown for detection of important corrections in an earlier draft, and some valuable discussions.

REFERENCES

1. Hocking W.K., "Measurement of turbulent energy dissipation rates in the middle atmosphere by radar techniques: a review" *Radio Sci.*, 20, 1403, 1985.

2. VanZandt, T.E., J.L.Green, K.S.Gage, and W.L.Clark, Vertical profiles of refractivity turbulence structure constant: Comparison of observations by the Sunset radar with a new theoretical model, *Radio Sci.*, 13, 819, 1978.

3. Tatarski, V., *Wave Propogation in a Turbulent Medium*, translated from Russian by Silverman, McGraw-Hill, N.Y., 1961.

4. Luebken, F-J., U. Von Zahn, E.V. Thrane, T. Blix, G.A. Kokin and S.V. Pachomov, In-situ measurements of turbulent energy dissipation rates and eddy diffusion coefficients during MAP/WINE, *J. Atmos. Terr. Phys.*, 49, 763, 1987.

5. Blix, T.A., E.V. Thrane, and O. Andreassen, In situ measurements of the fine-scale structure and turbulence in the mesosphere and lower thermosphere by means of electrostatic positive ion probes, *J. Geophys. Res.*, 95, 5533, 1990.

6. Kaimal, J.C., J.C. Wyngaard, Y. Izumi, and O.R. Cote, Spectral characteristics of surface layer turbulence, *Quart. J. Roy. Meteorol. Soc.*, 98, 563, 1972.

7. Caughey, S.J.,B.A. Crease, D.N. Asimakapoulos, and R.S. Cole, Quantitative bistatic acoustic sounding of the atmospheric boundary layer, Q. J. R. Meteorol. Soc, 104, 147-161, 1980.

8. Thrane, E.V., O. Andreassen, T. Blix, B. Grandal, A. Brekke, C.R. Philbrick, F.J. Schmidlin, H.U. Widdel, U. Von Zahn and F-J. Luebken, Neutral air turbulence in the upper atmosphere observed during the Energy Budget Campaign, *J. Atmos. Terr. Phys.*, 47, 243, 1985.

9. Dalaudier, F. and C. Sidi, Evidence and interpretation of a spectral gap in the turbulent atmospheric temperature spectra, *J. Atmos. Sci.*, 44, 3121, 1987.

10. Sidi, C. and F. Dalaudier, Turbulence in the stratified atmosphere: recent theoretical developments and experimental results, *Adv. Space Res.*, 10(10), 25, 1990

11. Barat, J., Some characteristics of clear air turbulence in the middle stratosphere, *J. Atmos. Sci*, 39, 2553, 1982.

the following article further develops the relation between C_n^2 & ε, and shows some examples of application of this theory.

Pergamon

PII: S1364-6826(97)00020-5

Journal of Atmospheric and Solar-Terrestrial Physics, Vol. 59, No. 14, pp. 1779–1803, 1997

1364-6826/97 $17.00+0.00

Upper and middle tropospheric kinetic energy dissipation rates from measurements of $\overline{C_n^2}$ — review of theories, *in-situ* investigations, and experimental studies using the Buckland Park atmospheric radar in Australia

W. K. Hocking[1] and P. K. L. Mu[2]

[1]Physics Department, University of Western Ontario, London, Ontario, Canada; [2]Department of Physics and Mathematical Physics, University of Adelaide, Adelaide, Australia
(*e-mail*: whocking@danlon.physics.uwo.ca)

(*Received* 15 *May* 1996; *in revised form* 15 *January* 1997; *accepted* 21 *January* 1997)

Abstract—We investigate the determination of the kinetic energy dissipation rate ε in the middle and upper troposphere by measurements of the refractivity structure function constant C_n^2. To begin, we review the literature on *in-situ* measurements of ε, to give a base for comparison with our own data. We then study the current literature concerning conversions of C_n^2 to ε, but find several available models. We intercompare these different theories. By using earlier boundary layer, tropospheric and stratospheric high resolution studies, we then determine the most appropriate theory for our purposes.

We then turn to experimental studies. Measurements of C_n^2 deduced by thermosondes are presented in order to show how the different models discussed above lead to quite different estimates of ε. In particular, we demonstrate that, if the Richardson number is not included in these determinations, some very mechanically active turbulent layers can be almost missed completely using temperature-sensitive techniques like thermosondes. However, if proper allowance is made for this effect, thermosondes can be a very good means of determination of atmospheric energy dissipation rates. Radar measurements of C_n^2 for determinations of ε are then presented, using data from the Buckland Park VHF radar near Adelaide, Australia (35°S, 138.5°E). The system was first carefully calibrated. Then radar data were incorporated with radiosonde data in order to optimize the measurement accuracies, utilizing the procedures described by Vanzandt *et al.* (1978, 1981) and Gage *et al.* (1980). In addition, we have developed a diagnostic test using correlation techniques between the radiosonde data and the radar data which can be used to determine when application of these procedures is appropriate. Finally, we present a comparison between results determined by the radar and energy dissipation rate distributions determined over recent years by other techniques. © 1997 Elsevier Science Ltd

INTRODUCTION

Turbulence is an important aspect of atmospheric motions. It is especially important in the process of diffusion of pollutants and contaminants in the atmosphere over both large and small scales. It is also important for vertical diffusion, possibly having impact at some latitudes in regard to diffusion of anthropogenic pollutants up into the stratosphere. Some such pollutants, such as chlorofluorocarbons, can interact with the stratospheric ozone layer and cause ozone destruction. Other important impacts of turbulence can be in relation to its impact on aircraft flight safety; occurrences of strong turbulence at upper levels of the atmosphere can cause discomfort for civil aircraft passengers, and in some cases can have more catastrophic effects. Identification and measurement of turbulence is thus an important goal of modern atmospheric studies.

Turbulence is the product of atmospheric events such as (amongst others) atmospheric gravity waves and wind shear induced Kelvin–Helmholtz instability. To describe the morphology of turbulence, it is necessary to calculate certain parameters associated with it. Two important factors are the refractive index structure constant C_n^2 and the kinetic energy dissipation rate ε, where the former is a measure of the refractive index fluctuations induced by the turbulence and the latter is a measure of the severity of the turbulence. More specifically, ε is equal to the energy deposited as heat into the atmosphere, per unit mass and per unit time.

126

There are a number of possible generation mechanisms which can lead to turbulence. Common sources of energy for turbulent velocity fluctuations are shear in the mean wind and breaking/overturning of short-period gravity waves. Other sources are jet streams and convection during the passage of a cold front or thunderstorm.

There are several methods which can be used in order to estimate the intensity of turbulence. For turbulence in which the entities which scatter the incident radar waves have scales much less than the radar resolution volume, an estimate of the turbulence can be made by measuring the half-power half-width of the broadened Doppler velocity spectra (Atlas, 1964; Frisch and Clifford, 1974; Doviak and Zrnic, 1984; Hocking, 1983, 1985, 1996; Hocking *et al.*, 1989; Cohn, 1995). In this regard, the article by Hocking (1996) is especially important in that it demonstrates the importance of determining and using the turbulence buoyancy scale in these calculations, an effect which was not fully appreciated in the past.

Another technique employs the spectral analysis of a sequence of wind observations, resulting in a generally $-5/3$ power law for the spectra. Energy dissipation rates can then be deduced, but this technique requires very fast temporal sampling and very good spatial resolution; it is beyond the capability of VHF radars. It is, however, the type of technique used with *in-situ* measurements of wind fluctuations employing high resolution anemometers (e.g. Lilly *et al.*, 1974; Kropfli, 1971). For radar methods, applied at the sorts of temporal and spatial scales used by most radars, this technique actually produces spectra of gravity wave and 2D turbulence motions.

The remaining method, which is the one used predominantly herein, is based on measurements of the refractive index structure constant. From this the energy dissipation rate is derived, enabling determination of the severity of the turbulence (Vanzandt *et al.*, 1978; Gage *et al.*, 1980; Vanzandt *et al.*, 1981). The structure function constant can be deduced in a variety of ways, including optical, *in-situ* and radar.

We will shortly examine in some detail the theory relating to this latter technique, as it will form the basis for our own measurements. However, before doing this it is expedient to examine the current level of knowledge about typical turbulent energy dissipation rates in the troposphere using other procedures. This will then give us a base against which we can compare the measurements which we demonstrate later in this article. There is some uncertainty about certain aspects of the conversion from C_n^2 to ε, so we need such a reference to be certain that our results are sensible. For this reason, the following summary will concentrate generally on *in-situ* measurements.

TYPICAL ENERGY DISSIPATION RATES IN THE TROPOSPHERE AND LOWER STRATOSPHERE

In this section we present typical values of energy dissipation rates which were measured in the lower atmosphere. We concentrate in this short review on measurements which were made by *in-situ* instrumentation, such as wind anemometers (acoustic, cup, wind vane, etc.) and accelerometers. In general we ignore radar measurements for the time being, since the theory used to produce radar measurements is the subject of our investigations and it would not be wise to include such previous radar data in this set if we want it to be an independent reference base. We also similarly ignore measurements made using acoustic radars and lidars.

Figure 1 shows measurements of energy dissipation rates by a variety of methods, but in the main *in-situ*. Boundary layer data were generally recorded using anemometers mounted on towers and tethered balloons, whereas upper level data were generally made with accelerometers and anemometers mounted on aircraft. Pao and Goldburg (1969) describe some of the types of instrumentation used on aircraft, and Caughey *et al.* (1978), Readings and Rayment (1969) and Mousley *et al.* (1981) discuss some of the different anemometers used for boundary layer studies.

Many of these higher altitude data were produced in the 1960s and 1970s, when there were some major campaigns dedicated to measurements of this type. For example, Lilly *et al.* (1974) has reported some such high altitude studies, while Vinnichenko and Dutton (1969) summarized the results of the so-called HICAT series of experiments. However, more recent studies have also been performed. In particular we note the measurements of Lee *et al.* (1988) and Bohne (1981). These data covered a variety of conditions, from quiet to thunderstorm activity.

We also note that data exist for altitudes above 20 km, principally because of balloon measurements by Barat (1982, 1983) and Barat *et al.* (1984), but since we are primarily interested in the troposphere and lower stratosphere, we have placed a ceiling of 20 km on our graph. Barat's data generally lie, however, in the range between 10^{-4} and 10^{-3} m^{2}s^{-3} for altitudes of 20–30 km.

Various summaries of these upper atmosphere *in-situ* studies have also appeared. One such important summary is that by Vinnichenko *et al.* (1973) who determined, based on a large dataset of measurements,

56c

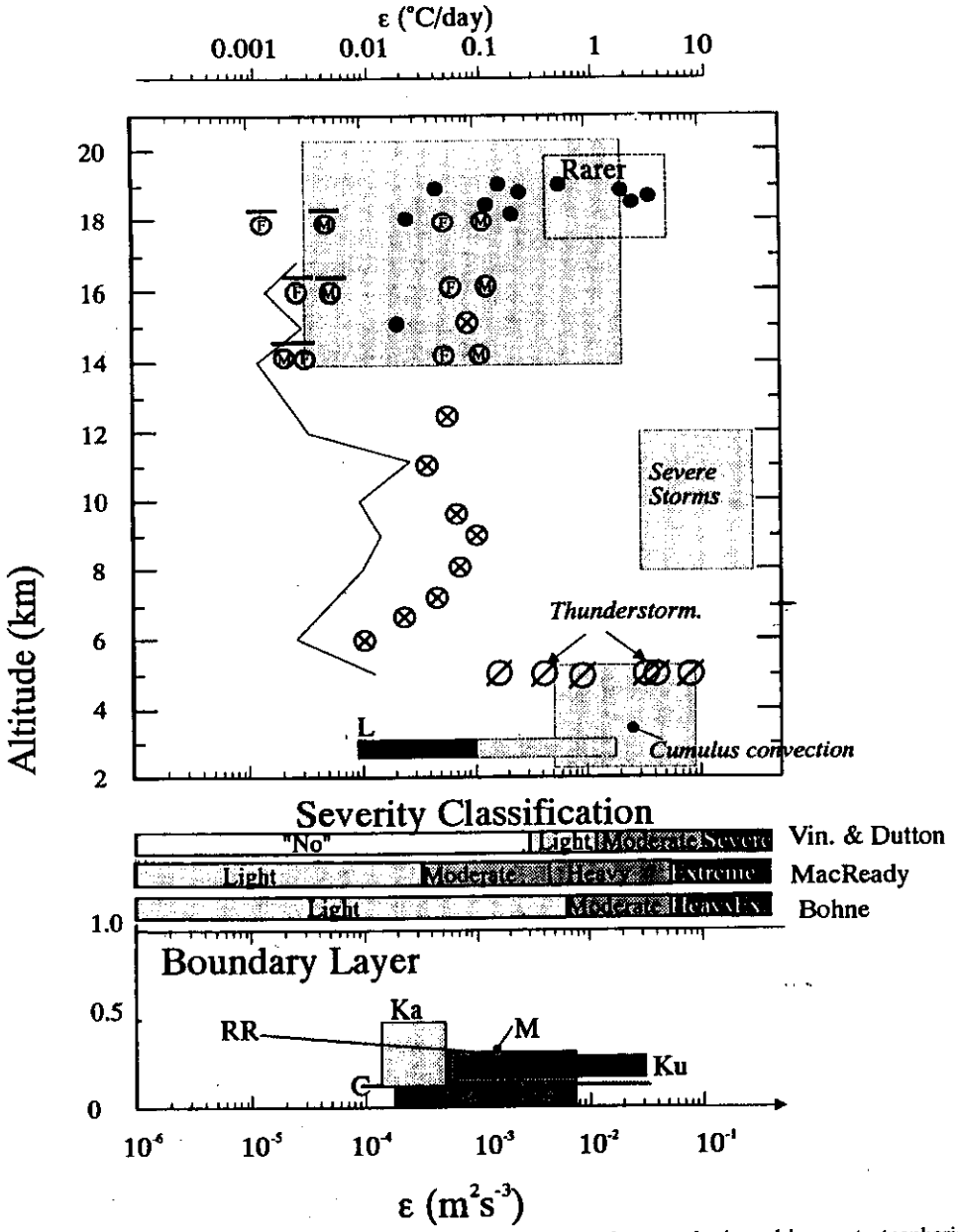

Fig. 1. Presentation of a variety of mainly *in-situ* measurements of tropospheric and lower stratospheric measurements of kinetic energy dissipation rates (exceptions from *in-situ* data being Crane (1980) and Kung (1966). Note that there are scales in both $m^2 s^{-3}$ (at the base) and °C/day (at the top of the figure). Some of these data come from campaigns comparing in-situ measurements and acoustic radars and lidars, but even in those cases we have generally only presented the in-situ data. The following symbols are used:

Upper panel: (•) Vinnichenko and Dutton (1969) (*HICAT*); (–) Crane (1980); (⊗) Kung (1966); (∅), Bohne (1981), Table 2; ((F)) Lilly *et al.* (1974) (over flatlands and water); ((M)) Lilly *et al.* (1974) (over mountains). The long black rectangle denoted "*L*" refers to Lee *et al.* (1988), Fig. 2, with about 90% of the data being in the black region. The large shaded rectangles are summaries of the results of Chen (1974). Note that the data taken from Lilly *et al.* (1974) are plotted in two ways: the data with the overbar refer to averages over all space and time, with laminar regions included in the average as zero energy dissipation rate, whilst the points without the overbars refer to average values calculated exclusively from actual turbulent layers.

Lower panel (Boundary Layer): (RR) Readings and Rayment (1969); (Ka) Kaimal *et al.* (1976), Fig. 4; (C) Caughey *et al.* (1978) (Ku) Kunkel *et al.* (1980), Table 2; (M) Mousley *et al.* (1981).

The severity classifications shown are from Table 2, and from Lee *et al.* (1988), Table 4.

128

Table 1. Approximate rates of occurrence of turbulence intensities as presented by Vinnichenko *et al.* (1973), Table 2.

Typical ε $m^2 s^{-3}$	Percent occurrence
1.0×10^{-4}	89%
30×10^{-4}	7.8%
80×10^{-4}	3.0%
700×10^{-4}	0.09% (storms etc.)

Table 2. Approximate range of turbulence intensities as categorized by Vinnichenko and Dutton (1969).

Category	ε $m^2 s^{-3}$
no turbulence	$< 30 \times 10^{-4}$
light turbulence	$> 30 \times 10^{-4}$ and $< 120 \times 10^{-4}$
moderate turbulence	$> 120 \times 10^{-4}$ and $< 10^{-1}$
severe turbulence	$> 10^{-1}$

that the distribution of strengths of turbulence followed that shown in Table 1. In classifying ε values, Vinnichenko and Dutton (1969) considered energy dissipation rates as falling within four categories (as generally reported on the basis of reactions of aircraft encountering the turbulence) which they termed 'no', 'light', 'moderate' or 'severe' turbulence, according to the values specified in Table 2. In the same year Trout and Panofsky (1969), using the geometric mean values of measured energy dissipation rates from different sources, associated 'no', 'light', 'moderate' and 'severe' turbulence with ε values of 1.5×10^{-4}, 30×10^{-4}, 85×10^{-4} and 675×10^{-4} $m^2 s^{-3}$, respectively. All these measurements of ε were made using clear-air turbulence spectra. The nomenclature of 'no', 'light', 'moderate' and 'severe' is of course somewhat subjective, but these authors felt that the values cited were appropriate levels. However, they noted that values within typically $\pm 50\%$ of the quantities quoted could be equally representative of each category. In Fig. 1, we show not only the classification scheme due to Vinnichenko and Dutton (1969), but also two more recent schemes denoted by 'Macready' and 'Bohne'. Both schemes were taken from Lee *et al.* (1988), Table 4. The discrepancies between the schemes are clear, indicating the subjective nature of these classification schemes. We generally follow the scheme of Vinnichenko and Dutton (1969). We draw on these classification schemes, together with Fig. 1, in our subsequent measurements of ε utilizing C_n^2.

THE RELATION BETWEEN C_n^2 AND ε—REVIEW OF THEORIES

Theoretical studies of turbulence have concentrated somewhat on scales which are somewhere within the *inertial subrange*. In this family of scales, the turbulence is assumed to be isotropic; that is, the statistical properties of turbulent motions are independent of direction. For VHF radars, the spatial scale $l = \lambda/2$ which determines the backscattering from isotropic turbulence (the so-called Bragg scale) will generally fall within the *inertial subrange* up to lower mesospheric heights, particularly if the radar returns originate from regions of moderate to violent mixing and turbulence (Hocking, 1985). Within the troposphere, where most of our radar studies concentrate, the inertial range approximately covers the range from a centimetre or so for the inner scale out to several hundred metres for the buoyancy scale (e.g. see Hocking, 1985, Fig. 1; Strauch *et al.*, 1986). This fact allows us to utilize these well established inertial-range theories about turbulence in our determinations. The salient points of these theories will now be discussed.

Throughout this article, we consider only the case of backscatter of radio signals caused by inhomogeneities produced by turbulence. We recognize that there are other physical processes that can generate refractive index fluctuations which may in turn cause radio wave backscatter, but such processes generally involve production of horizontally aligned entities like specular reflectors (e.g. Gage and Green, 1978; Röttger and Liu, 1978; Tsuda *et al.*, 1986; Hocking *et al.*, 1990, 1991). We can therefore avoid consideration of these in our radar work by dealing only with off-vertical radar beams in all of our studies, so henceforth we do not discuss these reflectors in any more detail.

The refractive index structure constant C_n^2 is a measure of the variability of the refractive index field. It can be measured directly with a radar of the type used in these studies, once the radar system has been calibrated properly. The calibration procedure is described shortly but, once the absolute value of the transmitter power and received power are known, C_n^2 is deduced through the relation

$$\overline{C_n^2} = 66.4 \frac{P_R z^2 \lambda^{1/3}}{P_T A_{Rm} e_R^2 \alpha (0.5L)} \qquad (1)$$

where P_R is the received power, z is the distance to the scatterers from the radar, λ is the radar wavelength, P_T is the transmitted power, A_{Rm} is the radar's effective area, e_R is a loss factor which describes power losses in the cables, transmitter and receiver of the system, α is a factor describing how the true gain of the radar beam differs from the ideal directivity (α is generally close to 1), and L is the actual transmitted pulse length (so that $0.5L$ is the effective pulse length) e.g. Hocking (1985), equation (35). Cohn (1994) investigated and generally verified the $\lambda^{1/3}$ dependence. Some authors

use the signal-to-noise ratio to determine the received power, using values for the noise level based on known strengths of extraterrestrial noise, but we prefer an absolute calibration of the system using a standard noise source because it is more accurate and less susceptible to variations in ionospheric absorption and the effects of man-made noise.

C_n^2 is sometimes used as a crude measure of the intensity of turbulence, because the more violent the turbulent mixing, the more intense are the fluctuations associated with the inhomogeneities in the refractive index field. However, as pointed out by Ottersten (1969), use of C_n^2 as an estimate of the intensity of turbulence will only be valid when there exists a strong correlation between the vertical gradient of the potential refractive index M and the mean vertical wind shear $d\bar{u}/dz$, in which case C_n^2 is roughly proportional to $\varepsilon^{2/3}$ (see shortly). This is sometimes not true. It is far better to use radar measurements of C_n^2 to deduce estimates of ε, since the latter is a more reliable estimator of the strength of the turbulence. However, the conversion from C_n^2 to ε is complicated by the fact that the relation depends on the mean potential refractive index gradient, M, which itself depends on the potential temperature gradient and the variation of the humidity as a function of height.

The equation for the gradient of the radio index of refraction is given by (e.g. Tatarskii, 1961; Vanzandt *et al.*, 1978; Gossard *et al.*, 1984):

$$M = -77.6\times10^{-6}\frac{P}{T}\left(\frac{\partial \ln\theta}{\partial z}\right)\times\left[1+\frac{15500q}{T}\left(1-\frac{1}{2}\frac{\partial \ln q/\partial z}{\partial \ln\theta/\partial z}\right)\right] \quad (2)$$

where z is height, θ is the potential temperature, q is the specific humidity, T is the absolute temperature and P is the atmospheric pressure in millibars. The term in square brackets was denoted as χ by Vanzandt *et al.* (1978); indeed this particular form of the equation was first introduced by these authors. Note that χ tends to 1 as the humidity terms tend to zero. In the lower troposphere M depends very much on the humidity gradient and the potential temperature gradient, both of which vary considerably, so it is not usually accurate to interpret C_n^2 as a direct measure of turbulence intensity. Since ε is a more direct measure of turbulence severity, it is this parameter which we seek.

Before giving explicit expressions for ε, however, we first need to discuss the type of energy dissipation rates which we can measure. The radar volume (i.e. the volume defined by the radar beam-width and the pulse length) is generally not filled with turbulence, at least for radars with pulse lengths of 500 m–1 km. Usually only a fraction F of the radar volume is filled with turbulence, so that the backscattered power is only produced by scatter from within a portion of the radar volume. Hence when we use measurements of C_n^2 to estimate the intensity of turbulence, we are actually determining an average over the radar volume. Thus henceforth we write the measured energy dissipation rates and structure function constants with an overbar, to emphasize that they represent a spatial average. This has not been necessary until now because we have been discussing C_n^2 and ε in general terms.

An expression relating the mean energy dissipation rate per unit mass $\bar{\varepsilon}$ and the mean refractive index structure constant $\overline{C_n^2}$ is (Vanzandt *et al.*, 1978; Gage *et al.*, 1980)

$$\bar{\varepsilon} = \left(\gamma\overline{C_n^2}\frac{\omega_B^2}{F^{1/3}}M^{-2}\right)^{3/2} \quad (3)$$

where ω_B is the Brunt Väisälä frequency ($\omega_B^2 = g(\partial\ln\theta/\partial z)$). The parameter F represents the fraction of the radar volume which is filled by turbulence, while γ is a constant to be discussed in much more detail shortly. Vanzandt *et al.* (1978) used a value of $\gamma \simeq (0.7)^{-1}$, but other variations are seen, some which even suggest that γ is not a constant.

On substituting for M in (2), we obtain

$$\bar{\varepsilon} = \gamma^{3/2}2.01\times10^{15}\left(\frac{T}{P}\right)^3\left(\frac{\overline{C_n^2}}{F^{1/3}\omega_B^2}\right)^{3/2}\chi^{-3}, \quad (4)$$

where χ is given by the expression

$$\chi = \left[1+\frac{15500q}{T}\left(1-\frac{1}{2}\frac{\partial \ln q/\partial z}{\partial \ln\theta/\partial z}\right)\right]. \quad (5)$$

Sometimes we write (4) as

$$\bar{\varepsilon} = C_t\left(\frac{T}{P}\right)^3(\overline{C_n^2})^{3/2}\chi^{-3}, \quad (6)$$

where $C_t = \gamma^{3/2}\times2.01\times10^{15}(F^{1/3}\omega_B^2)^{-3/2}$. Values of C_t are tabulated later.

Assuming that turbulence is the cause of the radar scatter, and assuming that pressure, temperature and humidity measurements are available from radiosondes, equation (4) (or (6)) and (5) permit determination of the kinetic energy dissipation rate from measurements of the radar-derived refractive index structure constant. The above relationships are not new, having been used in several presentations over recent years. For example, preliminary estimates of typical intensities of turbulence were reported by

/30

Crane (1977, 1980), who compared radar observations of C_n^2 with simultaneous measurements of temperature, humidity and pressure obtained from radiosonde soundings. Subsequent models which compare radar-derived measurements of C_n^2 with radiosonde data have become more sophisticated, the most complete being those by Vanzandt *et al.* (1978), Gage *et al.* (1980), Vanzandt *et al.* (1981), Fairall *et al.* (1991), and Gossard *et al.* (1982, 1984, 1985). Other experimental reports using adaptations of these formulae include ones by Hocking *et al.* (1989), Cohn (1995) and Jain *et al.* (1995).

However, despite the apparent similarities of these works, there are in fact fundamental differences. Each of these articles made different assumptions in their derivations of ε, the major variants being the ways in which 'F' and 'γ' were treated. Different articles used different values for γ, with some even taking it to be dependent on the Richardson number R_i (which is the Brunt–Väisälä frequency squared divided by the square of the vertical shear in the horizontal vector wind). Many authors (in fact most) did not even consider the fraction F, in effect assuming it to be 1.0. It is important to intercompare these different hypotheses; we begin by examining the 'constant' γ.

The 'constant' γ

Vanzandt *et al.* (1978) used the equation $\varepsilon = b(\mathrm{d}u)/(\mathrm{d}z)^3\, L^2$, where L is the 'outer scale' of the turbulence and $(\mathrm{d}u)/(\mathrm{d}z)$ is the shear in the mean wind, in their derivations. They assumed that $b = 1.0$ in deriving equation (3). However, subsequent studies have suggested that b is not 1.0 (e.g., see Hocking, 1992), and estimates of ε obtained by equation (3) may be over-estimates by a factor of up to 6 times if the Vanzandt *et al.* (1978) value of γ is used. But the discrepancy becomes even more serious than this. Several authors have provided proofs that γ is a function of Richardson number. In essence, this dependence arises because C_n^2 is related to the potential energy contained in the turbulence, whereas ε is a measure of the kinetic energy, so that the interrelationship between them depends on the ratio of kinetic to potential energy in the turbulent region. To give an extreme example, if the Brunt–Väisälä frequency is zero (so that the Richardson number is zero) then there can be no potential energy contained in the displaced eddies, but the kinetic energy can be quite high, giving zero for the ratio of potential divided by kinetic energy. Clearly the potential energy is not zero for other choices of R_i, so it seems that this ratio must be Richardson number dependent. Thus since the relationship between C_n^2 and ε depends on the ratios of potential to kinetic energy, and since this ratio is Richardson number dependent, it might not be surprising to find that γ could depend on the Richardson number.

Examples of references which demonstrate this Richardson number dependence include Ottersten (1969), Crane (1980), Gossard *et al.* (1982, 1987) and Hocking (1992). For example, Ottersten (1969) gives

$$\gamma = \frac{1}{a^2}\left(\frac{1-R_f}{R_i}\right) = \frac{1}{a^2 P_r}\left(\frac{P_r - R_i}{R_i}\right) \tag{7}$$

where a^2 is a constant, R_i is the gradient Richardson number, R_f is the flux Richardson number (Plate and Arya, 1969), and $R_f = P_r^{-1}\, R_i$, P_r being the turbulent Prandtl number, K_m/K_T, where K_m and K_T are the turbulent momentum and heat diffusion coefficients, respectively. Gossard *et al.* (1982, 1984) present an expression in which γ effectively obeys

$$\gamma = \frac{1}{B_\theta}\,\frac{P_r - R_i}{R_i} \tag{8}$$

where $B_\theta = 3.2$. Sengupta *et al.* (1987) produce an even more complex version of equation (3) which includes a correlation coefficient between temperature and humidity perturbations (their equation (21)). However, they then assume that this correlation coefficient is 1.0, which reproduces equation (3) with γ identical to the last equation.

Hocking (1992) assumed to first order a turbulent Prandtl number of unity and obtained, via energy balance arguments, the following expression for γ:

$$\gamma = \frac{3}{22}\,\frac{|1-R_i|}{|R_i|} \tag{9}$$

All these values differ but, even more importantly, some differ from the assumption that γ is a constant. Which γ should we adopt? The apparent discrepancy between an assumed constant for γ and the Richardson number dependence also intrigued Gossard and Frisch (1987), and they designed experiments to test the hypothesis that P_r might adjust as the Richardson number varied in such a way that $(P_r - R_i)/R_i$ remains constant. Figure 2, from Gossard and Frisch (1987), shows the results of their studies and of others before them. It is clear that the turbulent Prandtl number does seem to vary as a function of Richardson number, but it is not really clear that the relationship can be easily described by a simple function. Gossard and Frisch (1987) claimed that the data approximately obey the relation

$$\frac{B_\theta}{B_w}\,\frac{R_i}{P_r - R_i} \simeq \left(\frac{g\overline{\theta^2}}{\theta_0 \overline{w^2}}\right)\Big/\left(\frac{\partial \theta_0}{\partial z}\right) \simeq 1/2.2 \tag{10}$$

where $B_u \simeq 2.7$ and $B_\theta \simeq 3.2$. This corresponds to a value of γ of 0.81. The quantity between the two '$\simeq$' symbols in equation (10) is also proportional to the ratio of potential to kinetic energy in the turbulent patch (see Hocking, 1992).

Equation (10) is plotted in Fig. 2, but it is clear that this equation is only an approximation. Indeed, for values of R_i less than about 0.1, it is just as good (if not better) to simply take $P_r = 1.0$ (with a maximum error of about 30%). To compound matters even further, the measurements presented by Gossard and Frisch (1987) were essentially only boundary layer measurements, because they were made with an instrumented tower. Sidi and Dalaudier (1990) measured the same quantity in the upper troposphere and lower stratosphere, and found different values yet again for γ; specifically, they obtained $\gamma \simeq 0.21$ and $\gamma \simeq 0.36$ in the lower stratosphere and upper troposphere, respectively—and all estimates have associated large error bars. The theory presented by Gossard and Frisch (1987) predicted $\gamma \simeq 0.25$.

Of course none of these approximations is better than actually being able to measure both R_i and P_r, but this is generally not possible. Before deciding about the best possible choice of γ, we examine how important it is to include the Richardson number dependence of γ if it is at all feasible—especially for Richardson numbers in the range between 0 and 0.25.

Thermosonde studies and the importance of the Richardson number

In order to examine the importance of this Richardson number dependence of γ, we now turn to some data collected using thermosondes carried on balloons. The data were provided to us by James H. Brown (personal communication), and arise from a series of high resolution measurements of the temperature structure function constant, C_θ^2. Specifically, the turbulence probe was comprised two very sensitive fine wires (which acted as cold wire temperature-dependent resistive elements) separated by one metre; the temperatures measured by the two wires were differenced and squared to give the structure function value at a separation of one metre. The structure function is given by $C_\theta^2 r^{2/3}$ in the inertial range of turbulence, so that at a separation of one metre the structure function is equal to C_θ^2. For compatability with optical C_n^2 data, the values of C_θ^2 were then converted to C_n^2 by dividing by $(80 \times 10^{-6} \times P/T^2)^2$ (see Brown *et al.* (1989) for more details). Note that this conversion produces in effect an optical C_n^2, since it does not deduce a contribution caused by to the humidity term.

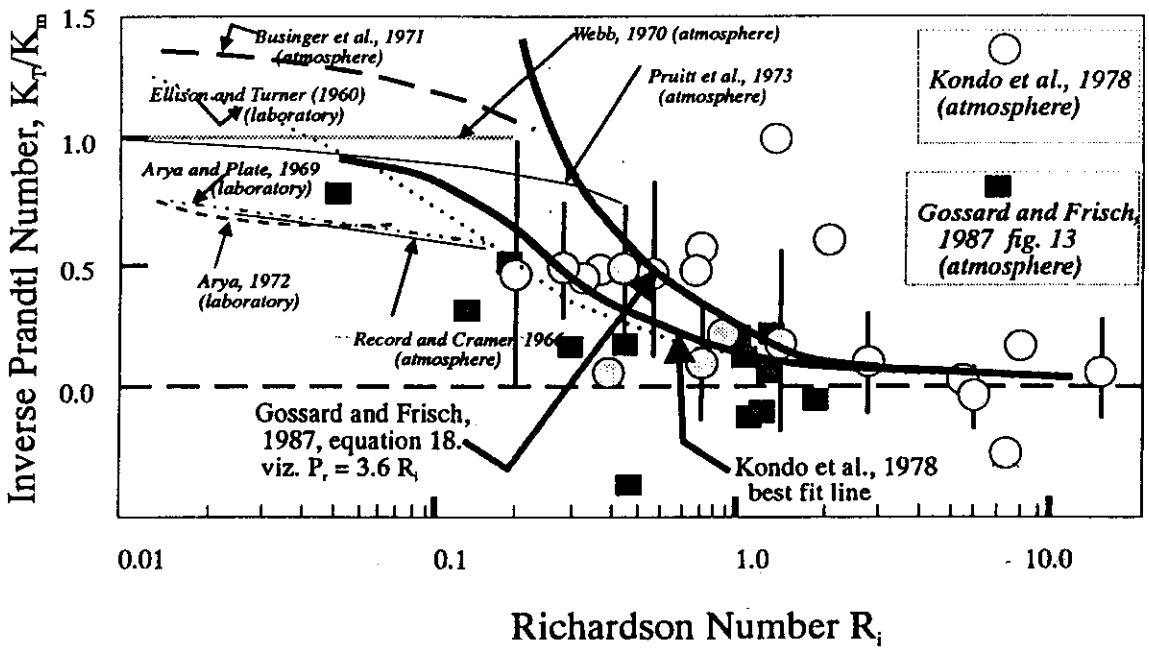

Fig. 2. Graphs of the inverse turbulent Prandtl number P_r^{-1} plotted as a function of gradient Richardson number R_i, from a variety of references (from Gossard and Frisch, 1987). Also shown are proposed curves by Kondo *et al.* (1978), and Gossard and Frisch (1987), equation (18). One point by Gossard and Frisch (1987), with $P_r^{-1} = 26$ at $R_i = -0.3$, is not presented.

132

However, this is not a drawback—in fact it would probably have been just as useful to leave the data as C_0^2, rather than converting to C_n^2 at all. Nevertheless, the conversion does permit us to make crude comparisons with the radar data later on. Simultaneous high resolution measurements of winds and temperatures were also available, so that the Brunt–Väisälä frequency and gradient-Richardson number could also be evaluated.

Figure 3 shows data from flight L4035 at Penn State University on 30 April 1986, 23:06 local time. The values of C_n^2 (optical) are shown to the left, while the Richardson number profile is shown in the middle. The panel to the right, of most interest to us here, shows two separate estimates of ε, using equation (4) but with F set to 1.0 (and of course $\chi = 1.0$, since we are only interested in optical C_n^2). The approximation $F = 1$ is quite valid because of the very high resolution of the studies.

We have used two values for γ. First, the discrete dots use a value of $\gamma = 0.4$, which we have chosen as the average of the four values quoted from different references earlier (viz. average of 0.81, 21, 0.36 and 0.25). While not based on any strong physical reason, this value does ensure that our estimates of ε agree with all the previous theories to within a factor of 3 or less; it is also closer to the 'upper atmosphere' values of Sidi and Dalaudier (1990), which are probably more appropriate once we leave the boundary layer. It is also interesting that this exactly matches the value proposed for γ by Hocking (1992) for the special case $P_r = 1.0$ and $R_i = 0.25$.

The continuous line in this figure uses a value of γ equal to (3)/(22) ($|1 - R_i|/|R_i|$) (see equation (9)); we have set γ to zero if R_i exceeds 1.0. This has been done because layers with $R_i > 1$ are in general not active turbulence, but rather decaying turbulence; we wish to emphasize the most active layers. Note that this choice for γ effectively assumes that $P_r = 1.0$—but, as seen in Fig. 2, this is a reasonable approximation out to $R_i = 0.2$, being in error by no more than a factor of two even at $R_i = 0.25$.

The profiles are clearly different, and we highlight several important features. First, consider layer 'A'. Note that when we use $\gamma \simeq 0.4$, the layer seems to be very weak. But when we use the second formulation for γ, we see a layer of turbulence with a strength approaching $10^{-2}\,m^2s^{-3}$—a layer of 'moderate' mechanical turbulence and quite dominant in the figure. It seems very likely that the second situation is the true one—indeed the assumption that γ equals a constant quite clearly breaks down for $R_i < 0.2$, as can be seen

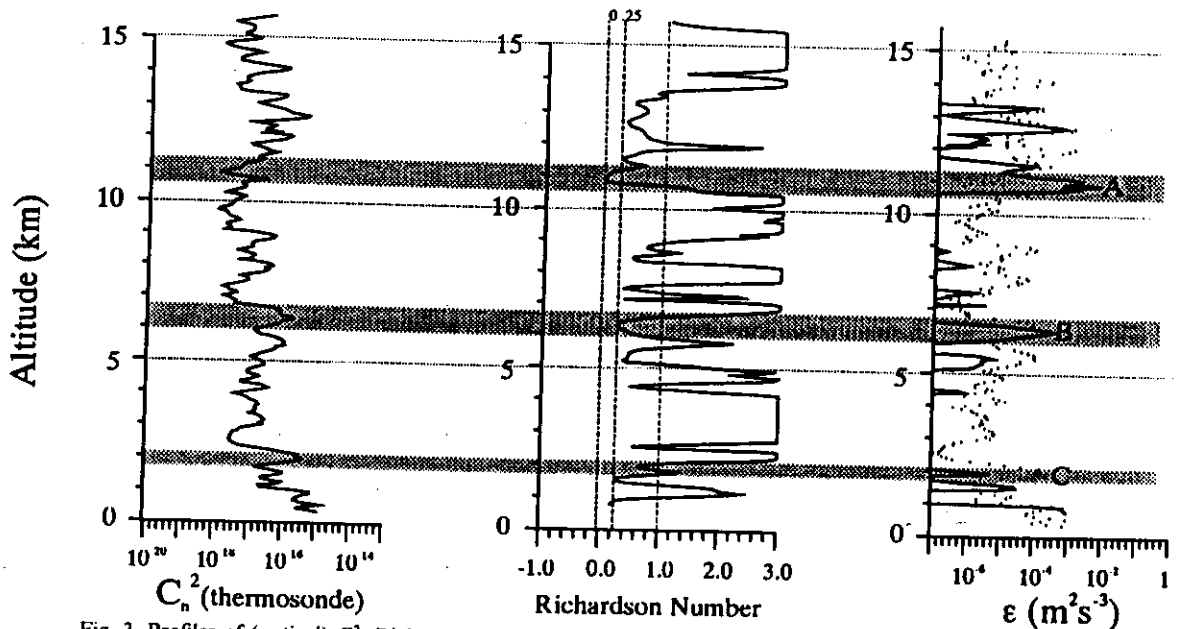

Fig. 3. Profiles of (optical) C_n^2, Richardson number, and two different estimates of the turbulent energy dissipation rate, using data from a balloon flight (courtesy of James H. Brown (private communication)). The balloon carried a pair of thermosondes separated by one metre for estimation of C_n^2, plus other high resolution instrumentation. The layers denoted by 'A', 'B' and 'C' are especially important, and are discussed in the text.

by the departure of the data from the line denoted by 'Gossard and Frisch, equation (18)' in Fig. 2. Since the Richardson number is very close to zero in this case, we can no longer expect an approximately constant value of γ. We also expect the layer to be quite active because of the low Richardson number—but it does not show strongly in the C_n^2 profile because the turbulence is embedded in a layer which is almost adiabatic (either driven that way by the turbulence or pre-existing that way before the turbulence was created). As a consequence, a parcel of air in this layer will show no (or at least little) deviation in temperature from its surroundings when displaced vertically, thereby producing a zero value for the temperature perturbations and therefore for the temperature structure function. This is a weakness of using thermosondes of this type to look for mechanically turbulent layers—they cannot 'see' layers embedded in an adiabatic temperature profile—and these are often the strongest and most active layers. Similar problems can arise with radars—it is quite possible for C_n^2 to be zero in a very active layer which has an adiabatic temperature profile. However, as seen from equation (2), this requires *both* a zero potential temperature gradient *and* a zero gradient in relative humidity, which is a less likely event whenever there is some humidity around. It is much more likely in the stratosphere.

Before proceeding, we make one further point about the thermosonde. The experiments for which this instrument was designed were involved with searches for layers of so-called 'optical turbulence'. These are layers of turbulence which cause significant fluctuations in optical refractive index and which substantially disturb the phase fronts of light waves passing through them. They destroy viewing conditions for astronomical studies, and interrupt the passage of other types of light such as laser radiation. For such studies, the value of C_n^2 (optical) is more important than ε, so the thermosondes are clearly well suited to this purpose. Our point here is not to discredit these instruments, but merely to note that they can also be used to measure the mechanical strength of turbulence, provided that care is taken. We have indicated the type of care required in such calculations.

We now return to our discussion about the layer of turbulence denoted by 'A', and make two main points. First, it is important to include the Richardson number dependence of γ in determinations of ε, especially in cases where the Richardson number is close to zero (<0.2). Second, it is quite possible that low values of C_n^2 can correspond to very active regions of mechanical turbulence, a possibility which must always be borne in mind.

Two other layers were highlighted in Fig. 3. Layer 'B' is a case where the Richardson number exactly equals 0.25; it is seen that the two different formulae used for γ produce identical estimates of γ. Finally, layer 'C' is a case where a layer of large C_n^2 appears. By using $\gamma = 0.4$, it would appear that this is a layer of relatively strong turbulence (dots) but, when we use equation (9), we see that the layer is very weak indeed; the only reason that it shows so well is that the potential temperature gradient is very strong, so that even a modest displacement of a parcel of air vertically produces a large difference between the temperature of the parcel and its immediate environment, thereby making for large C_θ^2 values.

The C_n^2 — ε relation in radar work

Despite the lessons learned in the last section, we (and indeed most radar investigations of ε) do not have sufficient resolution, or indeed sufficient supplementary equipment, to enable the Richardson number to be determined to resolutions of a few metres; generally such radars have resolutions of a few hundred metres. In the results to be presented, our radar had a vertical resolution of about 0.5 km, while our wind measurements had a vertical resolution of 500–1000 m. We therefore must adopt the procedure of taking γ equal to a constant, which we propose to be $\gamma = 0.4$, as used in the last section, a compromise between the various values proposed by various authors. We regard (3) and (4) as being accurate to within a factor of 2–3 or so. Nevertheless, it is still possible to determine the general variation of ε with time. The level of accuracy deduced in our calculations is still sufficient to classify the turbulence according to Table 2, given that the energy dissipation rate is a quantity with a large natural variability.

We noted that, with the thermosondes, a zero potential temperature gradient means that the thermosonde sees no fluctuations in temperature. For radars, the problems related to such 'transparent' layers are not quite as serious as those for thermosondes, because even if the temperature gradient is adiabatic it is possible that the humidity gradient may be non-zero, thereby still allowing the radar to illuminate the layer. However, it could well be that layers might exist in which both the potential temperature and the humidity have zero gradients. This might especially be true in very well mixed layers, where the turbulence itself might drive both quantities to be uniformly mixed within the layer. At upper heights, where q itself approaches zero, the problem may well be worse.

There is little that we can do at this stage except to recognize that the problem exists. Future simultaneous high resolution and radar studies are needed to determine the frequency of occurrence of such layers.

The filling factor, F

We now turn to a more detailed discussion of the filling factor F. Determination of F is generally not possible directly, so it is here that the theory of Vanzandt *et al.* (1978), 1981 becomes especially important. These papers developed a relation between the fraction F and kilometre-scale wind shears and temperature gradients, so that F can be estimated from radar and radiosonde data.

Aircraft measurements were used to show that F lies in the range $0.01 < F < 0.1$ (Gage *et al.*, 1980), but no aircraft measurements were available in our experiment. Using the statistical model proposed by Vanzandt *et al.* (1978), Gage *et al.* (1980) treated the product $F^{1/3}\,\omega_B^2$ as a single parameter, and determined it by the relation

$$F^{1/3}\omega_B^2 = \frac{\sigma_\mu^2}{4} F^{1/3}\tau_c^2 \qquad (11)$$

where σ_μ^2 is the variance of the microshear, i.e. the variance of the wind shears at scales much less than the radar vertical resolution. We analyze our data in 'layers', where the layer thickness is typically chosen to be equal in depth to the pulse-length of the radar (about 0.5 km). According to Vanzandt *et al.* (1978) and Gage *et al.* (1980), σ_μ is equal to $0.010\,s^{-1}$ in the troposphere. The parameter τ_c is the normalized critical shear which is defined as (s_c'/σ_μ), where s_c' is the critical shear defined as the windshear value which must co-exist with the existing temperature profile in order to produce a Richardson number of 0.25 within the layer under consideration.

In our radar experiments, we took some pains to measure F. The quantities F and $F^{1/3}\,\omega_B^2$ were evaluated in the following way, following Vanzandt *et al.* (1978). First, radiosonde data were used to produce plots of temperature and horizontal winds as a function of height. The wind data had only about 500 m–1 km resolution, whilst the temperature was displayed with a resolution of about 50 m. A detailed profile of the Brunt–Väisälä frequency as a function of height was then obtained from the temperature data. Both the temperature profile and the Brunt–Väisälä frequency profile were then convolved with a Gaussian function with a width of about 500 m or 1 km (depending on the radar pulse length which was being used by the radar at the time of the experiment), in order to make them compatible with the radar and wind data. Examples of both smoothed and unsmoothed profiles of ω_B^2 are shown in Fig. 4. The 'critical shear' at which turbulence is expected was then determined using $s_c^{2'} = 4\omega_B^2$. Finally, F was determined by evaluating the integral described in equation (10) of Vanzandt *et al.* (1978), which essentially determines the probability of turbulence occurring in the radar volume for the measured values of the mean wind-shear s and the Brunt–Väisälä frequency. The procedure is based upon the assumption that turbulence will exist wherever the

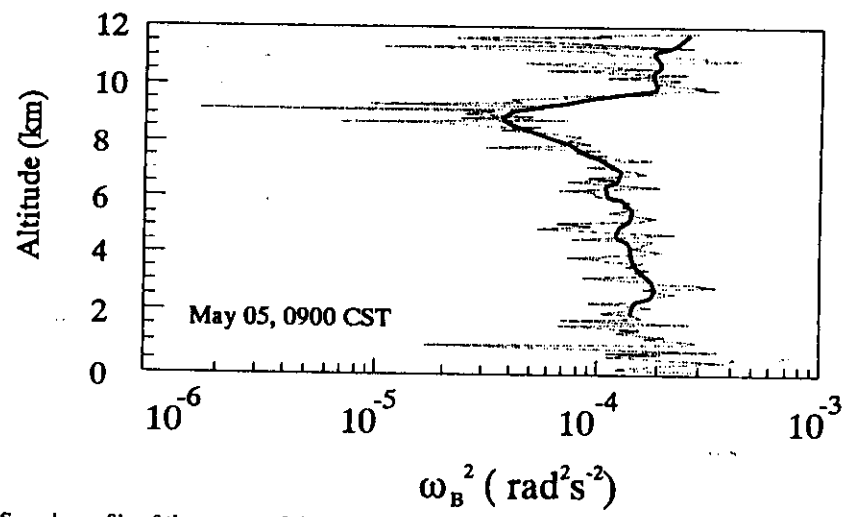

Fig. 4. Sample profile of the square of the Brunt–Väisälä frequency, in this case for a radiosonde flight at 09.00 on 5 May 1991. The dash–dot profile shows the data at 50 m resolution, and the solid line shows the result of convolving the high resolution data with a Gaussian function of approximate width 1 km.

Richardson number is locally less than 0.25. We also note that, whilst the radar was capable of measuring the eastward component of the winds by Doppler methods, we could not measure the northward component because the beam could not be steered in that direction. Hence we mainly use the radiosonde winds in all our analyses.

We evaluate both F and $F^{1/3}\,\omega_B^2$; the latter quantity varies only slightly for different atmospheric conditions, so that equation (4) is a fairly robust equation with respect to calculation of $F^{1/3}\,\omega_B^2$. Finally, we note that, since the 'original' model of Vanzandt *et al.* (1978) was proposed for the calculation of $\overline{C_n^2}$ in the free atmosphere, there were two subsequent models which are improvements to the original; they are Vanzandt *et al.* (1981) and Warnock and Vanzandt (1985), the latter of which deals principally with improvements in the application of numerical techniques. We feel that comparisons with the original model are adequate for the purposes of the current study.

RADAR DATA—EXPERIMENTAL PROCEDURES AND RESULTS

We now turn to a discussion of a series of combined radar and balloon measurements of ε using the Adelaide VHF atmospheric radar. We utilize equation (4) and equation (5) to determine this quantity, with $\gamma = 0.4$ as discussed above. In addition, we evaluate F using numerical calculations based on the original statistical model of $\overline{C_n^2}$ by Vanzandt *et al.* (1978).

The following discussion focuses on the results from observations made using the 54.1 MHz Doppler radar at Buckland Park, South Australia (35°S, 138.5°E). Equation (4) forms the basis of our derivations, which we apply using radar measurements of $\overline{C_n^2}$ and radiosonde measurements of T, P and q to determine ε. We also examine the degree of correlation between profiles of $\overline{C_n^2}$ and M. This is especially important in determining the likely effects of variations in χ near the radar and near the radiosonde. We note that accurate estimates of χ are necessary for reasonable application of equation (4). In conditions of low humidity, χ is close to 1, so that equation (4) is particularly easy to apply. Unfortunately, conditions of low humidity prevail only occasionally in the troposphere, though $\chi \sim 1$ occurs more generally in the stratosphere. In this work we use balloon measurements to determine χ. Provided that atmospheric conditions near the radar are not too different to those near the radiosonde, radiosonde estimates of χ lead to quite reasonable estimates of ε over the radar.

Instrumentation

The radar, described in some detail by Vincent *et al.* (1987), functioned as a narrow beam Doppler radar with a one way half-power half-width of 1.6°. The radar beam was generally pointed at 11° off-vertical (usually to the West), in order to eliminate the effects of specular reflections (e.g. Gage and Green, 1978; Röttger and Liu, 1978; Tsuda *et al.*, 1986; Hocking *et al.*, 1990, 1991). The typical pulse repetition frequency was 4096 Hz, and coherent integration was performed over 1024 successive points. The peak power transmitted was 40 kW. The radar was calibrated carefully for absolute determination of signal strengths before use by using a noise generator as a reference (e.g., see Cohn (1994) for a discussion on calibration procedures). The efficiency of the radar system was determined by comparing the strength of radio sky noise received by the system to that received with a single, accurately matched dipole, during periods when there was no dominant VHF radio source at the radar frequency in the sky (This ensured that the received VHF skynoise was moderately isotropic in nature.). The efficiency factor of the radar was determined to be about 40%, a factor which was used to convert the received signals to absolute values of $\overline{C_n^2}$. We emphasize that the skynoise measurements were only used to determine the efficiency of the radar; $\overline{C_n^2}$ itself was found by proper calibration using a noise source (e.g., see Cohn, 1994).

Whilst Gage *et al.* (1980) discussed the possibility of using climatological values for T and P in their determinations of ε, we prefer to use radiosonde data (specifically temperature, humidity and horizontal wind speed) coupled with the radar data to improve our accuracy. Determination of χ is especially important. The radiosondes were flown by the Adelaide Weather Bureau from Adelaide airport, some 35 km South of the radar site (see Figs 5 and 6). The analysis presented here is a case study of three mornings and three evenings of data taken during the approach and passage of a cold front in the autumn month of May 1991; significant dates and times are tabulated in Table 3.

The radiosondes used were Vaisala RS80-15 instruments, with a thermocap capacitive bead to measure temperatures, a humicap thin film capacitor to measure humidity and a capacitive aneroid to measure pressure. Temperatures were measured to a resolution of ±0.1°C, relative humidity to ±1%, and pressure to ±0.1 hPa. The respective accuracies were ±0.2°C, ±2% and ±0.5 hPa. Response times were typically 2–4 s near ground level, 5–8 s at 100 hPa (approximately 16 km altitude) and 15–25 s at 10 hPa (approximately

136

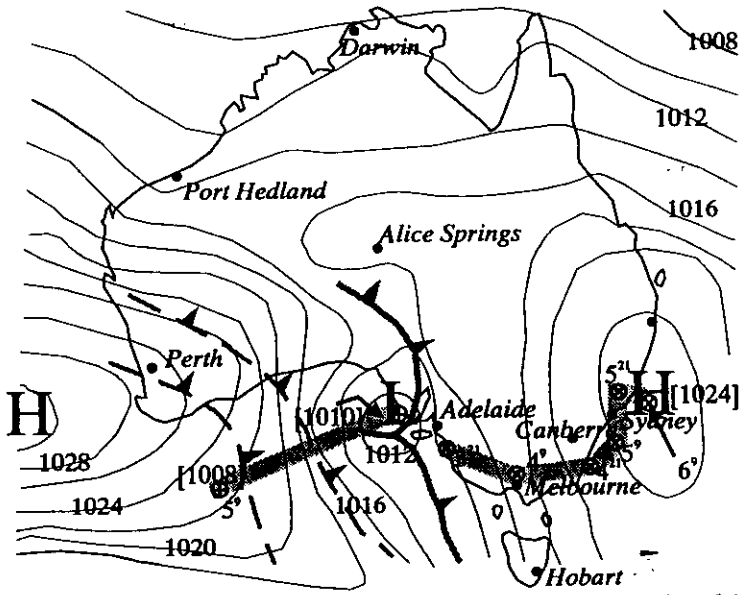

Fig. 5. Weather map for 6 May 19.91 at 09.00 local time, with trajectories of the motion of the major high and low pressure cells involved in this study. The centre of the high pressure cell on 3,4,5 and 6 May is shown as '⊗', and the low pressure's centre on 5 and 6 May are indicated by '⊕'. Numbers by the ⊗ and ⊕ indicate day numbers in May, where a superscript '9' refers to 09.00 and a superscript '21' refers to 21.00 local time.

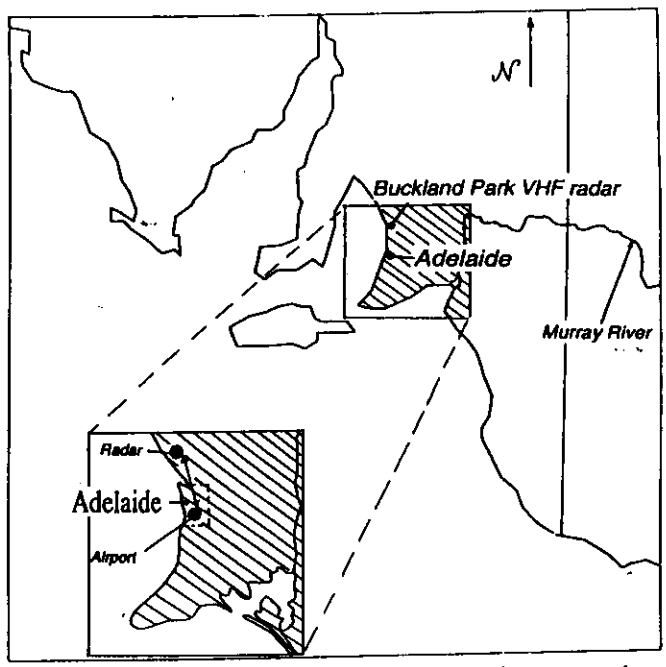

Fig. 6. Map of the area in which the experiments took place. The larger map shows southern South Australia, and the inset shows the relative positions of the radar and Adelaide airport, where the balloon launches occured. The radar and the airport were about 35 km apart.

Table 3. Values of ground-level pressure P_{grnd} (hPa), the mean vertical wind shears $\bar{s}$ (rescaled to be in units of 10^{-3} s^{-1}), the average fraction of the radar volume which is turbulent F, model parameter $F^{1/3}\tau_c^2$ and the model constant C_t divided by 10^{22} (see the line following equation (6)), tabulated as a function of time. We have used $\gamma = 0.4$, as suggested in section 3.3. Note that the quantity $F^{1/3}\omega_B^2$ can be determined simply by multiplying $F^{1/3}\tau_c^2$ by 0.25×10^{-4} (see equation 11), so we have not tabulated both quantities. Also given are the correlation coefficient r, the associated 95% confidence limits for r (denoted r_L and r_U) and the slope m of the best fit line for a scatter plot between $\log_{10}M^2$ and $\log_{10}$(power × height^2).

Troposphere Date/Time	P_{grnd}	$\bar{s} \times 10^3$	F	$F^{1/3}\tau_c^2$	$\overline{C_t}/10^{22}$	$r(r_L, r_U)$	m
3 May, 21.00 CST	1030.7	2.86	0.0371	1.5658	0.208	0.946 (0.834, 0.985)	0.9838
4 May, 09.00 CST	1020.9	2.79	0.0303	1.5734	0.206	0.469 (−0.080, 0.800)	0.4119
21.00 CST	1024.7	1.95	0.0295	1.5191	0.218	0.847 (0.574, 0.950)	0.9248
5 May, 09.00 CST	1015.9	2.25	0.0228	1.5431	0.212	0.458 (−0.122, 0.785)	0.4749
21.00 CST	1014.9	3.26	0.0300	1.6140	0.199	0.904 (0.718, 0.970)	0.7992
6 May, 09.00 CST	1019.1	3.90	0.0620	1.5847	0.204	0.917 (0.753, 0.974)	0.9605

32 km altitude). These quantities were digitized onto a personal computer at high temporal resolution and then smoothed to give data at 10 s intervals, or approximately 50 m resolution. Winds were also determined from the radiosonde by tracking the balloon by radar, but the resolution of these data was typically about 1 km.

Experimental program

The VHF radar ran continuously between 3 and 6 May 1991, but we concentrate our analysis on periods during which radiosonde flights were made. The radiosondes were actually launched at around 08.20 and 20.20 Australian Central Standard Time (Universal Time + 9:30) on each day, and the flights lasted for about 40 mins before telemetry stopped. The radar data presented here were typically determined from a 4 h wide window centred on the launch times of the balloons, where the windows generally covered the periods 07.00–11.00 and 19.00–23.00 inclusive.

During the period beginning at 09.00 CST on 3 May (Australian Central Standard Time) and ending at 21.00 CST on 4 May, a high-pressure system was the dominant feature over the region. For the latter part of the observation period, the effects of an approaching cold-front started to become important, with the high moving first in an eastward direction and then later towards the north-east. The ground level pressure readings for the six periods of study are given in Table 3, and Fig. 5 shows the general features in more detail. It also shows the paths of the centres of the high and low pressure systems which were important in this study.

Table 3 also shows a variety of parameters which summarize some important conditions for each experimental run. Quantities which are indicated by an overbar are averages over the whole height range which was recorded-typically from 2 to 8.5 km. In order to match the radar data, the 'mean shears' presented here were determined with 1 km height resolution. From the table, we see that the fractional volume that was turbulent varied from 2.3% to 6.2%, which is within the range given by Gage *et al.* (1980). In addition, the calculated values for $F^{1/3}\tau_c^2$ lie between 1.5 and 1.6 (approximately), which also agrees with their estimated value of 1.5. The fact that this parameter is so nearly constant is what makes equation (4) so useful, allowing us to estimate the turbulent energy dissipation rate with a reasonable degree of certainty. We have of course only considered a few examples, but these did cover a wide variety of atmospheric conditions. Note that we have not specifically tabulated $F^{1/3}\ \omega_B^2$ in the interests of saving space; it is proportional to $F^{1/3}\tau_c^2$, as indicated in the table caption.

An important result for interpreting the energy dissipation rate determinations is the relation between the height profiles of received power (after correction for the range, i.e. Power × z^2) and the mean square gradient of generalized potential refractive index, M^2. Whilst we have noted that equation (4) can to some extent be reduced to a dependence on climatological values, its application is improved if we use radiosonde data. Application of this technique also relies on assumed similarities between χ at the radar and radiosonde sites. Thus application of this equation becomes all the more reliable if the conditions at the radar and the radiosonde are similar. Therefore we created scatter plots in which the two variables to be compared were (i) the log of the 4 h mean range-corrected power at each height step and (ii) the log of the mean square gradient of potential refractive index as deduced from the radiosonde at the matching height step. We then calculated the correlation coefficient r and slope m between the two data sets. The correlation between M^2 and the backscattered

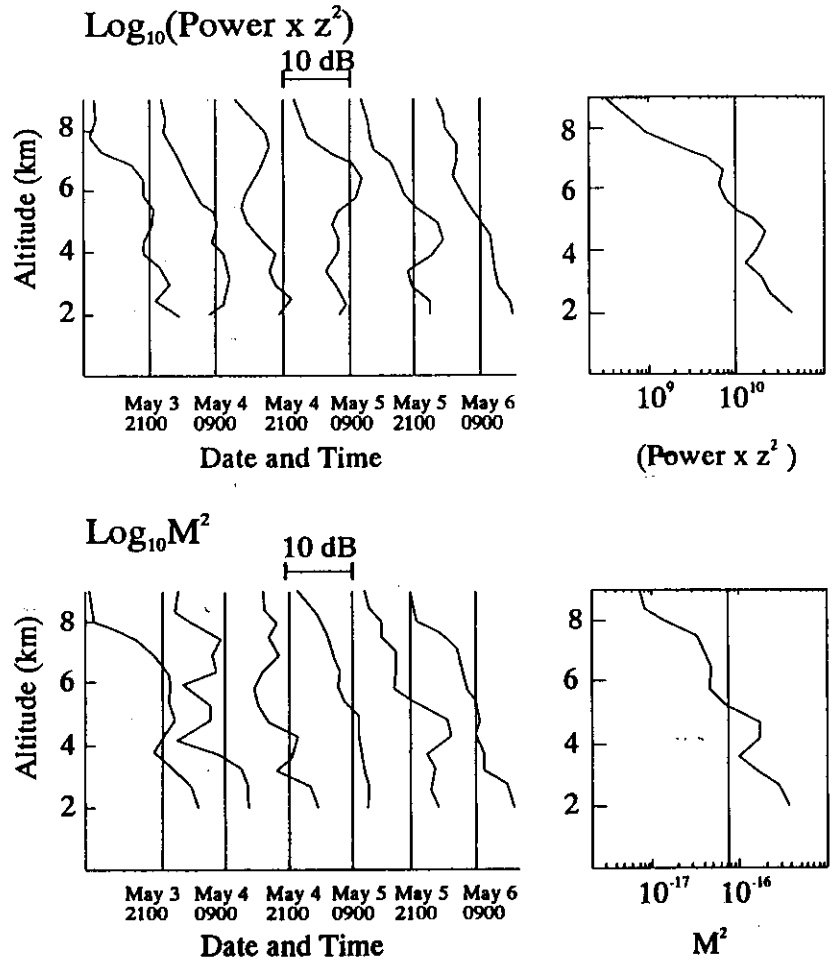

Fig. 7. Profiles of $\log_{10}(\text{Power} \times z^2)$ and $\log_{10}M^2$ averaged over 4 h for the entire six periods: the total average profile is shown on the right. The vertical lines are centred at $\log_{10}(\text{Power} \times z^2) = 10^{10}$ and $\log_{10}M^2 = -16.2$, respectively. As discussed in the text, we consider a good correlation between M^2 and the radar power to be indicative of moderately similar humidity profiles at the radar and the balloon – such similarity is required in order to combine the radiosonde and radar data to make useful estimates of ε.

power can be taken as a measure of the similarity between the regions, since a good correlation indicates that the refractivity profiles at the two sites were very similar. We consider this correlation to be a very important indicator of whether or not we can make meaningful estimates of ε. Figure 7 shows height profiles of $\log[\text{Power} \times z^2]$ and $\log[M^2]$, while the correlation coefficients r and slopes m for each of the cases studied are given in Table 3. The correlation coefficients in four cases were very good, in excess of 0.84, and in addition the lower 95% confidence limits were well above zero in these cases. However there were two cases for which the correlations were very poor, namely those for 4 and 5 May, both at 09.00 CST. We interpret a correlation which is substantially greater than zero at the 95% confidence level to mean that we can apply χ measured at the radiosonde to our radar data and thence produce a reliable estimate of the energy dissipation rates.

A note of caution when interpreting results based on these correlation values must be made. Our comparisons were made between a 4 h average at the radar and a balloon profile which represents a continuum of instantaneous measurements as a function of height, but in which the data at different heights were sampled at different times spread over a 40 min period. Thus the type of correlation would very much depend on the position of the ascending balloon relative to the radar site, as well as the spatio-temporal variation of the relevant atmospheric parameters. If the cor-

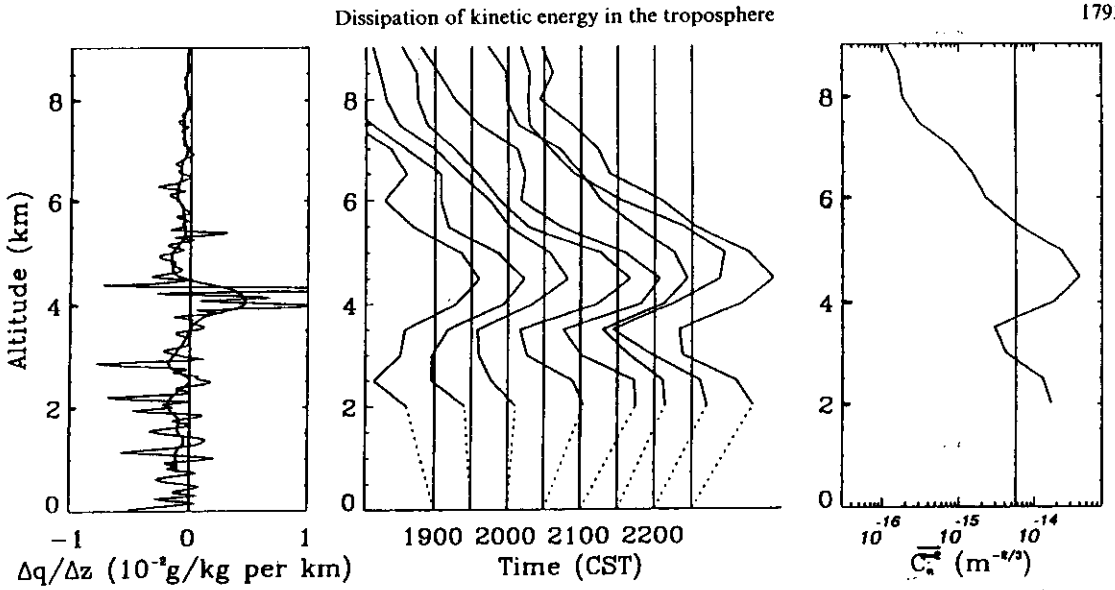

Fig. 8. Profiles of $\overline{C_n^2}$ averaged over one half hour for the entire fifth period (5 May 1991, 21.00): the total average profile is shown on the right and the humidity gradient profile on the left. The vertical lines are centred at $\log_{10} \overline{C_n^2} = -14.25$, and the horizontal scaling for the middle panel is the same as that used in the right hand panel.

relation between the radar and the balloon is good, it is probable that fairly stable atmospheric conditions exist, so that we are probably quite safe in assuming that χ is similar at the two sites. However, even on occasions when the weather conditions over the two sites might seem to a casual observer to be similar, there may be substantial differences in the profiles recorded by the two instruments. In such cases, we need to look more deeply into the data, and an examination of the temporal behaviour of $\overline{C_n^2}$ at the radar can be a good indicator of the overall stability of the atmosphere. Those cases in which there was poor correlation between the height profiles of scattered power and M^2 correspond to cases in which the atmospheric conditions over the radar and near the balloon were very variable.

Presentation of results

We now present a selection of data from the campaign for illustration. Figure 8 shows profiles of the gradient of the specific humidity and $\overline{C_n^2}$ for 5 May at 21.00. We have chosen to plot these two parameters in this figure because there have been some studies which indicate that the humidity profile is a major contributor to peaks in the backscattered power (e.g. Tsuda *et al.*, 1988), and we wish to examine this possibility. In the left-hand graphs two profiles of $(dq)/(dz)$ are shown, which correspond to different types of averaging and filtering that were applied to the raw data: the profile showing the finer details represents raw radiosonde data that were filtered and averaged to give interpolated values every 10 s, which gives about 50 m resolution; for the other profile, a Gaussian convolution was applied to the 50 m resolution data to give approximately 1 km resolution values. The middle graph shows half hour means of $\overline{C_n^2}$, and the right-hand graph shows $\overline{C_n^2}$ averaged over the interval shown.

This particular balloon flight was chosen because there was good correlation between M^2 measured with the balloon and (Power $\times z^2$) measured with the radar; thus we are fairly certain that conditions at the radar and in the vicinity of the balloon were similar. It is quite clear from the figure that the region of strongest radar scatter correlates very well with a region in which the magnitude of the humidity gradient was very large. This was not an uncommon feature throughout the campaign, supporting earlier observations by Tsuda *et al.* (1988), who also showed that regions of enhanced $\overline{C_n^2}$ generally correlated with regions of large humidity gradient. This re-emphasizes the importance of knowing the humidity gradient profile fairly well in order to make reasonable estimates of ε.

Figures 9–11 show a more detailed set of graphs describing the data from three separate selected days. They include profiles of potential temperature θ (K), χ, specific humidity q (g/kg), horizontal wind speed u (m/s), wind direction and vector wind shear s (units of $10^{-3}s^{-1}$) (magnitude only) as well as height and

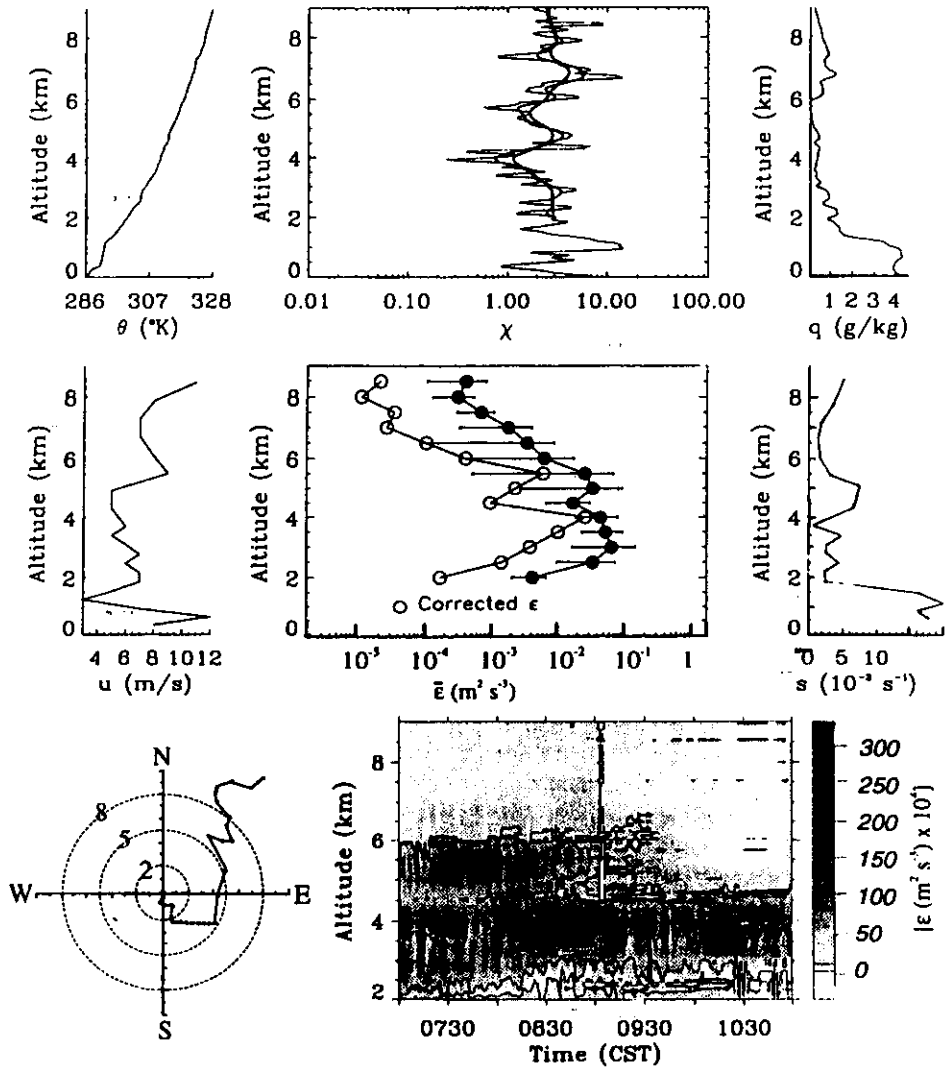

Fig. 9. For 4 May 1991, 09.00, plots of potential temperature, correction factor χ, specific humidity, wind speed, $\bar{\varepsilon}$, vertical wind shear, wind direction and the energy dissipation rates (the second period). In the plots of wind direction, the length of the vector from the origin to any point represents its height, and the direction of the same vector represents the direction of the wind at that height. In the height profiles of energy dissipation rates, the filled circles show values without correction for χ, and the open circles show the values after correction. Blank areas in the contour plots represent missing data. The correlation between $\overline{C_n^2}$ from the radar and M^2 from the radiosonde was poor on this occasion (see Table 3); thus, the estimates of $\bar{\varepsilon}$ in this figure are less likely to be reliable than in cases where the correlation was good, although the values are at least qualitatively representative of the energy dissipation rates at the time (see text).

contour plots for the mean energy dissipation rate per unit mass ($m^2 s^{-3}$). The height profiles of $\bar{\varepsilon}$ are not only spatial averages but also 4 h temporal averages. The filled circles represent 'raw' values, obtained by taking $\chi = 1$ in equation (4), whilst the open circles represent values obtained by utilizing the measured values of χ. The profiles of the humidity correction factor χ are also very important because this is the most sensitive factor in equation (4). For this parameter, three profiles are shown on the same plot; the profile showing the finer details represents raw radiosonde data that were filtered and averaged to give interpolated values every 10 s, which gives roughly 50 m resolution; for the other two profiles, a Gaussian filter was applied to the 50 m resolution data to give approximately 1 km and 2 km resolution data.

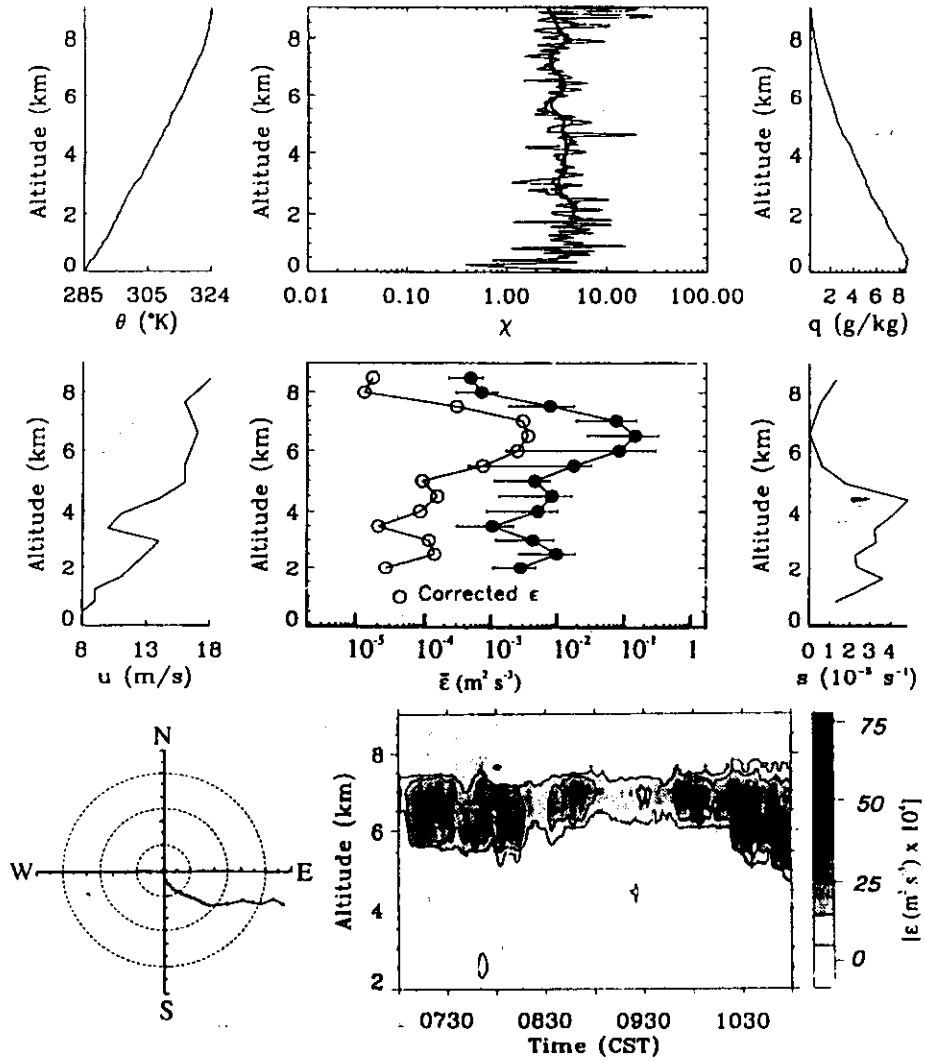

Fig. 10. As for Fig. 9, but for 5 May 1991, 09.00 (fourth period).

respectively. Note that the latter two profiles show generally similar structure, indicating that the buoyancy scale of the turbulence was something less than or of the order of 1 km. This smoothing also ensured that the χ-data had similar resolution to all the other types of parameters used in our determinations.

We emphasize here that it is necessary to exercise some caution in presenting contour plots of $\bar{\varepsilon}$, because they were derived assuming that the values of χ and $F^{1/3}\,\omega_B^2$ throughout the time interval plotted remain constant and equal to the values deduced during the radiosonde ascent. Of course this may not be entirely true, but as long as χ is moderately small (less than say 3 or 4) then we can ascribe most of the variability to true changes in the energy dissipation rate. However, if χ is large (of the order of 10, as actually occurred at 21.00 on 3 May (not shown)), the variability in χ is more likely also to be large. Thus in such cases the variability in the calculated values of $\bar{\varepsilon}$ may be caused as much by the variability in χ as to true variability of the turbulence intensity (particularly when we note that the calculated values of $\bar{\varepsilon}$ depend on χ^{-3}). Therefore we must exercise some caution when interpreting such plots.

Similar graphs were produced for all periods of the campaign, but we have selected three for conciseness. Nevertheless, these give a fair representation of the types of situations encountered. Figure 12 shows all the profiles of the energy dissipation rates deduced around the times of each of the six balloon releases.

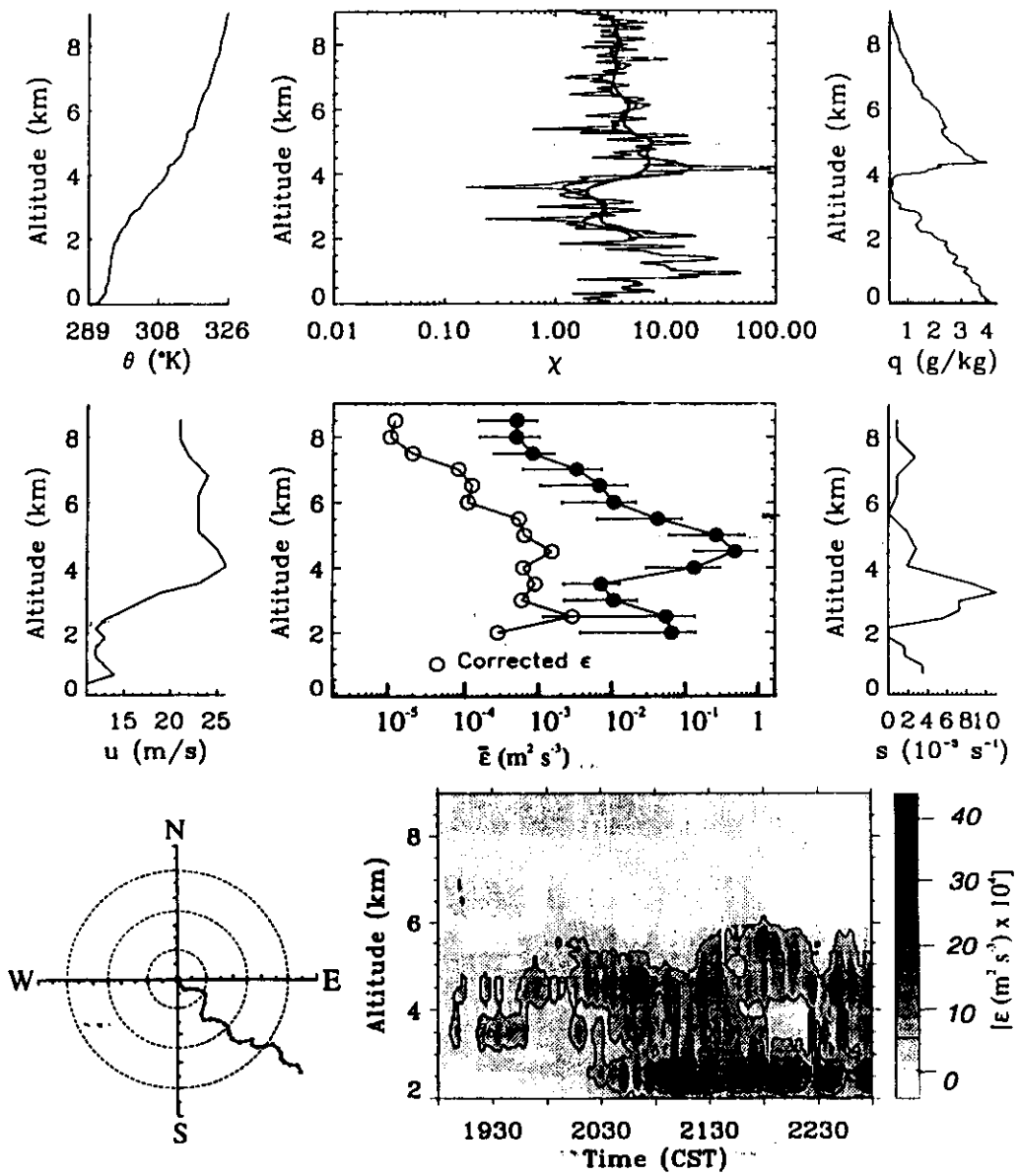

Fig. 11. As for Fig. 9, but for 5 May 1991, 21.00 (fifth period); the radar–radiosonde correlation was very good in this case.

Figure 13 shows the distribution of all measurements made in all six periods, while Fig. 14 shows a type of 'inverse-cumulative' graph; i.e. the probability of $\bar{\varepsilon}$ exceeding the abscissa.

Discussion of individual periods

We now consider each of the periods of observation in turn, highlighting important features, and conclude with some pertinent general observations.

3 May, 21.00 CST. The dominant feature on this occasion was a high pressure system which existed over both the radar and the airport. Turbulence strengths were in general weak above 3 km altitude; indeed according to the categories in Table 2 there was *no* turbulence at these higher heights. A layer of moderate turbulence appears to have existed at 2–3 km altitude, probably because of convective processes. This was a generally stable period, as might be expected in the presence of a high pressure system.

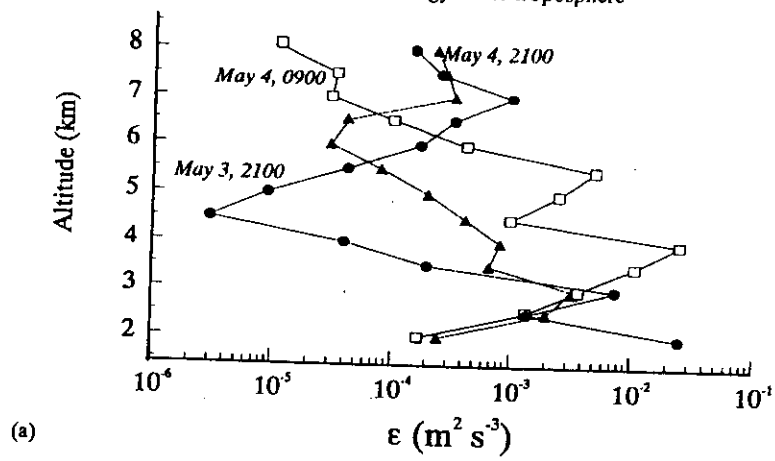

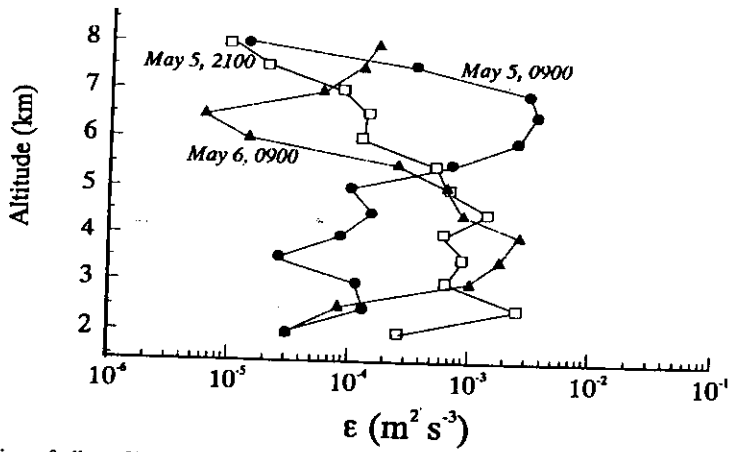

Fig. 12. Collection of all profiles of turbulent energy dissipation rates deduced in this study. The data for 5 May 1991, 09.00 are probably the least reliable quantitatively, as discussed in the text.

Apart from Fig. 7, no other graphs from this period are presented.

4 May, 09.00 CST. This interesting case exhibited very poor correlation between the echo power and the mean square gradient of the radio index of refraction M^2, even though at the time the region was dominated by a high-pressure system. Figure 9 shows the pertinent graphs relevant to the period. Table 3 shows a correlation coefficient of only 0.469, and the profiles in Fig. 7 are dissimilar. However, it should be noted that, whilst the high pressure system still dominated the weather, the low pressure system which was to arrive later was starting to move in from the West, and possibly starting to exert some influence. Although we have not presented graphs of $\overline{C_n^2}$ as a function of time, these are available, and one noticeable feature at the greater heights (above 5 km) was a fair degree of variability of $\overline{C_n^2}$ at this time, with variations of up to 3 orders of magnitude (between 10^{-17} and 10^{-14} $m^{-2/3}$). The large variations in $\overline{C_n^2}$ with time within this region mean that the atmosphere was very disturbed, with accompanying larger variability in backscatter returns. Hence we might expect that there were also substantial spatial variations, giving rise to differences in the conditions existing at the two sites (radar and radiosonde).

Despite the poor correlation between M^2 and $\overline{C_n^2}$, we do see that χ is moderately small ($\sim$2–3) and the

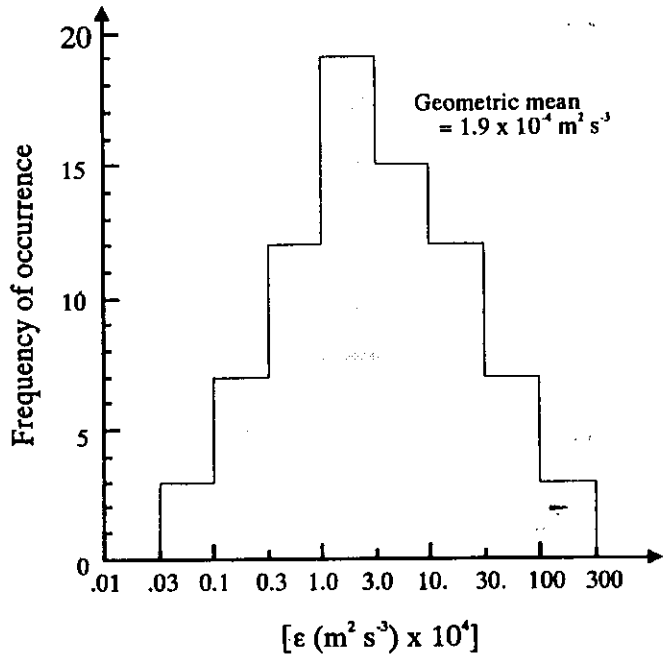

Fig. 13. Histogram showing the distribution of energy dissipation rates (logarithmic scale) for the whole six balloon flights of the campaign.

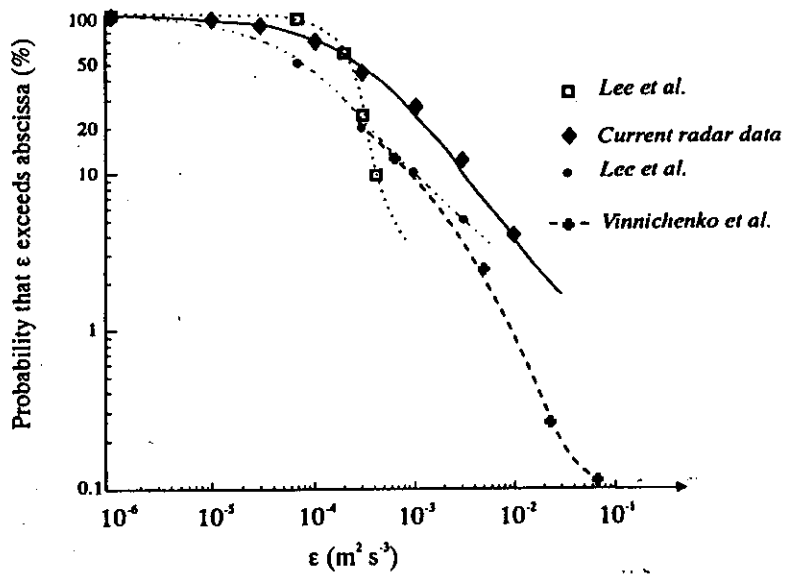

Fig. 14. Inverse cumulative distribution of energy dissipation rates deduced in this study, compared to other distributions deduced from other sources. (□) Lee *et al.* (1988), Fig. 7 [data from 1927 to 20.11 UT, 15 June 1983]; (●) Lee *et al.* (1988), Table 7, [pressure-based data, 18.10 to 18.46 UT, June 1983.]; (◇) current radar data; (- - + - -), Vinnichenko *et al.* (1973) [also see Table 1, this article]. Details are discussed in the text.

smoothed values never exceed 4 (Fig. 9). Thus, though we should not normally determine energy dissipation rates for this period, we feel that in this case it is warranted. The generally small values of χ permit greater reliability in our estimates of $\bar{\varepsilon}$, despite the poor correlation, and further, the temporal variability of χ is less likely to be important since the values are small. Hence we choose to plot $\bar{\varepsilon}$ in Fig. 9, despite the poor correlation coefficient.

The resultant levels of turbulence which are deduced, even despite the fact that they may have some uncertainty associated with them, support the notion that the atmosphere was very disturbed at the time. There occurred regions of moderate turbulence, some lasting for as long as 15 min. The whole atmosphere seems to have been quite unstable and variable; the region in which the most intense turbulence was detected was between 3.5 and 4 km, with the turbulence being significantly intermittent in nature. Equation (4) shows that if $\bar{\varepsilon}$ is very variable spatially, then we might expect $\overline{C_n^2}$ and M^2 measured at two displaced sites to show poor correlation; indeed this is seen.

Reference to the height profiles of the horizontal wind speed and the respective wind shear shows a very strong shear region below 2 km altitude (below the minimum height of detectability of the radar) and another region of moderate shear around 4–5 km. This latter region of shear is caused more by a change in direction of the mean wind than by a change in wind magnitude, and this rotational shear may well be the reason for the strong turbulent layer around 4 km altitude. The reason for the less continuous layer at 5–6 km is not clear.

4 May, 21.00 CST. This is another case for which no plots (apart from Fig. 7) are shown. The period showed very good correlation between the humidity gradient peaks and the $\overline{C_n^2}$ peaks — this was especially true at 2.5, 4 and 7.5 km altitude. The $\bar{\varepsilon}$ contours showed mainly 'no' or light turbulence, though no contour graphs are presented for this period.

5 May, 09.00 CST. This is one of two periods that showed very poor correlation between log[Power $\times z^2$] and log[M^2] in Fig. 7; the other, on 4 May, 0900, has been discussed already. The primary reason for the poor correlation is the existence of a strong layer of radar scatter at about 7 km altitude which does not appear in the profiles of M^2 deduced with the balloon data.

The relevant detailed graphs for this period are shown in Fig. 10. The plot of χ as a function of altitude in Fig. 10 shows a profile in which the smoothed values are remarkably constant with height, while q and θ are also quite smoothly varying with height. Thus, though we might not normally calculate the energy dissipation rates in this case because of the poor correlation of M^2 and $\overline{C_n^2}$, we can feel fairly confident that calculations of $\bar{\varepsilon}$ as a function of height (and even time) allow us to see the existence of any layers of turbulence. Profiles and contour plots of $\bar{\varepsilon}$ have therefore been plotted and, despite the fact that absolute values of $\bar{\varepsilon}$ might be uncertain, it is seen clearly that a layer of turbulence existed in the region between 5 and 7 km. The layer exhibited some intermittent light turbulence embedded in regions of weaker turbulence. Most of the rest of the atmosphere was clear of any turbulence. The absolute values of $\bar{\varepsilon}$ for these data are probably the least reliable of all cases because of uncertainty about the values of χ in the layer.

5 May, 21.00 CST. This was another example of excellent correlation between the humidity gradient profile and the $\overline{C_n^2}$ profiles. Table 3 shows a correlation coefficient of 0.904, while the profiles in Fig. 7 are very similar. Another interesting aspect of this comparison is the fact that the peak in $\overline{C_n^2}$ was just above the region of the maximum humidity gradient layer. This is probably caused by a slight tilt in the layer, giving different heights at the two sites; it emphasizes that one must be especially careful when combining the two data sets to determine $\bar{\varepsilon}$—a difference in heights of the peak in humidity gradients and $\overline{C_n^2}$ can in some cases give rise to 'artificial' layers of turbulence, though this does not seem to have occurred in this particular case. The relevant data are plotted in Fig. 11.

Part of the atmosphere below 6 km exhibited light turbulence, and in the latter portion of the period this turbulence was very intermittent, particularly above 3 km. A strong wind jet is observed, peaking at about 4 km altitude, with some corresponding turbulence at these heights (see Fig. 11). There is also a very large contribution to the echo power from the specific humidity at 4 km altitude but, despite the fact that this may lead to uncertainties in the $\bar{\varepsilon}$ profile, we still feel that the observation of light turbulence at this height was real. The layer of turbulence just above 2 km was possibly generated by convective processes.

6 May, 09.00 CST. The contour plot for this period (not shown) showed a similar situation existing to that for the previous period. The intermittent nature of atmospheric turbulence was also well displayed, just as in Fig. 11. Once again a strong intermittent layer was clearly evident at around 4–5 km. This layer of turbulence occurred at a height where χ was small, so the intermittency in this case is likely to have been true turbulence intermittency. The region was also close to a layer of strong rotational shear at 5–6 km, which may have been associated with the turbulence.

DISCUSSION

Figure 12 shows all energy dissipation rate profiles measured during the campaign. The lower graph generally shows days when the low pressure cell dominated the weather; the upper graph shows times when the high pressure cell dominated or when the site was in transition from domination by the high to domination by the low pressure cell. As a rule, it seems that, whenever turbulent layers appeared at 2–3 km, they were not generally associated with any particular wind shear. They were possibly convective in origin, or may have been associated with land and sea breezes. Layers of turbulence at the higher altitudes seemed more often to be associated with either wind shears or wind jets. Perhaps surprisingly, there seems to be no real evidence of less upper level turbulence on days when the high pressure cell was dominant than on days when the low pressure cell was prominent.

Figure 13 shows the distribution of kinetic energy dissipation rates over the full campaign. The distribution is quite consistent with the data shown in Fig. 1, with a geometric mean around $2\times10^{-4}\,m^2s^{-3}$. Figure 14 shows a form of 'cumulative probability', using the probability that the abscissa is exceeded rather than the probability that the value is less than the abscissa. For comparison, two similar distributions from Lee *et al.* (1988) (who used two types of sensors in their measurments—one based on wind fluctuations and one based on pressure fluctuations) are also shown, as well as a very approximate distribution based on Table 1. We have presented the data measured with the pressure-based instrument; data from the wind-based instrument were comparable to the pressure-based data. The data represented by the '+' symbol in Fig. 1 were originally presented by Vinnichenko *et al.* (1973) as simply percentage probabilities for particular 'typical' values, but we have converted the data to the type of format in Fig. 14 by simply summing from the large number end and assigning the sum to the geometric mean of the two energy dissipation rate levels at which the sum stops. For example, we have considered the boundary between $\varepsilon = 1.0\times10^{-4}$ and 30.0×10^{-4} to be $\sqrt{(30*1.0)}\times10^{-4} \simeq 5.5\times10^{-4}\,m^2s^{-3}$, and have then taken the percentage of time for which ε exceeds $5.5\times10^{-4}\,m^2s^{-3}$ as $0.09+3.0+7.8\simeq11\%$. This is of course only a crude conversion, which is why we have also fitted the dashed line as another indicator. Nevertheless, because of the log–log nature of the plot, even variations of the percentages of the order of a factor of 2 will not substantially shift the curve, so that it still represents a reasonable summary of the measurements of Vinnichenko *et al.* (1973).

A comparison between the four graphs in Fig. 14 shows at least broad similarity. There is a tendency for the radar to 'pick out' stronger layers; for example, according to the radar data the chance of exceeding $\varepsilon = 10^{-2}\,m^2s^{-3}$ is about 4%, whereas the *in-situ* data suggest that it is more like 1%. However, this is not surprising because a radar has a poorer sensitivity to regions of small turbulence than an *in-situ* instrument. Indeed a radar will often not even recognize a truly laminar region, due to overflow of the pulse from neighbouring turbulent regions. In general, the agreement is reasonable, considering the fact that all the data were measured at different locations and different times using different techniques.

It should be noted that turbulence is not energetically important on large scales in the atmosphere, as can be seen from Fig. 1. Even an energy dissipation rate of $10^{-2}\,m^2s^{-3}$ corresponds to a heating rate of only 1 K per day. However, measurements of the type presented here are still important in the atmosphere, both from the point of view of diffusion as well as from the point of view of aircraft safety. In both regards, refining radar measurements of ε is an important objective, since radars offer the best potential to achieve continuous coverage in height and time. Because of the intermittent nature of turbulence, such coverage is especially important. A single balloon or *in-situ* probe is very likely to miss many cases of strong, short-lived turbulence; yet such bursts of activity are the very thing which can cause the most severe aircraft damage. Thus, despite the overall lack of importance of turbulence in the large scale energy budget, we feel that studies of the type which we have presented are still of considerable significance.

There is another procedure which can be used to measure atmospheric turbulence strengths by radar, and that is the so-called spectral width method. We are fully aware of the importance of this technique, but have chosen not to utilize it in this paper because of insufficient space. We have instead chosen to concentrate our studies here completely on the C_n^2 method, in an attempt to try and clarify the various different models used with this technique. Now that we feel more comfortable that we have established a suitable model for this C_n^2 method, a logical next step will be comparisons with the spectral width method. This will serve as an important follow-up to the work of Cohn (1995), but with an improved C_n^2 method. Such a follow-up study should also use the improved spectral-width method described by Hocking (1996).

Finally, we return briefly to a discussion of an important issue which has implications for radar studies of turbulence, namely that of 'transparent' layers, viz. layers of (possibly even strong) turbulence which

appear invisible to the radar because the potential temperature and humidity gradients within the turbulent layer are both zero. Certainly our experimental results show substantial variability in both parameters (Figs 4, 9–11) and as a rule the two parameters are not generally correlated. As a consequence, we might expect that the probability of zero gradients in both quantities is small, so that the number of such transparent layers should be small. However, this conclusion cannot be definitive, because it is likely that, though the correlation might be small, it is still possible that both quantities could be driven to zero in well mixed layers by the turbulence itself. This would have little impact on the overall correlation between the two types of gradients, which could remain small, but would be important for the occurrence of transparent layers. We have no way of confirming or refuting the existence of such well mixed layers; it is a topic which certainly deserves study in the future. However, our feeling is that in the main the radar sees most layers of turbulence, although it certainly need not be true that the strongest values of C_n^2 should relate to the most turbulent layers. Studies of humidity and potential temperature gradients in well mixed layers should be strongly encouraged in the future.

CONCLUSION

We have examined in some detail the theories available for the conversion of $\overline{C_n^2}$ to kinetic energy dissipation rates $\bar{\varepsilon}$. *In-situ* high resolution thermosonde data were used to examine the importance of an expected Richardson number dependence of the 'constant' of proportionality γ. We have proposed that, wherever possible, this Richardson number should be measured and incorporated, especially for R_i close to zero. For Richardson numbers further removed from zero (greater than, say, 0.2) it seems valid to take γ to the truly constant; we have proposed a value of 0.4.

We have presented observations of potential refractive index gradient profiles, humidity profiles, and radar backscatter profiles, for a variety of radiosonde launches during which simultaneous radar observations were made. A statistical model has been used to help infer the strengths of atmospheric turbulence. We were careful to obtain good humidity profiles, because we have found that the humidity gradient is a major contributor to the potential refractive index gradient. This agrees with earlier observations due to Tsuda *et al.* (1988).

In the treatment of the model parameter $F^{1/3}\omega_h^2$, it is often assumed that this can be approximated by a constant value, which is calculated from a statistical analysis of the wind shears. We were able to verify that, at least for our data, this was indeed almost constant. Some caution may be required if the model is applied to other data.

The moderately large spatial separation of 35 km between the location of the radar and the radiosonde launch-site is a crucial factor in the interpretation of the results, but nevertheless we have done all that we can to consider this difference in our determinations and discussions. In particular, we have taken pains to examine the correlation between M^2 as measured by the radiosonde and $\overline{C_n^2}$ as measured by the radar, and have used this as an indicator of whether $\bar{\varepsilon}$ can be reliably deduced from the data. This was an important aspect of this work. We should also note that, even if the radiosonde was launched at the radar, it would still have blown away from the radar, so that by heights of 5 or 6 km there would in any case have been a significant horizontal separation (typically between 5 and 20 km) between the radar and the radiosonde.

Despite the moderate distance separating the radar and the radiosonde launch site, there appear to be numerous cases when there is very good correlation between regions of enhanced $\overline{C_n^2}$ and the humidity gradient, in agreement with observations made by Warnock *et al.* (1988) and Tsuda *et al.* (1988), among others. Indeed we emphasize that layers which produce very strong backscatter need not be the most turbulent layers, but instead are often height regions where the magnitude of (dq/dz) is large. We must be especially careful not to assume simply that strong backscatter is always associated with strong turbulence.

There are often cases of very good correlation between $\log[\text{Power} \times z^2]$ (as measured by the radar) and $\log[M^2]$ (as measured by the radiosonde), and when this occurs we feel that we can make reliable estimates of the turbulent dissipation rates. Where poor correlation exists, this was interpreted as being caused by different weather conditions above the radiosonde launch site and the radar. It could also imply that the atmosphere is very variable during the measurement run, or that the trajectory of the balloon borne radiosonde was directed away from the radar site. Our estimates of $\bar{\varepsilon}$ are less reliable in such cases, especially if χ is very different from 1.

In most cases, the atmosphere is either free of turbulence or has light and/or moderate turbulence. Turbulence in all categories is generally very intermittent in nature, which is in general agreement with other more detailed studies of turbulence (Tennekes, 1973). Our distributions of turbulence levels are in broad agreement with other data collected by *in-situ* techniques, so that it seems that the combined use of

148

radiosonde data and radars offers a useful way to measure strengths of atmospheric turbulence.

Acknowledgements—The authors especially thank James H. Brown, of the USAF Phillips Laboratory (Geophysics Directorate) PL/GPOS for suppling the raw data used to prepare Fig. 3, and also for his advice concerning this manuscript. We also acknowledge discussions with R. A. Vincent, of the University of Adelaide, and would like to thank the office of the Bureau of Meteorology in Adelaide for their assistance with the radiosonde data. We also thank Trevor Harris for the use of his contour procedures. This work was partly supported by the Australian Research Council (ARC) and by the Natural Sciences and Engineering Research Council of Canada.

REFERENCES

Arya, S. P. S. (1972) The critical condition for the maintenance to turbulence in stratified flows. *Quart. J. Roy. Meteorol. Soc.* **98**, 264–273.

Arya, S. P. S. and Plate, E. J. (1969) Modeling of the stably stratified atmosphericboundary layer'. *J. Atmos. Sci.* **26**, 656–665.

Atlas, D. (1964) *Advances in Geophysics*. Academic Press, New York.

Barat, J. (1982) Some characteristics of clear air turbulence in the middle stratosphere. *J. Atmos. Sci.* **39**, 2553–2564.

Barat, J. (1983) The fine structure of the stratospheric flow revealed by differential sounding. *J. Geophys. Res.* **88**, 5219–5228.

Barat, J., Cot, C. and Sidi, C. (1984) On the measurement of the turbulent dissipation rate from rising balloons. *J. Atmos. Ocean. Tech.* **1**, 270–275.

Bohne, A. R. (1981) *Radar Detection of Turbulence in Thunderstorms*. Report # AFGL-TR-81-0102 (ADA 108679), Air Force Geophys. Lab., Hanscom Air Force Base, MS, U.S.A.

Brown, J. H., Dewan, E., Murphy, A. and Thomas, P. (1989) *Study of Possible Solar Heating Effects on Thermosonde Probes - Error Analysis*. Report # GL-TR-89-0178 (ERP 1034), Air Force Geophys. Lab., Hanscom Air Force Base, MS, U.S.A.

Businger, J. A., Wyngaard, J. C., Izumi, Y. and Bradley, E. F. (1971) Flux-profile relationships in the atmospheric surface layer. *J. Atmos. Sci.* **28**, 181–189.

Caughey, S. J., Crease, B. A., Asi-Makopoulos, D. N. and Cole, R. S. (1978) Quantitative bistatic acoustic sounding of the atmospheric boundary layer. *Quart. J. Roy. Meteorol. Soc. and* **104**, 147–161.

Chen, W. Y. (1974) Energy dissipation rates of free atmospheric turbulence. *J. Atmos. Sci.* **31**, 2222–2225.

Crane, R. K. (1977) *Stratospheric Turbulence Analysis*. Report # AFGL-TR-77-0207 (ADO 47740), Air Force Geophys. Lab., Hanscom Air Force Base, MS, U.S.A.

Crane, R. K. (1980) A review of radar observations of turbulence in the lower stratosphere. *Radio Sci.* **15**, 177–193.

Cohn, S. A. (1994) Investigations of the wavelength dependence of radar backscatter from atmospheric turbulence. *J. Atmos. Ocean. Tech.* **11**, 225–238.

Cohn, S. A. (1995) Radar measurements of turbulent eddy dissipation rate in the troposphere: a comparison of techniques. *J. Atmos. Ocean. Tech.* **12**, 85–95.

Doviak, R. J. and Zrnic, D. S. (1984) *Doppler Radar and Weather Observations*. Academic Press, Orlando, FL.

Ellison, T. H., Turner, J. S. (1960) Mixing of dense fluid in a turbulent pipe flow, Part 2. *J. Fluid. Mech.* **8**, 529–544.

Fairall, C. W., White, A. B. and Thomson, D. W. (1991) A stochastic model of gravity-wave-induced clear-air turbulence. *J. Atmos. Sci.* **48**, 1771–1790.

Frisch, A. S. and Clifford, S. F. (1974) A study of convection capped by a stable layer using Doppler radar and acoustic echo sounders. *J. Atmos. Sci.* **31**, 1622–1628.

Gage, K. S. and Green, J. L. (1978) Evidence for specular reflection from monostatic VHF radar observations of the stratosphere. *Radio Sci.* **13**, 991–1001.

Gage, K. S., Green, J. L. and Van-Zandt, T. E. (1980) Use of Doppler radar for the measurement of atmospheric turbulent parameters from the intensity of clear air echoes. *Radio Sci.* **15**, 407–416.

Gossard, E. E., Chadwick, R. B., Neff, W. D. and Moran, K. P. (1982) The use of ground-based Doppler radars to measure gradients, fluxes and structure parameters in elevated layers. *J. Appl. Meteorol.* **21**, 211–226.

Gossard, E. E., Chadwick, R. B., Detman, T. R. and Gaynor, J. (1984) Capability of surface-based clear-air Doppler radar for monitoring meteorological structure of elevated layers. *J. Climate and Appl. Meteorol.* **23**, 474–485.

Gossard, E. E., Gaynor, J., Zamora, R. J. and Neff, W. D. (1985) Finestructure of elevated stable layers observed by sounder and *in-situ* tower sensors. *J. Atmos. Sci.* **42**, 2156–2169.

Gossard, E. E. and Frisch, A. S. (1987) Relationship of the variances of temperature and velocity to atmospheric static stability — application to radar and acoustic sounding. *J. Climate and Appl. Meteorol.* **26**, 1021–1036.

Hocking, W. K. (1983) On the extraction of atmospheric turbulence parameters from radar backscatter Doppler Spectra I Theory, . *J. Atmos. Terr. Phys.* **45**, 89–102.

Hocking, W. K. (1985) Measurement of turbulent energy dissipation rates in the middle atmosphere by radar techniques: A review. *Radio Sci.* **20**, 1403–1422.

Hocking, W. K., Lawry, K. and Neudegg, D. (1989) Radar measurements of atmospheric turbulence intensities by both C_n^2 and spectral width methods. *Middle Atmosphere Program Handbook*, Vol. 27, pp. 443–446. SCOSTEP Secretariat, Univ. Illinois.

Hocking, W. K., Fukao, S., Tsuda, T., Yamamoto, M., Sato, T. and Kato, S. (1990) Aspect sensitivity of stratospheric VHF radiowave scatterers, particularly above 15 km altitude. *Radio Sci.* **25**, 613–627.

Hocking, W. K., Fukao, S., Yamamoto, M., Tsuda, T. and Kato, S. (1991) Viscosity waves and thermal-conduction waves as a cause of 'specular' reflectors in radar studies of the atmosphere. *Radio Sci.* **26**, 1281–1303.

Hocking, W. K. (1992) On the relationship between the strength of atmospheric radar backscatter and the intensity of atmospheric ' turbulence. *Advances in Space Research* **12(10)**, 207–213.

Hocking, W. K. (1996) An assessment of the capabilities and limitations of radars' in measurements of upper atmosphere turbulence. *Advances in Space Research* **17(11)**, 37–47.

Jain, A. R., Rao, Y. J., Rao, P. B., Anandan, V. K., Damle, S. H., Balamuralidhar, P., Kulakarni, A. and Viswanathan, G. (1995) Indian MST radar 2. First scientific results in ST mode. *Radio Science* **30**, 1139–1158.

Kaimal, J. C., Wyngaard, J. C., Haugen, D. A., Cote, O.

R., Izumi, Y., Caughey, S. J. and Readings, C. J. (1976) Turbulence structure in the convective boundary layer. *J. Atmos. Sci.* **33**, 2152–2168.

Kondo, J., Kanechika, O. and Yasuda, N. (1978) Heat and momentum transfers under strong stability in the atmospheric surface layer. *Journal of the Atmospheric Sciences* **35**, 1012–1021.

Kropfli, R. A. (1971) Simultaneous radar and instrumented aircraft observations in a CAT layer. *J. Appl. Meteor.* **10**, 796–802.

Kung, E. C. (1966) Large scale balance of kinetic energy in the atmosphere. *Mon. Weather Rev.* **94**, 627–640.

Kunkel, K. E., Eloranta, E. W. and Weinman, J. A. (1980) Remote determination of winds, turbulence, spectra and energy dissipation rates in the boundary layer from lidar measurments. *J. Atmos. Sci.* **37**, 978–985.

Lee, Y., Paradis, A. R. and Klingle-Watson, D. (1988) *Preliminary Results of the* 1983 *Coordinated Aircraft-Doppler Weather Radar Turbulence Experiment*, Vol. 1. Report # DOT/FAA/PM-86/11 (A197894), Lincoln Lab., MIT, Lexington, MS, U.S.A.

Lilly, D. K., Waco, D. E. and Adelfang, S. I. (1974) Stratospheric mixing from high-altitude turbulence measurements. *J. Appl. Meteor.* **13**, 488–493.

Mousley, T. J., Asimakopoulos, D. N., Cole, R. S., Crease, B. A. and Caughey, S. J. (1981) Measurement of boundary layer structure parameter profiles by acoustic sounding and comparison with direct measurement. *Quart. J. Roy. Meteorol. Soc.* **107**, 203–230.

Ottersten, H. (1969) Atmospheric structure and radar backscattering in clear air. *Radio Sci.* **4**, 1179–1193.

Pao, Y.-H. and Goldburg, A. (1969) *Clear Air Turbulence and its Detection*. Plenum Press, New York, NY.

Pruitt, W. O., Morgan, D. L. and Laurence, F. J. (1973) Momentum and mass transfers in the surface boundary layer. *Quart. J. Roy. Meteorol. Soc.* **99**, 370–386.

Plate, E. J. and Arya, S. P. (1969) Turbulence spectra in a stably stratified boundary layer. *Radio Sci.* **4**, 1163–1168.

Readings, C. J. and Rayment, D. R. (1969) The high-frequency fluctuation of the wind in the first kilometer of the atmosphere. *Radio Sci.* **4**, 1127–1131.

Record, F. A. and Cramer, H. E. (1966) Turbulent energy dissipation rates and exchange processes above a nonhomogeneous surface. *Quart. J. Roy. Meteorol. Soc.* **92**, 519–532.

Röttger, J. and Liu, C. H. (1978) Partial reflection and scattering of VHF radar signals from the clear atmosphere. *Geophys. Res. Lett.* **5**, 357–360.

Sengupta, N., Warnock, J. M., Gossard, E. E. and Strauch, R. G. (1987) *Remote Sensing of Meteorological Parameters with the Aid of a Clear-air Doppler Radar*. NOAA Technical Report # ERL 431-WPL 61), U.S. Department of Commerce, National Oceanic and Atmospheric Administration Environmental Research Labs., Boulder, CO, U.S.A.

Sidi, C. and Dalaudier, F. (1990) Turbulence in the stratified atmosphere: recent theoretical developments and experimental results. *Advances in Space Research* **10**, 25–36.

Strauch, R. G., Frisch, A. S. and Weber, B. L. (1986) Wind measurements in the upper troposphere with UHF and VHF radar, preprints. 23rd Radar Meteorology Conf. and Cloud Physics Conf., Snowmass, Colorado, American Meteorological Society, pp. 48–51.

Tatarskii, V. I. (1961) *Wave Propagation in a Turbulent Medium*. McGraw-Hill, New York.

Tennekes, H. (1973) Intermittency of the small-scale structure of atmospheric turbulence. *Boundary Layer Meteorol.* **4**, 241–250.

Trout, D. and Panofsky, H. A. (1969) Energy dissipation near the tropopause. *Tellus* **21**, 355–358.

Tsuda, T., Sato, T., Hirose, K., Fukao, S. and Kato, S. (1986) MU radar observations of the aspect sensitivity of backscattered VHF echo power in the troposphere and lower stratosphere. *Radio Sci.* **21**, 971–980.

Tsuda, T., May, P. T., Sato, T., Kato, S. and Fukao, S. (1988) Simultaneous observations of reflection echoes and refractive index gradient in the troposphere and lower stratosphere. *Radio Sci.* **23**, 655–665.

Vanzandt, T. E., Green, J. L., Gage, K. S. and Clark, W. L. (1978) Vertical profiles of refractivity turbulence structure constant: Comparison of observations by the Sunset radar with a new theoretical model. *Radio Sci.* **13**, 819–829.

Vanzandt, T. E., Gage, K. S. and Warnock, J. M. (1981) An improved model for the calculations of profiles of C_n^2 and ε in the free atmosphere from background profiles of wind, temperature and humidity, preprint volume. Proc. 20th Conf. on Radar Meteorology, American Meteorological Society, Boston, MS, pp. 129–135.

Vincent, R. A., May, P. T., Hocking, W. K., Elford, W. G., Candy, B. H. and Briggs, B. H. (1987) First results with the Adelaide VHF radar: spaced antenna studies of tropospheric winds. *Journal of Atmospheric and Terrestrial Physics* **49**, 353–366.

Vinnichenko, N. K. and Dutton, J. A. (1969) Empirical studies of atmospheric structure and spectra in the free atmosphere. *Radio Sci.* **4**, 1115–1126.

Vinnichenko, N. K., Pinus, N. Z., Shmater, S. M. and Shur G. N., (1973) *Turbulence in the Free Atmosphere* (translated from Russian, translations ed. J. A. Dutton). Consultants Bureau, NY.

Warnock, J. M. and Vanzandt, T. E. (1985) *A Statistical Model to Estimate the Refractivity Turbulence Structure Constant C_n^2 in the Free Atmosphere* Report # NOAA-TM-ERL-AL-10, NOAA Environmental Res. Labs., Boulder, CO, U.S.A.

Warnock, J. M., Sengupta, N. and Strauch, R. G. (1988) Comparison between height profiles of C_n^2 measured by the Stapleton UHF clear-air Doppler radar and model calculations, preprint volume. Eighth Symp. on Turbulence and Diffusion, American Meteorological Society, Boston, MS, U.S.A.

Webb, E. K. (1970) Profile relationships: the log-linear range, and extension to strong stability. *Quart. J. Roy. Meteorol. Soc.* **96**, 67–90.

6.6.3.2 Spectral width estimates for determining ε

When a backscatter radar with a narrow beam is used to study the atmosphere, it is possible to measure the mean square fluctuating velocity of the scatterers by utilizing the spectral width of the received signal. This is a complex process, however, with the need to pay careful attention to a variety of contaminant effects. We will therefore now outline the principles of this procedure.

Before we begin, however, we first need the spectral width of our received radar signal. A variety of methods can be used to determine this spectral width. One can utilize either the width of the autocorrelation function where it falls to one half of its value at zero lag, or the second lag of the autocorrelation function, or the second moment of the spectrum (e.g. see the discussion by WOODMAN, 1985). In all cases, one must be careful about the effects of noise, since noise can cause systematic errors. For example, noise produces a narrow spike at zero lag of the autocorrelation function, and this spike should be eliminated before proceeding with analysis. A procedure commonly used to determine the spectral width is least-squares fitting of a Gaussian-like function. In some cases, it is necessary to remove excessively large spikes from the spectra, a procedure which is especially necessary when there are "mirror-like" partial reflectors in the radar volume (e.g. Hocking, 1983b). The details of these procedures will not be considered here; we are more concerned with the interpretation of the spectral width.

What then can cause the broadening of the spectrum? Perhaps the most obvious is random motion of the scatterers. If each scatterer has a velocity superimposed upon the mean speed, then each produces a line in the spectrum with a different frequency, as illustrated in the following diagram.

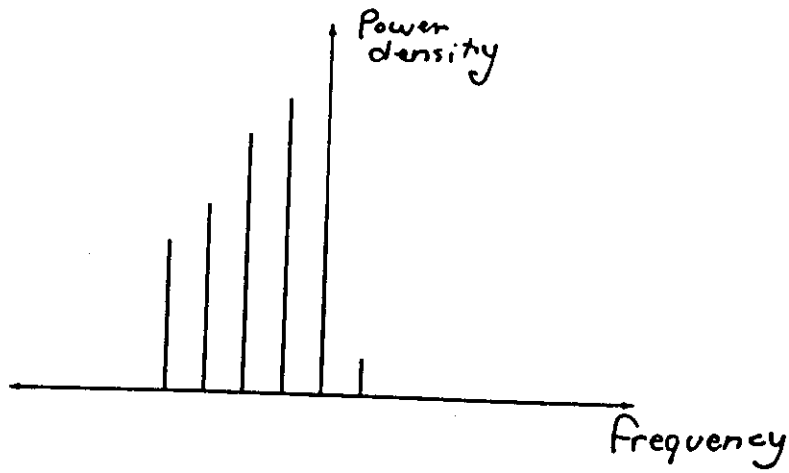

Fig. 21

If the scatterers have, for example, a Maxwellian distribution, then the vertical component of velocity (w) must have a Gaussian distribution, which is proportional to $exp\{-w^2/(2w^2_{RMS})\}$. Since for a vertical beam the Doppler shift from any scatterer is $f = \frac{2}{\lambda}.w$, the spectrum will have a shape of the form $exp\{-f^2/(2f^2_{RMS})\}$, where $f_{RMS} = \frac{2}{\lambda}.w_{RMS}$.

For some years in the early period of VHF middle atmosphere studies, it was assumed that this was the major cause of spectral broadening. However, for most VHF radars, this is not in fact the case. There are other causes of spectral broadening, which while understood by a few (e.g. Atlas,

1964; Sloss and Atlas, 1968; Atlas et al., 1969; Hocking, 1983a, b), were not generally appreciated in the Middle Atmosphere community. Fortunately, this attitude has changed recently. These effects will now be discussed.

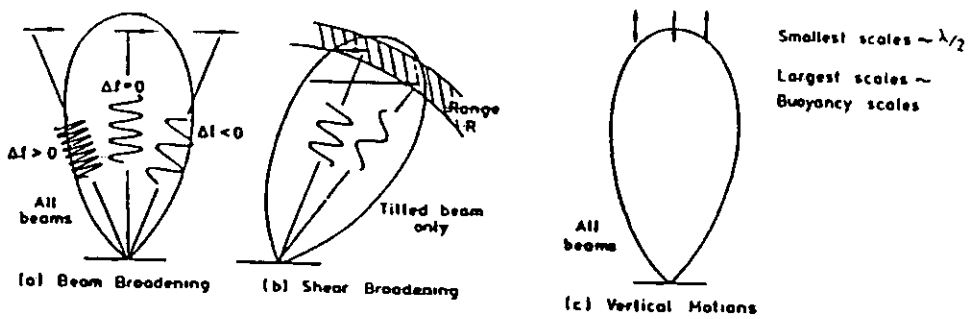

Contributors to the spectral broadening at any instant.

Fig. 22

For a vertically pointing beam, probably the main cause of the non-zero spectral width is the so-called "beam broadening", which is illustrated in fig. 22a.

Even if all the scatterers are moving horizontally at the same velocity, each scatterer will produce a different Doppler shift. The nett result is a spectrum of finite width. This spectral broadening has been modeled by several workers (e.g. Hitschfield and Dennis, 1956; Atlas, 1964; Sloss and Atlas, 1968; Atlas et al., 1969; Hocking, 1983a, b) , and for relatively narrow beams ($\leq$ about 5° half-power half-width), the spectral half-power half-width $f_{\frac{1}{2}b}$ obeys the approximate relation (in units of Hz)

$$f_{\frac{1}{2}b} = \frac{2}{\lambda}(1.0)\,|\,\underline{V}_{hor}\,|\,\theta_{\frac{1}{2}} \qquad (103)$$

where $\theta_{\frac{1}{2}}$ is the two-way half-power half-width of the polar diagram in radians, and $\underline{V}_{hor}$ is the *total* horizontal wind vector. The same approximation is also fairly accurate even for off-vertical beams, but it is important to note that the *total* wind speed should be used, and *not* just the component parallel to the tilt direction of the beam. This formula is based on the assumption that the scattering is statistically isotropic, an assumption which we will relax shortly. When one compares the spectral half-widths due to the non-fluctuating components of the wind-field to the experimental spectral half-widths measured with the vertical beam, one frequently finds that the two are very similar. For example, figure 23 from Hocking (1983) shows an almost 1:1 relationship between the two parameters when spectra produced from 11s data sets were used.

This point cannot be emphasized too strongly:- the spectral widths are often dominated by so called beam broadening.

There are other effects which alter the spectral width, particularly if the beam is tilted from the vertical. Horizontal fluctuating motions will alter the spectral width (e.g. see fig. 24), and so will changes of the mean wind with height, as occurs for example in a wind shear (e.g. fig 25). The former effect always broadens the spectrum, whilst the latter one can either reduce or increase the spectral width depending on the sign of the wind shear. These points are discussed in more detail by Hocking (1983a), for example.

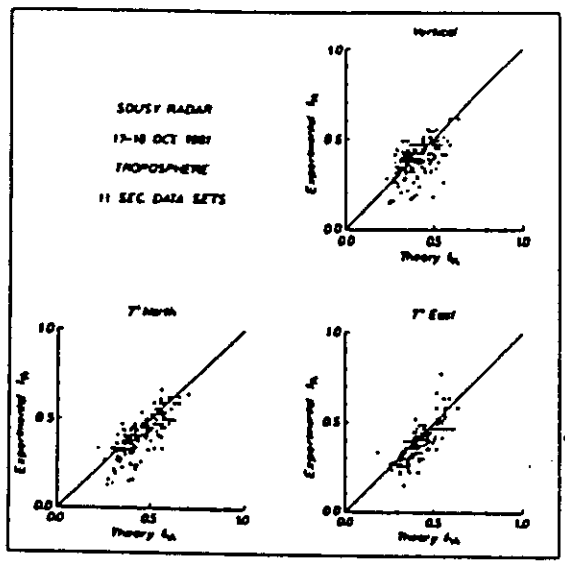

Scatter plots of experimental spectral half-power half-widths determined from 11 s data sets vs. the spectral half-width expected purely due to beam and wind-shear spectral broadening for the troposphere.

Fig. 23

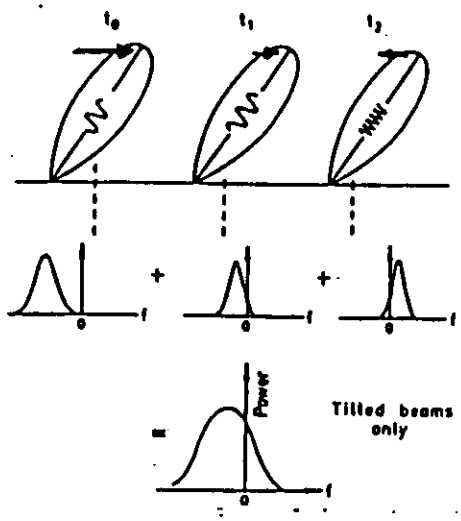

Illustration of spectral broadening by variation of horizontal wind with time.

Fig. 24

Of course the target parameter which is desired is the RMS fluctuating velocity of the scatterers, but this often contributes only a small fraction to the total spectral width. To determine the RMS fluctuating velocity, one should first use the measured mean wind speeds as a function of height, and the known polar diagram (radiation pattern) of the radar, to determine the spectral half-power half-width $f_{\frac{1}{2}nf}$ contributed by the non-fluctuating effects. Then the contribution from the fluctuating component f_{fluct} can be found through the relation

$$f^2_{fluct} = f^2_{\frac{1}{2}expt} - f^2_{\frac{1}{2}nf} \tag{104}$$

This arises because the experimental spectrum is approximately a convolution between the spectrum which would be produced if there were no fluctuating components, and the spectrum due to the fluctuating components alone (at least for very narrow beams ($\leq$ about 5° half-power half-width); the more general case has been modeled by Hocking, 1983a).

To properly consider all the contributions from the mean wind including wind shear, a more accurate computer model needs to be used (eg Hocking 1983a), but in many cases equation (104) serves as a useful approximation to obtain $f_{\frac{1}{2}nf}$.

Of course equation (104) is only a first-order estimate of the spectral half-width due to the non-fluctuating component, and it also assumes that the scatterers scatter isotropically. If the scatterers are anisotropic, as may be the case and as has been discussed previously, then the true contribution from non-fluctuating components will be less than that calculated with (104). That equation can still be used, but $\theta_{\frac{1}{2}}$ must be replaced by $\theta'_{\frac{1}{2}} = R.\theta_{\frac{1}{2}}$ where

$$R = \left[1 + \frac{\theta^2_{\frac{1}{2}}}{\theta^2_{s\frac{1}{2}}}\right]^{-\frac{1}{2}}, \tag{105}$$

$\theta_{\frac{1}{2}}$ being the true half-power half-width of the radar beam, and $\theta_{s\frac{1}{2}}$ is the half-power half-width of the polar diagram of backscatter due to the scatterers (i.e. $\theta_{s\frac{1}{2}} = \sqrt{ln2}.\theta_s$, θ_s being the aspect sensitivity factor (e.g. see Lesicar and Hocking, JATP, 1992)).

Having now determined the contribution due to non-fluctuating aspects of the wind field, and removed it from the experimentally determined spectral half-width, it is now necessary to decide what this residual contribution means, and how to interpret it. There are at least 3 possible contributions to this remaining contribution to the spectral width, namely the effects of fluctuations in the velocity due to turbulence, fluctuations due to buoyancy waves, and the decorrelation time associated with the decay of turbulent eddies. It is not always easy to separate out these terms.

In the case of a vertical beam, the most important effects are the vertical fluctuating component of the turbulent velocity, and both the vertical and horizontal components of the buoyancy-wave field. The horizontal component of the buoyancy field is important because although the beam is vertical, if the wave amplitudes are substantial the radial components of velocity fluctuations occurring near the edge of the beam may still contribute to the spectral broadening. This is especially true when wide beams are used, and is an argument for the use of narrow beams when studies of turbulence are made.

When off-vertical beams are used, both the vertical and horizontal fluctuating components of the turbulent velocity field are important. However, the horizontal components of the buoyancy-wave field become even more important in contributing to the spectral broadening; variations of velocity due to buoyancy waves occur both as a function of position within the radar beam and also as a

function of time during the period of data collection. This latter effect can be quite dominant, and swamp the contribution due to the turbulence. For example, fig. 25, taken from Hocking (1983b) illustrates this point, and shows the dramatic increase in spectral width recorded when an off-vertical beam is used as compared to a vertical beam. In this case the radar was an MF radar observing the mesosphere, and the beam-width was wider than for many VHF radars (about 4.5° half-width); data were collected for 12 mins in order to emphasize the effect. In normal VHF experiments the effect may not be so dramatic, but nevertheless occurs.

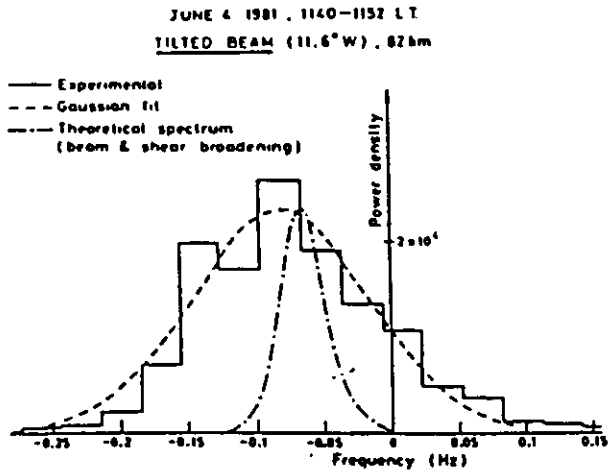

Fig. [..]: The solid curve shows a spectrum recorded with the Buckland Park 1.98 MHz radar, using a 10 min data length and a beam tilted 11.6° off-vertical. The dash-dot curve shows the approximate shape of the spectrum recorded with a vertically pointing beam at the same time.

Thus measurements of turbulent energy dissipation rates are best made using a vertical beam. The contribution due to turbulence can be envisaged as follows, and is illustrated in fig. 26. Backscatter occurs predominantly from scatterers with scales of the order of the radar half-wavelength, but these scatterers are carried around by the larger scales. The mean square fluctuating velocity measured by the radar is then the integrated effect from scales of the order of the radar half-wavelength out to scales comparable with the radar volume (e.g. Sato and Woodman, 1982; Hocking, 1983a).

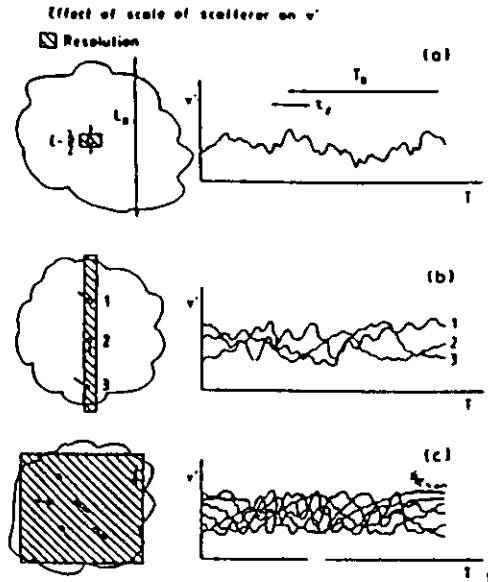

Illustration of the effect of scale of resolution on measured $\overline{v^2}$ values. (a) The motion of a single scatterer. In any time interval τ_p only a limited amount of velocity fluctuation occurs, but in the larger time interval T_p the full possible range of velocity fluctuations occur, as larger scales become more effective. (b) and (c) show that many scatterers contribute to the final signal received, each with a different velocity, so a full range of Doppler velocities is experienced in a very short time.

Fig. 26

For radars with pulse lengths and beam-widths comparable to the buoyancy scale of turbulence, scales even beyond the buoyancy scale may contribute to the mean square fluctuating velocity, although fortunately with reduced contributions. Let us say that the measured mean-square fluctuating velocity is due to a fraction $\mathcal{F}$ from scales within the inertial range of turbulence, and the remaining contribution comes from scales within the buoyancy range. The exact value of $\mathcal{F}$ depends on the radar configuration, sampling time, etc., and for the present we will not concern ourselves with its evaluation.

Then we may write (following Hocking 1983a, 1986) that the velocity variance observed with the radar is

$$\overline{v^2} = \int \Theta_{11}(k_1)dk_1 \tag{106}$$

where $\Theta_{11}(k_1)$ is the longitudinal one-dimensional spectrum function (e.g. see earlier) for the direction radial from the radar. The integration is performed over all scales which can affect the radar measurements, which for VHF radars means scales out to the radar pulse length or the buoyancy scale of turbulence, whichever is larger. For a radar pulse length of 600 m, say, this means that scales well into the buoyancy range will be effective, since the thicknesses of these layers is often well below 600 m (e.g. CRANE, 1980; BARAT, 1982) and the inertial range-buoyancy range transition scale is usually several times less than the layer thickness (e.g. BARAT, 1982). If it is assumed that a fraction $\mathcal{F}$ of the measured velocity variance resides in the inertial range and the rest in the buoyancy range, we may write that the measured velocity variance $\overline{v^2}$ obeys the relation

$$\int_{-k_\lambda}^{-k_B} \Theta_{11}(k_1)dk_1 + \int_{k_B}^{k_\lambda} \Theta_{11}(k_\lambda)dk_1 = \mathcal{F} \cdot v^2 \tag{107}$$

where k_B is the wave number of the buoyancy scale (transition scale between the inertial and buoyancy ranges) and k_λ is the Bragg backscatter wave number. For Kolmogoroff, inertial-range turbulence, and defining the turbulent energy dissipation rate as ε, we may take

$$\Theta_{11}(k) = .1244C_v^2 \mid k \mid^{5/3} = .1244C\varepsilon^{2/3} \mid k \mid^{5/3} \tag{108}$$

and solve for ε in terms of k_B, k_λ, and $\overline{v^2}$. C is well known from careful atmospheric experiments (e.g. CAUGHEY et al., 1978) to be close to 2.0.

This may then be used (e.g. Hocking, 1983a) to derive

$$\varepsilon = \varepsilon_* L_B / \left(L_B^{2/3} - \left(\frac{\lambda}{2}\right)^{2/3} \right)^{3/2} \tag{109}$$

where

$$\varepsilon_* = 2\pi \left(\frac{\mathcal{F}}{.3732C_v^2} \right)^{3/2} \left(\overline{v^2}\right)^{3/2} / L_B. \tag{110}$$

If $\mathcal{F}$ is taken to be 0.5 and $C_v^2 = 2.0$, then we can write approximately that

$$\varepsilon = 3.45 \left(\overline{v^2}\right)^{3/2} / L_B. \tag{111}$$

WEINSTOCK (1978b) has suggested that the Buoyancy scale relates to the Brunt-Vaisala frequency and the energy dissipation rate through the relation

$$L_B = \frac{2\pi}{0.62} \varepsilon^{\frac{1}{2}} \omega_B^{-\frac{3}{2}}$$

and using this relation with our earlier equations gives

$$\varepsilon = \left[\frac{12.24\mathcal{F}}{C_v^2} \right] \overline{v^2} f_B, \tag{112}$$

f_B being the Brunt-Vaisala frequency in Hz. Again taking $\mathcal{F} = 0.5$ and $C = 2.0$, we may write

$$\varepsilon \simeq 3.1 \overline{v^2} f_B \tag{113}$$

Notice that this also means that

$$L_B \simeq 1.1 \frac{\overline{v^2}^{\frac{1}{2}}}{f_B},$$

a useful relation for making radar estimates of the Buoyancy scale.

Of course $\overline{v^2}$ can be found from the relation

$$\overline{v^2} = f_{fluct}^2 / (2\ell n 2) \tag{114}$$

provided of course that $f_{\frac{1}{2}fluct}$ can be shown to be entirely due to the turbulence.

If $\mathcal{F}$ actually varies up to 1.0 or down to 1/4, then the estimates represented by these equations will be incorrect by a factor of 2-3. However, shortly we will present a revised and improved theory which gives a better feel for the values of $\mathcal{F}$.

These formulae assume that the scattering scale $\lambda/2$ lies in the inertial range. However, it should be noted that if scatter occurs from the viscous range, as may at times happen in the mesosphere, the formulae are still largely valid. It will be noted from (107) that the mean square velocity is an integrated effect due to all scales between $\lambda/2$ and L_B and this integration is dominated by the large scales. A change in the spectral form from (108) within the viscous range will not greatly affect the integral; at worst, the $\lambda/2$ term in (109) may need to be replaced with the inertial range inner scale.

When the radar volume has dimensions less than the buoyancy scale of turbulence, the formula becomes slightly modified. The parameter L_B is replaced by the larger of the pulse length and the radar beam-width at the height of scatter (which we will denote as L_r), and the constant of proportionality changes slightly. In this case k_B in equation (107) is replaced by a Fourier scale representative of the range of Fourier components in the pulse (or the beam-width, whichever is larger). For example, if the pulse is Gaussian in shape with a half-power half-width L_r, then its Fourier transform has a half-width at half-power of about $0.44 \times 2\pi/L_r$. This different situation means that for $L_r \ll L_B$, the following relation applies (e.g. Labitt, 1979; Bohne, 1982 (appendix C); Hocking, 1996 (see shortly))

$$\varepsilon \simeq 1.3 \left(\overline{v^2}\right)^{3/2} / L_r. \tag{115}$$

The constant (1.3) has changed considerably compared to the earlier formulae. The main reason is that the constant 1.3 assumes that there is no Buoyancy scale, and assumes that the $k^{-\frac{5}{3}}$ law applies over all scales; thus Fourier scales of small wavenumber, although only a small contribution to the pulse, make a large contribution to the integral. An improved mathematical discussion will be given shortly.

The relations above may be used to determine the turbulent energy dissipation rate if one knows the contribution to the spectrum from turbulent fluctuations. However, we still must decide whether all the remaining spectral width is indeed due to turbulent fluctuations. Even when vertical beams are used to measure the spectrum, there may still be a small contribution due to buoyancy waves, (as has already been discussed), but it is possible to make at least some attempt to separate the turbulent and buoyancy wave effects. Use of procedures which involve least-squares fitting to a Gaussian shape help, because buoyancy-wave fluctuations of specular reflectors, for example, can produce fairly non-Gaussian spectra. Thus spectra dominated by buoyancy-wave fluctuations are often rejected by such procedures. Another possibility is that used by Hocking (1988),who utilized the fact that the buoyancy-wave field tends to have only a small contribution (if at all) from oscillations with periods of less than 5 min. This is not to say, however, that using a data length of less than 5 mins eliminates the wave effects, since even a fraction of a wave cycle could cause significant contributions to the spectral width. However, one can predict how the spectral width might change as a function of data length in this case, and by comparing this prediction to the true variation in spectral width as a function of data length, can make some estimate of the relative contributions of buoyancy waves and turbulence. Such a process has some uncertainty associated with it, but is nevertheless of some value. An example was given in Hocking (1988).

We have not yet addressed the contribution due to the decorrelation time associated with the finite lifetime of the eddies. In fact provided that the radar wavelength is substantially less than the

buoyancy scale, this is not a major contribution, as will now be shown.

If the energy dissipation rate is again denoted ε, the typical eddy scale as ℓ and the velocity associated with such an eddy is denoted as v, then the typical lifetime τ of an eddy is

$$\tau \sim \frac{\ell}{v} \tag{116}$$

where

$$\varepsilon \sim \frac{v^2}{\tau}. \tag{117}$$

Hence

$$\tau \sim \frac{v^2}{\varepsilon} \sim \left(\frac{\ell}{\tau}\right)^2 \cdot \frac{1}{\varepsilon} \tag{118}$$

so that

$$\tau \sim \ell^{\frac{2}{3}} \varepsilon^{-\frac{1}{3}} \tag{119}$$

Thus the growth and decay of eddies produces an autocorrelation function with a half-width at a value of 0.5 of about τ , where τ is given by the above expression. If the autocorrelation function is taken to be Gaussian, then its Fourier transform is also Gaussian, with a half- power half-width of $0.22 / \tau$, and we will denote this as f_{dc} , where "dc" stands for "decorrelation". Thus

$$f_{dc} \simeq \frac{.22}{\tau} \sim .22\ell^{-\frac{2}{3}} \varepsilon^{\frac{1}{3}}, \tag{120}$$

where ℓ can be taken to be of the order $\lambda/2$.

(A special application of this theory in regard to PMSE will be presented shortly

Contrast this to the contribution due to fluctuating motions, which contribute out to scales of the order of the Buoyancy scale, L_B. In this case, we have already seen that if we take $\mathcal{F}$ as about 0.5, then

$$\varepsilon \simeq 3.5 \frac{v_{RMS}^3}{L_B}. \tag{121}$$

Then the half-power half-width of the spectrum due to the fluctuating motion of the scatterers is given by

$$f_{fluct(m)} \simeq .8 \left(\frac{2}{\lambda}\right) \varepsilon^{\frac{1}{3}} L_B^{\frac{1}{3}} \tag{122}$$

Hence the ratio of spectral half-widths due to the eddy motions and the decorrelation time of the eddies is

$$\frac{f_{fluct(m)}}{f_{dc}} \sim 4 \left[\frac{L_B}{\lambda/2}\right]^{\frac{1}{3}} \tag{123}$$

Physically this arises because the spectral width associated with the scatterer movement is related to the buoyancy scale L_B, (since we have seen that this width is due to the integrated effect of all scales up to L_B), whilst the decorrelation time depends only on the scale of the scatterers.

For a typical case with $\lambda/2$ equal to 3m, and L_B equal to say 200 m, the ratio is about 16. Since the total spectral width due to these two components combined is equal to the square root of the sum of the squares, the correction due to the decorrelation time in this case would be only a fraction of a percent. Thus provided the Buoyancy scale is greater than the Bragg backscatter scale by a few times, the decorrelation time of the eddies is only a minor correction to the spectral width and can usually be ignored.

It was mentioned earlier that information about the level of turbulence also exists in the correlation functions, and can be obtained from the Full Correlation Analysis technique using spaced antennas. Indeed, one of the output parameters of the Full Correlation Analysis is a parameter which is usually denoted as $T_{\frac{1}{2}}$ and represents the correlation function half-width which would be measured with a radar which moved along the ground with the velocity of the mean wind in the scattering region. Spectral beam-broadening has been removed from this parameter, although the effects of wind-shear have not. Thus the parameter $f_{\frac{1}{2}} = 0.22/T_{\frac{1}{2}}$ can be used in place of f_{fluct} in all the discussions above; the main potential problem is that there may be increased contributions from buoyancy waves if the polar diagram of the system is wide.

Provided the effects of gravity waves can be adequately separated, or even shown to be relatively unimportant, the procedures described above allows radars to be used to extract estimates of atmospheric turbulence.

It is also possible to infer the turbulent diffusion coefficient for a turbulent layer through the relation

$$K_M = c_2 \varepsilon / \omega_B^2 \tag{124}$$

e.g. WEINSTOCK, 1978a, b; LILLY et al. 1974). The constant c_2 is quoted to have a variety of values in the literature, ranging from about 0.25 to 1.25. The most commonly accepted value seems to be 0.8 (WEINSTOCK, 1978). Ideally it is also necessary to know the Brunt-Vaisala frequency averaged over the turbulent layer, but unfortunately it is not always possible to find this. Some authors use climatological values, but it is better to use radio-sonde determinations where possible.

6.6.3.2.1 A more general theory for spectral width determinations of ε

The above theoretical development is modestly complete, but there is one complication which needs to be now introduced. This is the effect of the pulse-length. We have already alluded to this in a general sense; but we now need to consider it in more detail.

The inclusion of these effects, and their impacts on radar measurements, are described in the following article.

160

Pergamon

Adv. Space Res. Vol. 17, No. 11, pp. (11)37–(11)47, 1996

0273-1177(95)00728-8
0273-1177/96 $9.50 + 0.00

AN ASSESSMENT OF THE CAPABILITIES AND LIMITATIONS OF RADARS IN MEASUREMENTS OF UPPER ATMOSPHERE TURBULENCE

W. K. Hocking

Physics Department, University of Western Ontario, London, Ontario, Canada N6A 3K7

ABSTRACT

The basic procedures used to determine atmospheric turbulence intensities from measurements made with atmospheric radars are outlined. The method which utilizes the spectral width of the signal is especially discussed, and missing assumptions which have not been fully considered in earlier derivations are considered in more detail. It is shown that previous relations linking spectral widths and turbulent energy dissipation rates will need modifications and these modifications reduce previous radar estimates of energy dissipation rates by up to a factor of 2 or 3.

INTRODUCTION

Radars, whilst not being able to provide the height resolution available with rocket and in situ measurements, offer the potential to study longterm variability of atmospheric turbulence because of their capability to record continuously and uninterrupted for long periods of time, often in an unattended mode. The two main procedures which are used to determine atmospheric turbulence strengths with radars are firstly, measurement of the absolute signal strength, and, secondly, measurement of the spectral width of the time series recorded with the radar. Both methods have been discussed in some detail in the past decade (e.g. /1,2,3,4,5/). In this document we will very briefly outline the techniques and highlight some of the difficulties in making these measurements, but one of the major tasks of this paper will be to point out deficient assumptions made in earlier derivations of relationships between energy dissipation rate and spectral width.

To begin, one chief advantage of atmospheric radars is their ability to measure on a continuous basis, often unattended. Such radars also have a moderately good height resolution (typically a few hundred metres), although certainly not comparable to the resolution which can be obtained with in-situ measurements. Disadvantages include the possible existence of anisotropic turbulence and contamination by processes such as gravity wave oscillations. The radars also tend to determine an average turbulence intensity over a volume of atmosphere which may approach a cubic kilometre. Nevertheless these limitations, whilst perhaps limiting somewhat the instantaneous precision available in measurements of turbulence with such radars, certainly permit radars to measure a long term morphology of the variation of mean turbulence intensities.

TURBULENT ENERGY DISSIPATION RATES BASED ON ABSOLUTE SIGNAL STRENGTHS

The absolute signal strength method essentially involves determining the backscattered power received with a radar and then using radar characteristics such as the beam width, wavelength, transmitter power, antenna gain and antenna effective area to determine an effective turbulence structure constant C_n^2. The relation specifically is as follows:

$$C_n^2 = \frac{92 P_{RT}^2 \lambda^{1/3}}{A_T G_{Tm} A_{Rm} e_T e_R (0.5 c\tau) \theta_{1/2}^2} \qquad (1)$$

where P_R is the received power, P_T is the transmitted power, r is the range, e_T and e_R are the transmitter and receiver system efficiencies, c is the speed of light in air, G_{Tm} and A_{Rm} are the transmitter gain and receiving area respectively, τ is the pulse length, and $\theta_{1/2}$ is the half-power half-width of the two-way polar diagram of the combined transmitter-receiver system /3/. For work in the middle atmosphere, the turbulence structure function C_n^2 can then be related to the energy dissipation rate through the following relation:

$$\epsilon = [\frac{3C_N^2\omega_B^2}{22\frac{|R_i|}{|1-R_i|}M_N^2}]^{3/2} \tag{2}$$

(/5/), where N is the electron density, M_N is the mean electron potential density gradient, ω_B is the Vaisala- Brunt frequency, and R_i is the gradient Richardson number. The refractive index structure constant C_n^2 is related to the electron density structure constant by

$$C_N^2 = (\frac{\partial N}{\partial n})^2 C_n^2 \tag{3}$$

The expression for $\frac{\partial N}{\partial n}$ can be determined from theory (e.g. /6,7/) Equivalent expressions for scatter from the troposphere and stratosphere have also been given in /5/.

However, although these relations seem moderately simple, there are complications involved in evaluating turbulence strengths by this method. In particular, the radar volume is often incompletely filled, and in order to make a meaningful estimate of the energy dissipation rate it is necessary to determine the fraction of the radar volume which is filled by turbulence. /1/ and /8/ have discussed this problem in some detail. /2/ have also shown how this fraction F can be determined in a climatological sense, but it is only an approximate calculation and can still lead to large errors in the energy dissipation rate. It should also be pointed out that the expression in equation (2) depends on the Richardson number. This is a deviation from earlier theories in which it was assumed that potential energy and kinetic energy are equipartitioned within a turbulent region. However it has been clearly shown that such equi-partition is not a valid assumption, and the inclusion of this Richardson number dependence is an important modification of recent theories. /5/ has discussed this in greater detail.

TURBULENT ENERGY DISSIPATION RATES BASED ON SPECTRAL WIDTHS

The second major method for determining energy dissipation rates is to measure the spectral width determined by the radar. This also has complications of its own, not the least of which is removal of the spectrum due to the mean motion of the wind through the radar beam. This process has been discussed extensively by /3,4,9,10,11,12/. The theory related to this process has been well developed, and once contaminating effects like beam broadening and wind shear broadening have been removed from the spectral width it is possible to make an estimate of the turbulent energy dissipation rate. However this assumes that gravity waves are not a significant contributor to the spectral width. In fact /13,14,15/ have discussed how temporal variations due to gravity waves may contaminate the spectral width even though the data length recorded may only be a small fraction of the period of the gravity waves. Nevertheless because of the rather oscillatory nature of the gravity waves the spectra produced due to their presence often have particularly obvious (and non-Gaussian) shapes which involve very peaked sections of the spectra. Such spectra can often be identified and removed, and indeed many routine procedures utilizing this method include criteria for rejection of non-Gaussian spectra.

Then once these effects such as gravity waves and beam broadening are deconvolved from the measured spectra, the remaining spectral width can be used to determine the energy dissipation rate. The essence of the idea is that the spectral width measured is the integrated effect of all scales within a turbulent patch which are within the range between the Bragg scale (i.e. 1/2 of the radar wave length) up to the largest scale of turbulence. Assuming a Kolmogoroff form for the turbulence spectrum we have the expression:

$$\sigma^2 \propto \int_{k=4\pi/\lambda}^{2\pi/L_B} \varepsilon^{2/3} k^{-5/3} dk, \tag{4}$$

where σ is the root mean square velocity deduced from the spectral width of the signal. Details concerning specifics about the type of spectrum involved and the relevant constants are discussed in more detail in /4/. In particular, it is necessary to consider the relative distribution of energy in the buoyancy and inertial ranges. Upon integration we obtain the following expression:

$$\sigma^2 \propto \varepsilon^{2/3}[L_B^{2/3} - [\frac{\lambda}{2}]^{2/3}] \tag{5}$$

and assuming that $L_B >> \lambda/2$ we have the following relationship:

$$\varepsilon = c_1 \frac{\sigma^3}{L_B} \tag{6}$$

The value of c_1 differs somewhat for different assumptions about the constants involved in the Kolmogoroff spectrum, but /4/ has given a value of c_1 of 3.5. This value assumes that the fluctuations producing the radar signal are produced in roughly equal proportion by scales in the buoyancy range and the inertial range. We shall re- address this assumption shortly.

If, in addition, we use the relation between the buoyancy scale L_B and the Vaisala-Brunt frequency which was specified by /16/ as

$$L_B = \frac{2\pi}{0.62} \varepsilon^{1/2} \omega_B^{-3/2} \tag{7}$$

we may then write

$$\varepsilon = c_0 \sigma^2 \omega_B \tag{8}$$

where c_0 is a constant. /4/ has given $c_0 = 0.49$.

Thus we have a very simple relationship between the energy dissipation rate, the mean square radial velocity measured with the radar and either the outer scale of turbulence or the Brunt-Vaisala frequency. However, one of the major purposes of this paper is to re-examine this very simple derivation. One can note that the key point in this derivation is an assumption that the integration proceeds only out to the buoyancy scale of turbulence. The possibility that the relative values of the buoyancy scale and the pulse length of the radar might somehow affect the constants has only been considered in a very crude sense. It will be a major objective of this paper to re-address the relative contributions from the inertial and buoyancy parts of this spectrum in greater detail.

In contrast to this expression, (which is commonly used in mesospheric and stratospheric radar studies), equations relating radar spectral widths and turbulent energy dissipation rates which have been presented in the meteorological literature have tended to ignore the possibility that the larger scales important in determining the radar spectral widths might be defined by the turbulence outer scales. Rather, they have assumed that either the length of the radar pulse, or the radar beam-width, (whichever is larger) is the most important parameter in determining the outer scale required in the above integrations. The initial derivation of this type of formula was presented by /12/, although a more thorough derivation was presented by Labitt/17/. A summary of the derivation produced by Labitt has been presented by /18/. In this document we will briefly outline the derivation produced by Labitt and then we will show how it is modified when one takes into account the existence of an outer scale of the turbulence.

RELATION BETWEEN THE RADAR SPECTRAL WIDTH AND THE STRENGTH OF TURBULENCE WHEN THE EFFECTS OF THE BUOYANCY SCALE ARE IGNORED

As discussed, the most thorough derivation of the relation between the radar spectral width and the strength of turbulence has been given by Labitt /17/. Labitt begins by noting that the mean variance of the signal is given by the following expression:

$$\sigma^2 = E(u_r^2) - [E(u_r)]^2 \tag{9}$$

where u_r represents the radial velocity and E represents the expectation value. The expectation is weighted by the radar volume, and it is assumed that the weighting takes the following form:

$$A(\underline{r}) = \frac{1}{(2\pi)^{3/2}ba^2} exp\{-[\frac{y^2+x^2}{2a^2} + \frac{z^2}{2b^2}]\} \tag{10}$$

Thence:

$$\sigma^2 = \int A(\underline{r})E(u_r^2)d\underline{r} - \int\int [A(\underline{r_1})A(\underline{r_2})E(u_r(\underline{r_1})u_r(\underline{r_2})d\underline{r_1}d\underline{r_2} \tag{11}$$

We now note that if we assume statistical stationarity and homogeneity then

$$E[u(\underline{r_1})u(\underline{r_2})] = E[u(\underline{r_1})u(\underline{r_1}+\underline{\delta r})] = B_{ll}(\underline{r_1}-\underline{r_2}) = B_{ll}(\underline{\delta r}) \tag{12}$$

where B_{ll} is the autocorrelation function. We now let $\phi_{ll}(\underline{k})$ be the Fourier transform of $B_{ll}(\underline{r})$, so that $B_{ll}(\underline{r}) = \int \phi_{ll}(\underline{k})exp\{i\underline{k}\cdot\underline{r}\}\underline{dk}$. ϕ_{ll} is called the longitudinal spectral function, and B_{ll} is the longitudinal autocorrelation function. Then we note that

$$E(u^2) = B_{ll}(0) = \int \phi_{ll}\underline{dk} \tag{13}$$

Substitution of these Fourier expressions in (11) leads to the following expression

$$\sigma^2 = \int \phi_{ll}(\underline{k})[1 - \int\int A(\underline{r_1})e^{i(\underline{k}\cdot\underline{r_1})}A(\underline{r_2})e^{i(\underline{k}\cdot\underline{r_2})}d\underline{r_1}d\underline{r_2}]\ \underline{dk} \tag{14}$$

Further manipulation then leads (for a near-vertical radar beam) to the expression

$$\sigma^2 = \int \phi_{ll}(\underline{k})[1 - e^{-[k_x^2b^2+k_y^2a^2+k_z^2a^2]}]\underline{dk} \tag{15}$$

Note that the term in square brackets is simply 1 minus the Fourier transform of the radar volume. If one then takes the classical Kolmogoroff spectrum, the spectrum of vertical velocities as a function of wave number $\underline{k}$ is:

$$\phi_{ll}(\underline{k}) = \frac{E(k)}{4\pi k^2}[1 - \frac{k_z^2}{k^2}], \tag{16}$$

where k is the magnitude of $\underline{k}$ and so is a scalar satisfying $k^2 = k_x^2 + k_y^2 + k_z^2$, α is a numerical constant with value $0.7655C$, (where $C = 2.0$ /19/), and furthermore $E(k) = \alpha\varepsilon^{2/3}k^{-5/3}$. Then the following expression for the velocity variance measured by the radar is obtained:

$$\sigma^2 = \frac{1}{2}\alpha\varepsilon^{2/3}\Upsilon. \tag{17}$$

where
$$\Upsilon = \int_{\theta=0}^{\pi}\int_{k=0}^{\infty} sin^3\theta k^{-5/3}[1-e^{-(a^2sin^2\theta+b^2cos^2\theta)}]dkd\theta. \tag{18}$$

Thence
$$\varepsilon = \frac{2\sqrt{2}}{[\alpha\Upsilon]^{3/2}}\sigma^3 \tag{19}$$

Finally, Labitt shows that the following expressions for Υ are valid: Firstly if $a \geq b$:

$$\Upsilon = 2\Gamma(\frac{2}{3})a^{2/3}F[\frac{-1}{3};\frac{1}{2};\frac{5}{2};1-\frac{b^2}{a^2}] \tag{20}$$

whilst if $b \geq a$:

$$\Upsilon = 2\Gamma(\frac{2}{3})a^{2/3}F[\frac{-1}{3}; 2; \frac{5}{2}; 1 - \frac{a^2}{b^2}] \tag{21}$$

The function Γ is the gamma function, and F is the confluent hypergeometric function; it turns out that the value for F is actually very insensitive to a/b, with it being approximately 1 (to within 10%) over all a and b in the case $a \geq b$, and within 25% of 1 in the second case. It should also be noted here that a and b are $1/e$ half-widths. If we use the more conventional half-power full widths of the pulse and the beam width, then we have $a = r\theta_f/(2\sqrt{(2\ell n2)} = r\theta_f/2.35$, and $b = L/2.35$, where r is the range to the scatterers, θ_f is the half-power-*full*-width of the beam, and L is the half-power full pulse length. In the case that $\alpha = 1.53$, we can write

$$\epsilon = 0.79\frac{\sigma^3}{S_m}.c_c \tag{22}$$

where S_m is the largest of the pulse length and the beam width, and c_c is a correction factor very close to 1. (Labitt used $\alpha = 1.36$, but we feel that the estimate given by /19/ of $C = 2.0$ and hence $\alpha = 1.53$ is more appropriate). Thus this equation looks very much like equation (6), except that the scale on the denominator is now related to the pulse length or beam width rather than the buoyancy scale, and the constant differs (0.79 compared to 3.5). The difference in the constants arises because in equation (6) some contribution to the variance is allowed due to scales larger than L_B, whilst equation (22) assumes a more abrupt cut-off at its largest scale.

Note especially the dependence of this relation on the largest of the beam width and the pulse length. Note also there is no dependence on a buoyancy scale L_B simply because there was no buoyancy scale permitted in the first place. In the following section we wish to re-address this derivation due to Labitt but allow the spectrum to simultaneously have a dependence on the outer scale.

COMBINING THE BUOYANCY PART OF THE SPECTRUM WITHIN THE LABITT-FORMALISM.

Fig. 1 shows two examples of how the spectrum might be modified if an outer scale is included in the spectral expression. Unfortunately there are almost no observational data describing the spectral form of $E(\underline{k})$ at small k, so we have simply tried to represent two possible extremes in this plot. We have maintained a Kolmogoroff spectrum at larger k. Because of this uncertainty about the nature of $E(\underline{k})$ at small k, we have decided to approach this problem by numerical integration, assuming various forms for the spectrum. Thus we return to equations (18) and (19), but we make an assumption that $E(k)$ is no longer given by the Kolmogoroff spectrum. Rather, we assume that it is given by the form shown below:

$$E(k) = \alpha\epsilon^{2/3}\frac{k^{-5/3}}{[1 + (k/k_B)^n]} \tag{23}$$

where n may equal -3 or n may equal -4/3. These values are not chosen for any particular physical reason except that they describe very nicely two rather extreme forms of the spectrum in the low wave number range. A value of $n = -3$ corresponds to the case of E proportional to $k^{4/3}$ at very small k and this essentially is equivalent to a cutoff in the spectrum at a wave number corresponding to an outer scale L_B. A value of $n = -4/3$ corresponds to a spectrum which varies as $k^{-1/3}$ at small k. (Note that the spectrum of vertical velocities should not be confused with that of horizontal fluctuations, which has a very different power law, but is often discussed more frequently in the literature). Representative spectra are illustrated in Fig. 1.

We will be evaluating a modified form of equation (18) for the work presented here-in: specifically, we will determine

$$\Upsilon = \int_{\theta=0}^{\pi}\int_{k=0}^{\infty} sin^3\theta\frac{k^{-5/3}}{[1 + (k/k_B)^n]}[1 - e^{a^2sin^2\theta + b^2cos^2\theta}]dkd\theta. \tag{24}$$

Note throughout all this work that (19) is still valid; it will be the value for Υ which will change as we vary n.

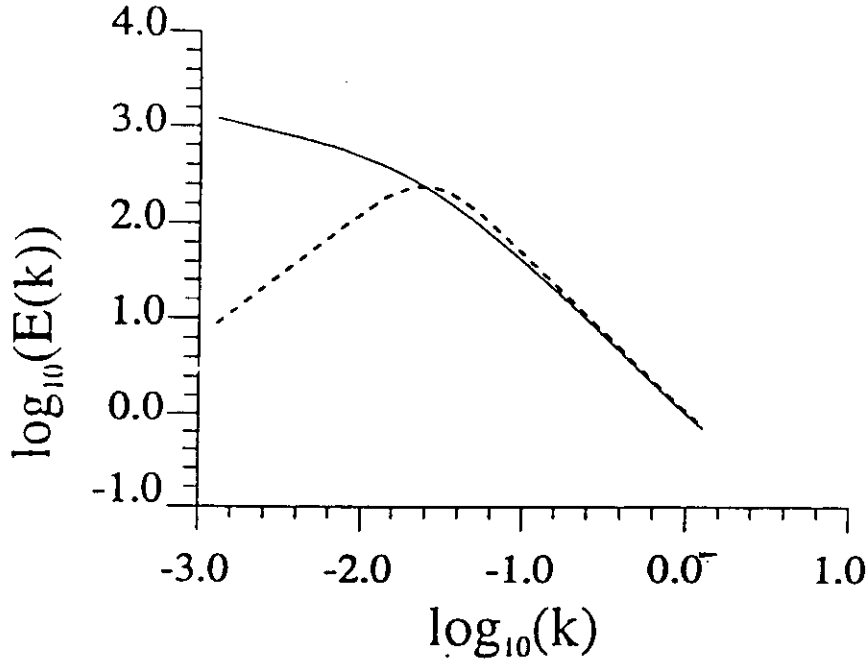

Fig. 1. Representative forms for the turbulent spectra $E(k)$, including typical possible variations at small k. Specifically these graphs show equation (23), for $n = -3$ and $-4/3$. The $n = -3$ case corresponds to a power law of the type $k^{4/3}$ at small k, and is represented by the broken line; the $n = -4/3$ case corresponds to a power law of the type $k^{-1/3}$ at small k, and is represented by the solid line. In both cases the buoyancy scale is the same and equals $250m$; the corresponding wavenumber lies very close to the peak in the broken curve.

We shall make the assumption throughout this derivation that the Kolmogoroff part of the spectrum which exists at large k and the spectral shape which exists at very small k are continuous as they merge into each other. The -1/3 slope is especially important because it represents a situation similar to that described by /20/ for vertical velocity fluctuations as a function of horizontal wavenumber as one passes from the turbulent regime at large k (small scales) to a gravity wave regime at small k (large scales). We expect that the variation as a function of horizontal wave number would be more important than the variation as a function of vertical wavenumber, because the beam width usually far exceeds the pulse length for vertically pointing radars. However, by considering both the spectral forms described above, we will in a broad sense cover both possibilities. (In fact it should be noted that if perchance the variation as a function of vertical wavenumber were to be more important than the variation as a function of horizontal wavenumber, then /20/ suggests that the spectral energy density should vary as k_z^{+1} - close to $k_z^{+4/3}$, and thus fairly similar to the "n = -3" case.) Also note that this contribution from gravity wave motions should not be confused with the earlier discussion, in which the effect of temporal fluctuations of the waves, and data length of the sample, was discussed. The effect discussed now represents a contribution due to spatial variability.

We begin by considering the case "n=-3." A numerical integration of equation (24) shows that over a wide range of scales, Υ can be represented closely by the following expression:

$$\Upsilon = (0.45 L_B)^{2/3} \tag{25}$$

Hence, using (19) we obtain the relation

$$\varepsilon = 3.3\frac{\sigma^3}{L_B} = 0.47\sigma^2\omega_B \tag{26}$$

This compares very favourably to the estimates made in earlier literature, in which the equation $\varepsilon = 0.49\sigma^2\omega_B^2$ has been given e.g. see equation (8). Fig. 2 shows a contour graph in which the ratio of the true value of ε relative to the above formula is shown for various beam widths and various outer scales L_B. The pulse length is chosen to be a fixed value of 150 m, although almost identical results would be obtained for other pulse lengths provided that the beam-width always exceeds the pulse-length (a condition chosen because it is almost always true in practice for VHF and MF radars). The area in which the Labitt formula is accurate is also highlighted; note that throughout most of the region described by this graph the dependence of ε on L_B is very important and the Labitt formalism is generally not valid.

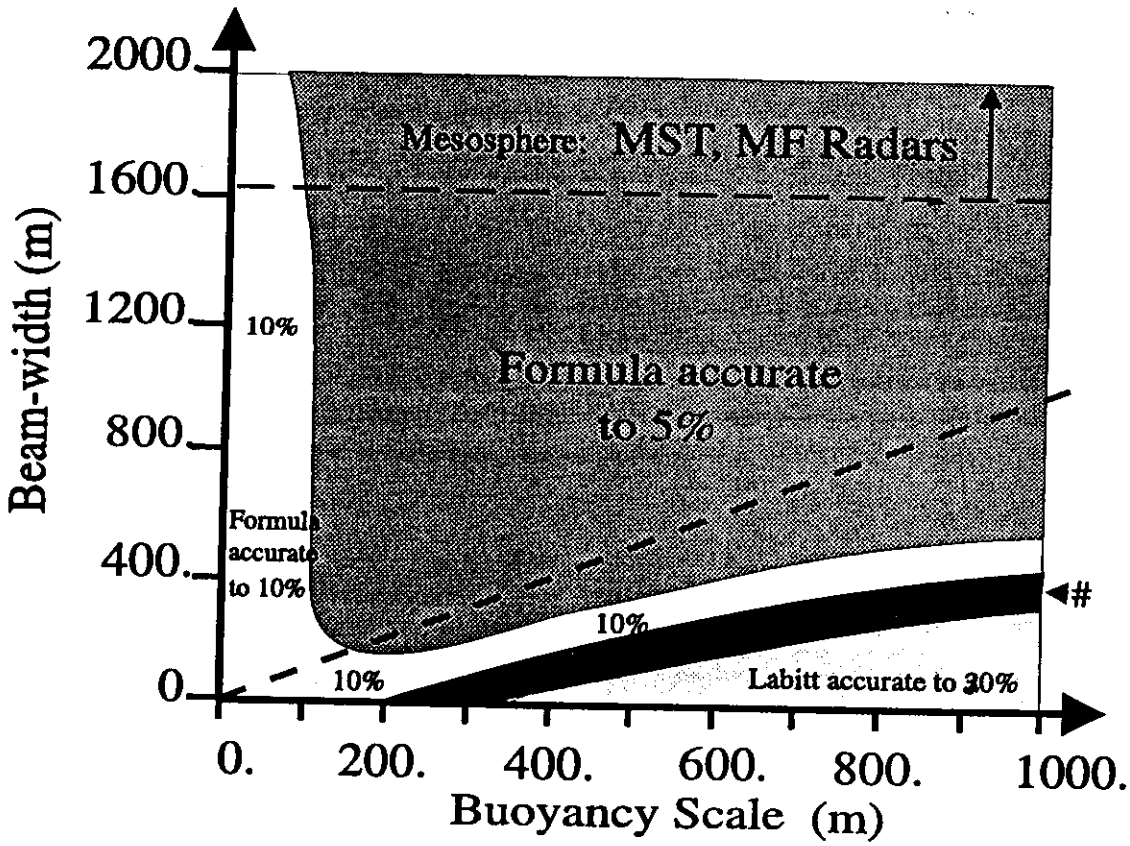

Fig. 2. Map showing the accuracy of equation (26) as a function of beam-width and buoyancy scale, assuming that the spectrum $E(k)$ varies as $k^{4/3}$ at small k (n = -3). Typically the true value of ε (as determined from an exact evaluation of (24) which is then applied in (19)) is less than that according to according to (26) in the bottom left-hand corner, and is generally slightly greater than (26) in the top right-hand corner, but in this graph we are only interested in knowing the deviation from 1.0, regardless of whether the ratio is less than or greater than 1. In the bottom right-hand corner Labitt's formula is more accurate (see equations (19) - (21)) , so in that region the true value of ε is compared to those equations. In the region indicated by a "#" symbol, neither formula is suitable, and (24) should be evaluated numerically for a suitably accurate solution. In these calculations, a pulse length of about 150m has been used, although the results will be insensitive to this value provided it is less than the beam-width.

The Labitt formalism is only valid if the outer scale L_B is several times larger than both the beam width and the pulse length, and the L_B dependence applies for all cases in which the beam-width

is more than one half of the buoyancy scale. Notice that although there is some variability in this ratio, the the variability is very small, generally less than 5%. Given the inaccuracies involved in making measurements of turbulence at distances a long way from the radar, a 5% error is almost insignificant.

It should be noted that this equation for $E(k)$ is the three dimensional spectrum integrated over all $\underline{k}$. This is not the same as the spectrum measured for a probe moving through the turbulence in a straight line, and the two types of spectra are often confused. For example, $E(k)$ given above for the Kolmogoroff spectrum is a true integration of the three-dimensional spectrum, whilst the types of spectra discussed by /20/, for example, represent the types of spectra measured by a probe moving in a straight line through the velocity field. However, provided the turbulence is isotropic and three-dimensional, and the spectra are governed by power laws, then the two different types of spectra have the same slope in log-log co-ordinates. Thus for our purposes, in which we are interested in form and not specifics about constants, and in which any constants are defined by letting the buoyancy wave spectrum run smoothly into the Kolmogoroff spectrum, we do not need to be too concerned about such details.

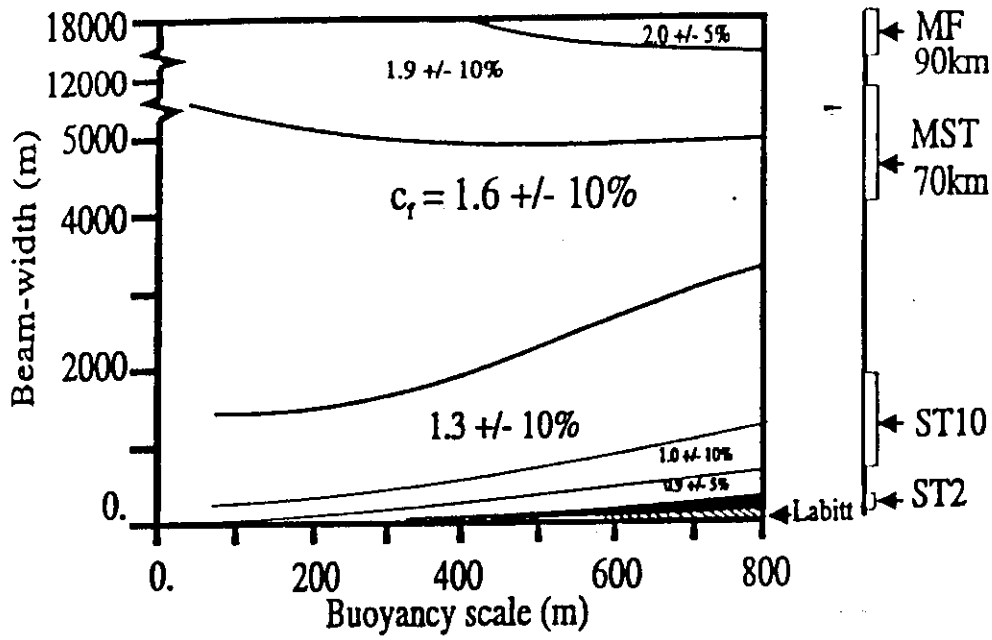

Fig. 3. Approximate contour graph showing the correction factor c_f in equation (27), as a function of buoyancy scale and beam-width. The region in which the Labitt formalism is more accurate than (27) is also shown in the bottom right-hand corner. The small darkened region above the "Labitt" region is an area in which neither (27) nor Labitt's formulas are appropriate. On the right of the graph is a one-dimensional map indicating relevant parts of the contour graph for different types of radars. These different categories are essentially based on beam-width, and in all cases it has been assumed that the beam half-power half-width lies approximately in the range 1.5° to 5°. A typical altitude for each type of radar is also indicated. "MF" refers to Medium Frequency radars, "MST" refers to Mesosphere-Stratosphere-Troposphere radars. ST10 means Stratosphere-Troposphere radars at typically 10 km altitude, and ST2 refers to ST radars at 2km altitude. There is no sense in going lower than 2 km since this is the near-field region for most ST VHF radars.

Let us now turn to the case of $n = -4/3$. In this case the spectrum goes as $k^{-1/3}$ as k tends to 0. Then in fact numerical integration of Equation (24) over a wide range of possible outer scales and possible pulse lengths and beam widths gives the following expression:

$$\epsilon = 3.3\frac{\sigma^3}{L_B}\frac{1}{c_f} = 0.47\sigma^2\omega_B[\frac{1}{c_f}]^{2/3} \quad (27)$$

where c_f is a correction factor. Even in this case, where the buoyancy range runs smoothly into the turbulence spectrum but the energy involved in the buoyancy range is higher than that in the turbulent spectrum, it can be seen that the dependence on L_B is still significant and the expression given by Labitt is generally not appropriate.

Fig. 3 shows the value of the correction factor over a wide range of beam widths and outer scales. Note that the region in which the Labitt formalism is approximately correct is indicated and is clearly only a small portion of the region. For MST radars the Labitt equation is almost never valid and the previous expression (27) is correct. Furthermore, the correction factor is a fairly slowly varying term which varies from as small as 0.9 for very small beam widths and very long outer scales up to a factor of as high as 2 for very broad beam widths (widths of several kilometres). The correction factor is dependent on the characteristics of the particular radar being used, but it is not a strong function of the radar parameters and a reasonable estimate can be made in almost all circumstances.

HORIZONTAL FLUCTUATING MOTIONS

In addition to the effects discussed above, there is an additional effect which can in certain circumstances produce an enhancement of the radar spectral width; the horizontal fluctuating motions as a function of horizontal scale can also be important in producing an artificial broadening of the spectral width. We shall examine this in an somewhat approximate manner.

First we shall assume, following /20/, that the spectrum of horizontal velocities follows a law of the type $E_{u^2}(k) = \beta k^{-5/3}$, and the vertical velocities have a spectrum as a function of horizontal wavenumber of the form $E_{w^2}(k) = \gamma k^{-1/3}$. We are interested in the contribution of each of these types of motions to the variance of radial velocities "seen" by a radar. In reality each of these spectra must be converted to a type of spectrum similar to that represented by ϕ_{ll} earlier, and then integrated over the radar beam , with a $sin^2\theta$ weighting included for the u^2 contribution , but this is beyond the scope of this paper. Hence we will content ourselves with the assumption that the result of these integrations will be power laws, with exponents differing by 4/3, just as the $E(k)$ expressions do. Then, assuming that each is equal in magnitude at $k = k_B$ (isotropic turbulence at this scale), the relative contributions to the radial velocity will be approximately

$$\frac{u^2_{rad}}{w^2} \sim [\frac{L_W}{L_B}]^{4/3}\theta^2_{1/2} \quad (28)$$

where L_W represents the beam half-power full width, L_B is the buoyancy scale, and $\theta_{1/2}$ is the half-power half-width of the radar beam. If we let the altitude of the scatterers be z, then for a vertical beam, we obtain

$$\frac{u^2_{rad}}{w^2} \sim 2^{4/3}\frac{z}{L_B}^{4/3}\theta^{10/3}_{1/2} \quad (29)$$

For $z < 10km$, $L_B \sim 500m$, and $\theta_{1/2} < 5°$, this ratio is less than .05, so that horizontal fluctuating motions make little contribution to the radial velocity in tropospheric studies. The contribution for scatter from 20 km altitude becomes around 10% - 15% for a 5° half-power half-width, but is still not important for beam half-widths less than 3° or so. However, in the case of mesospheric studies, the effect is more important, largely because of the much broader beam-width due to the greater range. Consider an altitude of scatter of 80 km. A beam half-power half-width of 2° gives a contribution to the mean square radial velocity due to horizontal fluctuations of only 5% relative to the vertical fluctuations, but a half-power half-width of 5° or 10° gives comparable contributions to the mean square radial velocity due to horizontal and vertical fluctuating motions! Such broad beam widths are often used by MF radars, for example, and some MST radars may even have beams out to 10° in half-width.

Of course the expression (29) is very likely an over-estimate, because it did not take account of the fact that the spectral shapes assumed are only valid for $k < k_B$, whereas the integrations were in effect done assuming that the power laws given were valid over all scales. Nevertheless there is a clear possibility that for large beam-widths, and for scatter from mesospheric heights, there may be an appreciable contribution to the mean square radial velocity measured by a radar due to horizontal fluctuating motions. Since it is likely that the above ratio is an over-estimate, we can conclude that this effect is not likely to be a concern for scatter from any altitude provided that the beam half-power half-width is less than 2°, and will not be a concern in most stratospheric-tropospheric experiments made with a vertical beam (even for half-power half-widths out to 5°). However,(remembering that ϵ is proportional to the cube of the root mean square radial velocity), the possibility of a bias in estimates of ϵ as high as 50% or even more exists for MF radars and wide beam MST radars making studies in the mesosphere. The integrals discussed above clearly need to be evaluated in much greater detail before the exact contribution can be determined, but the importance of this effect must be borne in mind.

CONSEQUENCES OF THIS NEW THEORY

In the following discussion, it will be assumed that the form of spectrum which varies proportionally to $k^{-1/3}$ at small k is the one which best matches the real case (fig. 3), based in part on the theory of /20/.

One immediate consequence of this theory is that many measurements of turbulent energy dissipation rates made with radars in the past, particularly radars with very broad beams and very long pulse lengths, will have overestimated the strength of atmospheric turbulence. As an example, Hocking /13,14/ has shown values of energy dissipation which vary between .08 and .16 W/kg. However the new theory shows that these measurements should more properly be considered as values varying between .03 and .05 W/kg. (There is a reduction of a factor of about $2^{2/3}$ due to the effect presented in fig 3., and then probably an extra 50% reduction due to contamination by horizontal fluctuating motions due to the effects discussed in the last section).) These values are much closer to the types of measurements made by rockets, e.g. /21,22,23,24/. Thus the radar measurements and the rocket measurements are now very much of the same order of magnitude.

One should also recognize that radars will tend to have a built-in bias in that they will tend to respond to stronger patches of turbulence and may not see weaker patches. A rocket, on the other hand, will see all turbulence of all strengths, but only along its trajectory. A small intense patch of turbulence may be seen by a radar but may be missed completely by a rocket, so one should never expect a perfect one-to-one relationship between rocket and radar measurements of turbulence. In fact on average radar measurements should be a little higher than the rocket measurements, but differences of factors of 2 or 3 at the most would be expected for long term averages (although instantaneous differences could be larger at times). However, larger average discrepancies than this have been recorded in the past,and although some of these differences may be geophysical, this new theory helps to better reconcile past rocket and radar measurements of atmospheric turbulence.

CONCLUSIONS

In this paper we have examined current methods of measurement of atmospheric turbulence by radars and highlighted some of the strengths and weaknesses of these techniques. Of particular importance, we have re- addressed the issue of the relationship between the spectral width measured by radars and the strength of atmospheric turbulence. We have shown that reduction factors c_f are necessary which may be as high as 2 and 3, particularly for wide beam radars (narrow beam radars are less affected - fig. 3. shows the correction factor for different beam widths); this will therefore reduce previous estimates of turbulence energy dissipation rate by values of this order. This may go a long way to explaining previously observed discrepancies between in situ and radar measurements of atmospheric turbulence. It would be of great interest to now carry out common volume measurements of turbulence by both radar and rocket.

REFERENCES

1. Van Zandt, T.E., J.L. Green, K.S. Gage and W.L. Clarke, "Vertical profiles of refractivity turbulence structure constant: comparisons of observations by the Sunset radar with a new theoretical model", *Radio Sci.*, 13, 819-829, 1978.
2. Gage, K.S., J.L. Green and T.E. VanZandt, "Use of Doppler radar for the measurement of atmospheric turbulent parameters from the intensity of of clear echoes", *Radio Sci.*, 15, 407-416, 1980.
3. Hocking, W.K. "Measurement of Turbulent Energy Dissipation Rates in the Middle Atmosphere by Radar Techniques, A Review", *Radio Sci.* , 20, 1403-1422, 1985.
4. Hocking, W.K., "Observation and Measurement of turbulence in the middle atmosphere with a VHF radar", *J. Atmos. Terr. Phys.*, 48, 655-670, 1986.
5. Hocking, W.K., On the relationship between the strength of atmospheric radar backscatter and the intensity of atmospheric turbulence, *Adv. Space Res.* 12(10), 207-213, 1992.
6. Hocking, W.K. and Vincent, R.A. "A Comparison between HF partial reflection profiles from the D-region and simultaneous Langmuir probe electron density measurements", *J. Atmos. Terr. Phys.* , 44, 843-854, 1982.
7. Sen, H.K., and A.A. Wyller, "On the generalization of the Appleton- Hartree magnetionic formulas", *J. Geophys. Res.*, 65, 3931-3950, 1960.
8. Warnock, J.M. and T.E. VanZandt, "A statistical model to estimate the refractivity turbulence structure constant C_n^2 in the free atmosphere, *Report NOAA-TM-ERL-AL-10, NOAA Environmental Research labs., Boulder, Co.*, 1985.
9. Hocking, W.K. "On the Extraction of Atmospheric Turbulence Parameters from Radar Backscatter Doppler Spectra – I: Theory", *J. Atmos. Terr. Phys.*, 45, 89-102, 1983.
10. Hocking, W.K. "Mesospheric turbulence Intensities Measured with a HF radar at 35°S", J. Atmos. Terr. Phys. 45,103-114, 1983b
11. Atlas, D., R.C. Srivastava and P.W. Sloss, "Wind shear and reflectivity Gradient effects on Doppler radar spectra, II", *J. Appl. Meteor.*, 8, 384-388, 1969.
12. Frisch, A.S. and S.F. Clifford, "A study of convection capped by a stable layer using Doppler radar and acoustic echo sounders, *J. Atmos. Sci.*, 31, 1622-1628, 1974.
13. Hocking, W.K., "Two Years of Continuous Measurements of Turbulence Parameters in the Upper Mesosphere and Lower Thermosphere made with a 2-MHz radar", *J. Geophys. Res.*, 93, 2475-2491, 1988
14. Hocking, W.K., "Seasonal variations of turbulence intensities in the upper mesosphere and lower thermosphere measured by radar techniques", *Middle Atmosphere Program Handbook*, SCOSTEP Secretariat, Dept. of Electr. Computer Eng., Univ of Illinois, Urbana, IL 61801, USA, 27, 439-442, 1989.
15. Murphy, D.J., W.K. Hocking and D.C. Fritts, "An assessment of the effect of gravity waves on the width of radar Doppler spectra", *J. Atmos. Terr. Phys.*, 56, 17-29, 1994.
16. Weinstock, J., "On the theory of turbulence in the buoyancy subrange of stably stratified flows", J. Atmos. Sci., 35, 634-649, 1978.
17. Labitt, M., "Some basic relations concerning the radar measurement of air turbulence", *Mass. Inst. of Technol., Lincoln Lab.*, Work. Pap. 46WP-5001, 1979.
18. Hohne, A.R., "Radar detection of turbulence in precipitation environments", *J. Atmos. Sci.*, 39, 1819-1837., 1982.
19. Kaimal, J.C., J.C. Wyngaard, Y. Izumi, and O.R. Cote, "Spectral characteristics of surface layer turbulence", *Quart. J. Roy. Meteorol. Soc.*, 98, 563, 1972.
20. Dewan, E.M., "The saturated-cascade model for atmospheric gravity wave spectra, and the wavelength-period (W-P) relations, *Geophys. Res. Letts.*, 21, 817-820, 1994.
21. Thrane, E.V., T.A. Blix, C. Hall, T.L. Hansen, U. Von Zahn, W. Meyer, P. Czechowsky, G. Schmidt, H.-U. Widdel, and A. Neumann, "Small scale structure and turbulence in the mesosphere and lower thermosphere at high latitudes in winter", *J. Atmos. Terr. Phys.*, 49, 751-762, 1987.
22. Luebken, E.-J., O. van Zahn, E.V. Thrane, T. Blix, O.A. Kokin and S.V. Pachomov, "In-situ Measurements of Turbulent Energy Dissipation Rates and Eddy Diffusion Coefficients During MAP/WINE", *J. Atmos. Terr. Phys.*, 49, 763-776, 1987
23. Blix, T.A., E.V. Thrane, and O. Andreassen, "In situ measurements of the fine-scale structure and turbulence in the mesosphere and lower thermosphere by means of electrostatic positive ion probes", *J. Geophys. Res.*, 95, 5533-5548, 1990.
24. Luebken, F.J., "On the extraction of turbulent parameters from atmospheric density fluctuations", *J. Geophys. Res.*, 97, 20385-20395, 1992.

Radio Science, Volume 32, Number 4, Pages 1425–1444, July–August 1997

Studies of polar mesosphere summer echoes over EISCAT using calibrated signal strengths and statistical parameters

W. K. Hocking

Department of Physics, University of Western Ontario, London, Ontario, Canada

J. Röttger

EISCAT Scientific Association, Kiruna, Sweden

Abstract. The EISCAT (European incoherent scatter) monostatic VHF radar operating on 224 MHz has been used to investigate characteristics of polar mesosphere summer echoes (PMSE) at Bragg scales of around 0.6 m. In particular, we look at four main parameters, two of which have not been studied in any real detail for these echoes. These parameters are absolute backscatter strengths, fading times, amplitude distributions, and turbulent energy dissipation rates. The calibrated signal strengths, combined with theoretical modeling, are used to demonstrate that specular reflection from even the sharpest background density gradients which have been measured thus far by rocket probes cannot be the cause of these echoes at VHF frequencies. We also demonstrate that specular reflections from the edges of the large electron density "bite-outs" (which are often observed in association with these echoes) cannot be responsible for the measured backscatter strengths. However, these same gradients can, in association with turbulence, cause measurable backscatter, but only provided that scatter is from within the inertial subrange of turbulent electron density fluctuation spectra. This requires large Schmidt numbers. We also use statistical studies of the amplitude distributions to show that our echoes were due to an ensemble of scatterers in the radar volume, rather than single entities. A new calculation concerning the expected lifetimes of the scattering entities in the presence of turbulence is also demonstrated, and then our measurements are used to show that the scatterers often have lifetimes in excess of those which are predicted for classical neutral turbulence. We use this latter point to supply additional evidence that the Schmidt number substantially exceeds 1.0.

Special calculation of scatterer lifetimes from $\tau_{\frac{1}{2}} \propto f_{\frac{1}{2}}$, in the case of high Schmidt Numbers

5. Lifetimes of Scatterers

In the following section, we wish to pursue the issue of the lifetimes of the scatterers and see how these relate to the fading times of the signals which we measure. Earlier, we ascribed the fading times measured to be indicators of the strength of turbulence, but we now wish to readdress this assumption. At frequencies of 50 MHz or so, scatterers with scales of the order of 3 m are involved, and it is generally assumed that these scatterers are sufficiently long-lived that their lifetimes do not impact on the fading times of the signal; that is, it is assumed that the scatterers exist pretty much unchanged for at least a few seconds (we will see verification of this assumption shortly). However, it is instructive to examine the lifetime of typical scatterers in different regimes of the turbulence spectrum. We will consider scatterer lifetimes for the cases in which the scatterer is in the inertial subrange and the viscous subrange of turbulence.

To begin, we need to define our visualization of a "scatterer" or "scattering eddy," at least in regard to the following calculations. In reality, a region of turbulence comprises a tangle of twisted and contorted shapes [e.g., see *Hocking and Hamza*, 1997], but it is common to represent them in a statistical sense as ellipsoids. When we refer to a scattering eddy, we will mean an ellipsoid of electron density perturbation with dimensions (scale) comparable to one half of the radar wavelength, which may rotate and move about. We envisage that there are also many other such "eddies" with different scales, but these do not produce substantial backscatter at our radar wavelength (e.g., see *Hocking* [1987b], for schematic diagrams of these eddies and calculations concerning their efficiency of backscatter).

In each case we will imagine that a typical scatterer has an eddy size with depth of the order of one half a radar wavelength, (i.e., it will have a scale of ≈0.67 m for a 224-MHz radar), although we emphasize that there are many other eddies of different size scattered around the region; we simply concentrate on the ones which give strongest backscatter. If the scatterer has a scale which places it in the viscous subrange (as, for example, we would expect in the case of 224-MHz scatterers if the Schmidt number is 1), the eddy will be destroyed in the time it takes for the velocity motion on one side of the eddy to diffuse across to the other; that is, the motions on opposite sides will be in the opposite directions, so that by the time the momentum on one side transfers to the other, the eddy will have self-destructed. Thus the eddy will have a lifetime of typically

$$\tau_\ell \approx (\lambda/2)^2 / \nu \qquad (17)$$

where ν is the molecular kinematic viscosity. *Kelley and Ulwick* [1988] used $\nu \approx 3$ m^2 s^{-1}, based on an observed temperature of 135 K, and this value is quite appropriate here as well. Thus at our scales, the lifetime is typically $\tau_\ell \approx 0.15$ s. Even if we assume that $\nu \approx 1.5$ m^2 s^{-1}, we still have $\tau_\ell \approx 0.3$ s. Thus scatterer lifetimes are very short, and it may be that in many cases (especially those of slower fading) the observed fading time is a measure of the scatterer lifetime, rather than either the strength of turbulence or even spectral beam broadening. It is probably true that the faster fading times (which we may take to be associated with more violent turbulent mixing) do give a fair estimate of turbulence strengths, so Figure 5 is still reasonably valid. However, in cases where $\tau_{0.5}$ is large, Figure 5 may overestimate the turbulent energy dissipation rate. Indeed, in such cases it is quite possible that the long fading times result from persistent layers which may even exist in a nonturbulent (laminar) environment. Such a suggestion has also been made by *Röttger and Pan* [1995]. Such points are not in the majority, but there are enough large values to make this a noteworthy issue. As an additional point, it is of interest to apply (17) to the case of 6-m radar wavelengths. In this case, $\tau_\ell \approx 3$ s for $\nu \approx 3$ m^2 s^{-1}, confirming our earlier expectations of a few seconds for the lifetimes of eddies at these scales.

If, on the other hand, the scatterer's scale places it in the inertial subrange, then the eddy is not destroyed by viscous diffusion, but rather by the tearing motion of smaller-scale eddies. In this case, we can write that the eddy size ξ is related to the lifetime τ through the relation $\xi^2 = \beta\varepsilon\tau^3$ [*Batchelor*, 1950], where $\beta \approx 1$, so we may write

$$\tau_\ell \simeq \left[(\lambda/2)^2/\varepsilon\right]^{1/3} \qquad (18)$$

The actual lifetime of the eddy will be the lesser of (17) and (18). For our 224-MHz scatterers, and assuming for the present that the plasma turbulence follows the neutral turbulence (i.e., assuming $S_c \approx 1$), we may take $\varepsilon \approx$

0.04 W kg^{-1} and show that the latter lifetime is about 2 s. Since this exceeds our earlier estimates (0.15 or 0.3 s), it means that such scales would have to be in the viscous subrange and so have a lifetime of less than 0.3 s if $S_c \approx 1$.

It is this fact which brings us to another major point of this paper. We note in Figure 3 that, in fact, there are values of $\tau_{0.5}$ up to 0.5 s and certainly many values in excess of 0.3 or 0.15 s. This should not be possible for a plasma spectrum which emulates that for neutral air turbulence; the eddies should destroy themselves more quickly than this in the case of $S_c \approx 1$. The only way in which such eddies can persist for so long is if the diffusion coefficient associated with the electrons is less than that for the neutrals by at least a factor 3 or 4. The diffusion of the electrons is determined not by the diffusion coefficient of the neutrals, ν, but rather by the ion diffusion coefficient D, and in this case $\tau_\ell \approx (\lambda/2)^2/D$. Thus the existence of such slow fading is evidence of an electron diffusion D considerably less than ν, or a Schmidt number in excess of 1; in this case, at least 3 or 4. In fact if D is small enough, then the eddies with scales of the order of 0.67 m will be in the inertial subrange, and so their lifetimes will then be governed by (18). Regardless of this final point, however, the fact remains that the cases of slower fading certainly cannot be accounted for if the plasma turbulence follows the spectral form of the neutral turbulence, and the only way in which such slow fading times are possible is if D is much less than ν, that is, if the electron diffusion is much slower than the diffusion of the neutrals.

REFERENCES

The following references are not by any means complete, but serve as a useful starting point for further sources of information.

Anadarao B.G., Raghavarao, R., Desai, J.N.: J. Atmos. Terr. Phys, 40, 157-163, 1978.

Barat, J.: J. Appl. Meterology, 21, 1480-1488, 1982a.

Barat, J.: J. Appl. Meterology, 21, 1489-1496, 1982b.

Barat, J.: J. Atmos. Sci., 39, 2553-2564, 1982c.

Batchelor, G.K.: The Theory of Homogeneous Turbulence, Cambridge University Press, 1953.

Batchelor, G.K., Roy, J.: Meteorol. Soc., 76, 133-146, 1977.

Battaner, E. Molina, A.: J. Geophys. Res., 85, 6803-6810, 1980.

Blamont, J.E., de Jager, C.: Ann. Geophys., 17, 134-143, 1961.

Blamont, J.: Planet Space Sci., 10, 89-101, 1963.

Blamont, J.E., Barat, J.: in Aurora Airglow, edited by B.M. McCormac, 156-159, Reinhold Pub. Co., 1964.

Blix, T.A., Thrane, E.V., Andreassen, O.: J. Geophys. Res., 95, in press 1990.

Blum, P., Schuchardt, K.G.H., von Zahn, U.: J. Atmos. Terr. Phys., 40,1131-1135, 1978.

Blum, P.W., Schuchardt, K.G.A.: J. Atmos. Terr. Phys., 40, 1137- 1142, 1978.

Booker, H.G., Cohen, R.: J. Geophys. Res., 61, 707-733, 1956.

Bradshaw, P.: "An Introduction to Turbulence its Measurement", Pergamon Press, 1975.

Chakrabarty, D.K., Beig, G., Sidhu, J.S., Chakrabarty, H., Narayanan, R., Modi, N.K., Das, S.R., Chakrabarty, P.: J. Atmos. Terr. Phys., 49, 975-980, 1987.

Chakrabarty, D.K., Beig, G., Sidhu, J.S. Das, S.R.: J. Atmos. Terr. Phys., 51, 19-27, 1989.

Chandra, S.: Planet. Space Sci., 28, 585-593, 1980.

Chanin, M.L., Hauchecorne, A.: J. Geophys. Res., 86, 9715-9721, 1981.

Colegrove, F.D., Hanson, W.B., Johnson, F.S.: J. Geophys. Res., 70, 4931-4941, 1965.

Colegrove, F.D., Johnson, F.S., Hanson, W.B.: J. Geophys. Res., 71, 2227-2236, 1966

Czechowsky, P., Ruester, R., Schmidt, G.: Geophys. Res. Letts., 6, 459-462, 1979.

Czechowsky, P., Inhester, B., Klostermeyer, J., Reid, I.M., Ruester, R., Schmidt, G.: Handbook for MAP, vol 28, 459-466, Scostep Secretariat, University of Illinois, U.S.A., 1989.

Danilov, A.D.: Adv. Space Res., 4, 67-78, 1984.

Desaubies, Y., Smith, W.K.: J. Phys. Oceanography, 12, 1245-1259, 1982.

Dewan, E.M.: Science, 211, 1041-1042, 1981.

Dewan, E., Grossbard, N., Quesada, A.F., Good, R.E.: Geophys. Res. Letts, 11, 80-83, 1984 with correction in Geophys. Res. Letts., 11, 624, 1984.

Dewan, E.M., Good, R.E.: J. Geophys. Res., 91, 2742-2748, 1986.

Dong, B., Yeh, K.C.: J. Geophys. Res., 93, 3729-3744, 1988.

Driscoll, R.J., Kennedy, L.A.: Phys. Fluids, 28, 72-80, 1985.

Ebel, A.: J Atmos. Terr. Phys., 42, 617-628, 1980.

Ebel, A.: J. Atmos. Terr. Phys., 46, 727-737, 1984.

Ebel, A., Manson, A.H., Meek, C.E.: J. Atmos. Terr. Phys., 49, 385-401, 1987.

Eckermann, S.D., Hocking, W.K.: J. Geophys. Res., 94, 6333-6339, 1989.

Eckermann, S.D., Vincent, R.A.: Pure Appl. Geophys., 130, 509- 532, 1989.

Elford, W.G., Roper, R.G.: Space Res., VIII, 42-54, 1967.

Fellous, J.L., Frezal, M.E.: MAP Handbook, Vol. 2, 323-332, Scostep Secretariat, University of Illinois,

U.S.A., 1981.
Fritts, D.C., Rastogi, P.K.: Radio Sci., 20, 1247-1277, 1985.
Fritts, D.C., Dunkerton, T.J.: J. Atmos. Sci., 42, 549-556, 1985.
Fritts, D.C., Chou, H-G.: J. Atmos. Sci., 44, 3610-3624, 1987.
Fritts, D.C., Vincent, R.A.: J. Atmos. Sci., 44, 605-619, 1987.
Fritts, D.C., Tsuda, T. Sato, T., Fukao, S., Kato, S.: J. Atmos. Sci., 45, 1741-1759, 1988.
Fritts, D.C., Blanchard R.C., Coy, L.: J. Atmos. Sci., 46, 423- 434, 1989.
Fritts, D.C., Yuan, Li.: J. Atmos. Sci., 46, 2562-2568, 1989.
Fukao, S., Sato, T., Kato, S., Harper, R.M., Woodman, R.F., Gordon, W.E.: J. Geophys. Res., 84, 4379-4386, 1979.
Fukao, S., M.D. Yamanaka, N. Ao, W.K. Hocking, T. Sato, M. Yamamoto, T. Nakamura, T. Tsuda and S. Kato, "Seasonal variability of vertical eddy diffusivity in the middle atmosphere, 1. Three-year observations by the middle and upper atmosphere radar", *J. Geophys. Res., 99*, 18973 - 18987, 1994.
Gage, K.S.: J. Atmos. Sci., 36, 1950-1954, 1979.
Gage K.S., Nastrom, G.D.: Radio Sci., 20, 1339-1347, 1985.
Gage K.S., Nastrom, G.D.: J. Atmos. Sci., 43, 729-740, 1986.
Garcia, R.R., Solomon, S.: J. Geophys. Res., 90, 3850-3868, 1985.
Garrett, C., Munk, W.: Geophys. Fluid Dynamics, 2, 225-264, 1972.
Garrett, C., Munk, W.: J. Geophys. Res., 80, 291-297, 1975.
Gibbins, O.T., Schwartz, P.R., Thacker, D.L., Bevilacqua, R.M.: Geophys. Res. Lett., 9, 131-134, 1982.
Gordiets, B.F., Kulikov, Yu N., Markov, M.N., Marov, Ma. Ya.: J. Geophys. Res., 87, 4504-4514, 1982.
Gossard, E. D., Hooke, W.H.: Waves in the Atmosphere, Elsevier Scientific Publ. Co., Amsterdam, 1975.
Greenhow J.S., Neufeld, E.L.: J. Geophys. Res., 64, 2129-2153, 1959.
Greenhow, J.S.: J. Geophys. Res., 64, 2208-2209, 1959.
Hauchecorne, A., Chanin, M-L., Wilson, R.: Geophys. Res. Letts., 14, 933-936, 1987.
Hesstvedt, E.: Geofys. Publik., 27, 1-35, 1968.
Hill, R.J., Clifford, S.F.: J. Opt. Soc. Am., 68, 892-899, 1978.
Hines, C.O.: Canadian J. Phys., 38, 1441-1481, 1960.
Hines, C.O.: The Upper Atmosphere in Motion, Am. Geophys. Union, Washington DC 433, 1974.
Hines, C.O.: J. Atmos. Sci., 45, 1269-1278, 1988.
Hirota, I.: J. Atmos. terr. Phys., 46, 767-773, 1984.
Hirota, I.: Middle Atmosphere Handbook, vol 16, 144-148, Scostep Secretariat, University of Illinois, U.S.A., 1985.
Hocking, W.K.: J. Atmos. Terr. Phys., 45, 89-102, 1983a.
Hocking, W.K.: J. Atmos. Terr. Phys., 45, 103-114, 1983b.
Hocking, W.K.: Radio Sci., 20, 1403-1422, 1985.
Hocking, W.K.: J. Geophys. Res., 93, 2475-2491, 1988.
Hocking, W.K., May, P., Roettger, J.: Pure Appl. Geophys., 130, 571-604, 1989.
Hocking, W.K.: Handbook for MAP, vol. 27, 439-442, Scostep Secretariat, University of Illinois, U.S.A., 1989.
Hodges, R.R.: J. Geophys. Res., 72, 3455-3458, 1967.
Holton,J.R.: J. Atmos. Sci., 39, 791-799, 1982.
Holton, J.R.: J. Atmos. Sci., 40, 2497-2507, 1983.
Houghton, J.T.: The Physics of Atmospheres, Cambridge University, 1977.

Hunten, D.M.: J. Geophys. Res., 79, 2533-2534, 1974.

Johnson, F.S., Wilkins, E.M.: J. Geophys. Res., 70, 1281-1284, 1965.

Johnson, F.S., Gottlieb, B.: Planet. Space Sci., 18, 1707-1718, 1970.

Johnson, F.S.: J. Atmos. Sci., 32, 1658-1662, 1975.

Jones, L.M., Peterson, J.W.: Meteorological monographs, 8, 176- 189, 1968.

Jones, W.L., Houghton, D.D.: J. Atmos. Sci., 28, 604-608, 1971.

Justus, C.G.: J. Geophys. Res., 71, 3767-3773, 1966.

Justus, C.G.: J. Geophys. Res., 72, 1035-1039, 1967a.

Justus, C.G.: J. Geophys. Res., 72, 1933-1940, 1967b.

Justus, C.G.: J. Geophys. Res., 73, 455-458, 1968.

Justus, C.G.: J. Atmos. Sci., 26, 1137-1141, 1969.

Kaimal, J.C., Wyngaard, J. C., Izumi, Y., Cote, O.R.: Q. J. Roy. Meteorol. Soc., 98, 563-589, 1972.

Kelley, M.C., Farley, D.T., Roettger, J.: Geophys. Res. Letts., 14, 1031-1034, 1987.

Kelley, M.C., Ulwick, J.C.: J. Geophys. Res., 93, 7001-7008, 1988.

Kellog, W.W.: Space Science Revs., 3, 275-316, 1964.

Keneshea, T.J., Zimmerman, S.P.: J. Atmos. Sci., 27, 831-849, 1970.

Keneshea, T.J., Zimmerman, S.P., Philbrick, C.R.: Planet. Space Sci., 27, 385-401 1979.

Klostermeyer, J.: Middle Atmosphere Program handbook, 28, 299- 308, Scostep Secretariat, University of Illinois, U.S.A., 1989.

Kochanski, A.J.: J. Geophys. Res., 69, 3651-3662, 1964.

Kolmogoroff, A.N.: Doklady Akad. Nauk USSR, 32, 16, 1941. German Translation in "Sammelbzur Statistischen Theorie der Turbulens", Akademi-Verlag, Berlin, 1958.

Korolev, S.S., Kolenik, A.G.: Geomag. Aeron., 19, 47-50, 1979.

Kraichnan, R.H.: Phys. of Fluids, 10, 1417-1423, 1967.

Layzer, D., Bedinger, J.F.: Planet. Space Sci., 17, 1891-1911, 1969.

Lhermitte, R.: J. Geophys. Res., 88, 725-742, 1983.

Lilly, D.K., Waco, D.E., Aldefang,S.I.: J. Appl. Meterol., 13, 488-493, 1974.

Lilly, D.K.: J. Atmos. Sci., 40, 749-761, 1983.

Lilly, D.K.: J. Atmos. Sci., 46, 2026-2030, 1989.

Lindzen, R.S.: J. Geophys. Res., 86, 9707-9714, 1981.

Lloyd, K.G., Low, C.H., McAvaney, B.J., Rees, D., Roper, R.G.: Planet. Space Sci., 20, 761-769, 1971.

Luebken, F.-J., von Zahn, U., Thrane, E.V., Blix, T., Kokin, G.A., Pachomov, S.V.: J. Atmos. Terr. Phys., 49, 763-775, 1987.

Manson, A.H., Meek, C.E.: J. Atmos. Terr. Phys., 42, 103-113, 1980.

Manson, A.H., Meek, C.E., Gregory, J.B.: J. Atmos. Terr. Phys., 43, 35-44, 1981.

Massie, S.T.: J. Geophys. Res., 85, 2155-2164, 1980.

Matsuno, T.: J. Meteorol. Soc. Japan, 60, 215-226, 1981.

McAvaney, B.J.: Small Scale Wind Structure in the Upper Atmosphere, Ph.D Thesis, University of Adelaide, 1970.

Meek, C.E., Reid, I.M., Manson, A.H.: Radio Sci., 20, 1383-1402, 1985.

Mueller, H.G.: Planet. Space. Sci., 16, 61-90, 1968.

Muller, P., Holloway, G., Henyey,F., Pomphrey, N.: Rev. Geophys., 24, 493-536, 1986.

Nastrom, G.D., Fritts, D.C., Gage, K.S.: J. Atmos. Sci., 44, 3087-3096, 1987.

Noel, T.M.: J. Geophys. Res., 68, 2862-2863, 1963.

Philbrick, C.R.: Middle Atmosphere Handbook, vol 2, 333-340, Scostep Secretariat, University of Illinois, U.S.A., 1981.

Rastogi, P.K.: J. Atmos. Terr. Phys., 43, 511-524, 1981.

Rees, D., Roper, R.G., Lloyd, K., Low, C.H.: Phil. Trans. Roy.,Soc., Lond, A 271, 631-666, 1972.

Reid, I.M.: J. Atmos. Terr. Phys., 48, 1057-1072, 1986.

Reid, I.M., Vincent, R.A.: J. Atmos. Terr. Phys., 49, 443-460, 1987.

Reid, I.M., Ruester, R., Schmidt, G.: Nature, 327, 43-45, 1987.

Rhines, P.B.: J. Fluid Mechanics, 69, 417-443, 1975.

Roettger, J., Rastogi, P.K., Woodman, R.F.: Geophys. Res. Letts., 6, 617-620, 1979.

Roper, R.G.: J. Geophys. Res., 71, 4427-4428, 1966.

Roper, R.G.: Turbulence in the Lower Thermosphere, in "The Upper Atmosphere Magnetosphere: Studies in Geophysics", 129, 117-129, National Research Council, U.S.A., 1977.

Rosenberg, N.W., Golmb, D., Zimmerman, S.P., Vickery, W.K., J.S. Theon, Space Res. XIII, 435-439, 1973.

Royrvik, O., Smith, L.G.: J. Geophys. Res., 89, 9014-9022, 1984.

Sato, T., Woodman, R.F.: J. Atmos. Sci., 39, 2546-2552, 1982.

Sato, T., Tsuda, T., Kato, S., Morimoto, S., Fukao, S., Kimura, I.: Radio Sci., 20, 1452-1460, 1985.

Scheffler, A.O., Liu, C.H.: Radio Sci., 20, 1309-1322, 1985.

Shibata, T., Fukuda, T., Maeda, M.: Geophys. Res. Letts., 13, 1121-1124, 1986.

Shimazaki, T.: J. Atmos. Terr. Phys., 33, 1383-1401, 1971.

Sidi, C., Teitelbaum, H.: J. Atmos. Terr. Phys., 40, 529-540, 1978.

Sidi, C., Lefrere, J., Dalaudier F., Barat, J.: J. Geophys. Res., 774-790, 1988.

Smith, S.A., Van Zandt, T.E.: Radio Sci., 20, 1331-1338, 1985.

Smith, S.A., Fritts, D.C., Van Zandt, T.E.: J. Atmos. Sci., 44, 1404-1410, 1987.

Strobel, D.F., Summers, M.E. Bevilacqua, R.M. DeLand, M.T., Allen, M.: J. Geophys. Res., 92, 6691-6698, 1987.

Strobel, D.: Pure Appl. Geophys., 130, 533-546, 1989.

Tatarski, V.: Wave Propogation in a Turbulent Medium translated from Russian by Silverman, McGraw-Hill, N.Y., 1961.

Tchen, C.M.: Phys. Rev., 93, 4-14, 1954.

Teitelbaum, H.: Space. Res. VI, 438-447, 1966.

Teitelbaum, H., Sidi, C.: J. Atmos. Terr. Phys., 38, 413-421, 1976.

Teitelbaum, H., Blamont, J.E.: Planet. Space Sci., 25, 723-734, 1977.

Thrane, E.V., Andreassen, O., Blix, T., Grandal, B., Brekke, A., Philbrick, C.R., Schmidlin, F.J., Widdel, H.V., Von Zahn, U., Luebken, F.-J.: J. Atmos. Terr. Phys., 47, 243-956, 1985.

Tsuda, T., Inoue, T., Fritts, D.C., Van Zandt, T.E., Kato, S., Sato, T., Fukao, S.: J. Atmos. Sci., 46, 2440-2447, 1989.

Van Zandt, T.E.: Geophys. Res. Letts., 9, 575-578, 1982.

Van Zandt, T.E.: Handbook for MAP,vol 16, 149-156, Scostep Secretariat, University of Illinois, U.S.A., 1985.

Van Zandt, T.E.: Radio Sci., 20, 1323-1330, 1985.

Van Zandt, T.E., Fritts, D.C.: J. Geophys. Res., 9723-9732, 1987.

Van Zandt, T.E., Fritts, D.C.: Pure Appl. Geophys., 130, 400-420, 1989.

Vincent, R.A., Ball, S.: J. Atmos. Terr. Phys., 39, 965-970, 1977.

Vincent, R.A., Stubbs, T.J.: Planet. Space Sci., 25, 441-455, 1977.

Vincent, R.A., Ball, S.M.: J. Geophys. Res., 86, 9159-9169, 1981.

Vincent, R.A., Reid, I.M.: J. Atmos. Sci., 40, 1321-1333, 1983.

Vincent, R.A.: J. Atmos. Terr. Phys., 46, 119-128, 1984.

Vincent, R.A.: Adv. Space Res., 7, 163-169, 1987.

Vincent, R.A., Fritts, D.C.: J. Atmos. Sci., 44, 748-760, 1987.

Von Zahn, U., Herwig, T.: Proc. NATO Advanced Study Institute, Spatind, Norway, April 12-22, eds. B. grandal J.A. Holtet, Reidel Publ. Co., 1977.

Weinstock, J.: J. Atmos. Sci., 35, 634-649, 1978a.

Weinstock, J.: J. Atmos. Sci., 35, 1022-1027, 1978b.

Weinstock, J.: J. Atmos. Sci., 38, 880-883, 1981.

Weinstock, J.: Geophys. Res. Letts., 9, 863-865, 1982.

Weinstock, J.: J. Atmos. Terr. Phys., 46, 1069-1082, 1984.

Widdel, H.-U.: J. Atmos. Terr. Phys., 49, 723-741, 1987.

Wofsy, S.C., McElroy, M.B.: J. Geophys. Res., 78, 2619-2624, 1973.

Woodman, R.F., Guillen, A.: J. Atmos. Sci., 31, 493-505, 1974.

Woodman, R.F., Kugel, R.P., Roettger, J.: Radio Sci., 15, 233- 242, 1980.

Woodman, R.F.: Radio Sci., 15, 423-430, 1980.

Woodman, R.F., Rastogi, P.K.: Geophys. Res. Letts., 11, 243-246, 1984.

Yeh, K.C., Dong, B.: J. Atmos. Terr. Phys., 51, 54-50, 1989.

Zimmerman, S.P., Champion, K.S.W.: J. Geophys. Res., 68, 3049- 3056, 1963.

Zimmerman, S.P.: J. Geophys. Res., 71, 2439-2444, 1966.

Zimmerman, S.P.: Space Res. VI, 425-437, 1966.

Zimmerman, S.P.: J. Geophys. Res., 73, 463-454, 1968.

Zimmerman, S.P., Trowbridge, C.A., Kofsky, I.L.: Space Res., XI, 907-914, 1971.

Zimmerman, S.P., Rosenberg, N.N.: Space Res., XIII, 623-628, 1972.

Zimmerman, S.P., Trowbridge, C.A.: Space Res., XIII, 203-208, 1973.

Zimmerman, S.P.: J. Geophys. Res., 78, 3927-3938, 1973.

Zimmerman, S.P., Pereira, G.P., Murphy, E.A., Theon, J.: Space Res., XIII, 209-215, 1973.

Zimmerman, S.P., Murphy, E.A.: in Proc. NATO Advanced Study Institute, Spatind, Norway, April 12-22, eds. B. Grandal, J.A Hostet, Reidel Publ. Co., 1977.

Zimmerman, S.P., Keneshea, T.J.: MAP Handbook, Vol.2, 311-322, Scostep Secretariat, University of Illinois, U.S.A., 1981.

Zimmerman, S.P., Keneshea, T.J.: J. Atmos. Terr. Phys., 48, 491- 507, 1986.